USING SINGLE PARTICLE ICP-MS TO STUDY OCCURRENCE AND BEHAVIOR OF ENGINEERED, NATURAL, AND INCIDENTAL NANOPARTICLES IN FRESHWATER STREAMS

by

Logan N. Rand

A thesis submitted to the Faculty and the Board of Trustees of the Colorado School of Mines in partial fulfillment of the requirements for the degree of Doctor of Philosophy (Geochemistry).

Golden, Colorado

Date _____

Signed: _____

Logan N. Rand

Signed: _____

Dr. James F. Ranville
Thesis Advisor

Golden, Colorado

Date _____

Signed: _____

Dr. Thomas Gennett
Professor and Department Head
Department of Chemistry

ABSTRACT

The use of engineered nanoparticles (ENPs) in numerous industrial and consumer applications is steadily increasing, which has led to concern about their environmental release. However, the study of ENP fate and transport has been met with significant technical challenges. Low (parts per trillion) concentrations and the frequent complexity of environmental media makes accurate detection difficult, even without the added possibility of ENP alteration via aggregation, surface modification, and degradation (dissolution). Additionally, there are many mineral analogues to ENPs and these natural nanoparticles (NNPs) are not easy to distinguish from ENPs. Human activities also result in many incidental nanoparticle (INP) byproducts in the environment. The Ph.D. dissertation research described in this thesis contributes to the current attempts to improve environmental nanoparticle (NP) analysis and better understand NP behavior in natural systems, with the focus being on streams and the application of single particle inductively coupled plasma-mass spectrometry (spICP-MS) for NP measurement.

Two field studies in this thesis demonstrate the utility and limitations of the technique for quantifying changes to NP populations in dynamic natural water systems, including semi-urban recreational streams and a mining-impacted stream. Total metal mass concentrations, oxybenzone, and NPs were examined during stream recreation in Clear Creek, Colorado, Truckee River, Nevada, and Salt River, Arizona and in some instances significant increases in Ti NP concentrations and sizes were observed by spICP-MS. The study on the mining-impacted system found a decrease in Fe INP concentration and size occurred that could be related via multiple linear regression to seasonal and remediation-related water chemistry changes in the North Fork of Clear Creek, Colorado.

Additionally, the ability of spICP-MS to analyze aggregated NPs was examined and compared between instruments with magnetic sector versus time-of-flight mass analyzers. The results support the detectability of small (up to 200 nm) aggregates of CeO_2, goethite, and kaolinite NPs based on changes to size distributions and signal pulse clumping, as well as simultaneous pulses of multiple elements, depending on the analytical capabilities of the instrument used.

This dissertation advances the ability to measure ENPs, NNPs, and INPs in the environment and contributes to our understanding of anthropogenic effects on stream NPs.

TABLE OF CONTENTS

LIST OF FIGURES

LIST OF TABLES

LIST OF ABBREVIATIONS

Acid mine drainage ..... AMD
Continuing calibration verification CCV
Deryagin-Landau-Verwey-Overbeek ..... DLVO
Detection limit ..... DL
Deionized ..... DI
Dissolved organic carbon ..... DOC
Dynamic light scattering ..... DLS
Electrical double layer ..... EDL
Electron microscopy ..... EM
Energy-dispersive x-ray spectroscopy ..... EDS
Engineered nanoparticle ..... ENP
High resolution ..... HR
Incidental nanoparticle ..... INP
Inductively coupled plasma-atomic absorption spectroscopy ..... ICP-AES
Inductively coupled plasma-mass spectrometry ..... ICP-MS
Isoelectric point ..... IEP
Multiple linear regression ..... MLR
Nanoparticle ..... NP
National Institute of Standards and Technology ..... NIST
Natural nanoparticle ..... NNP
Natural organic matter ..... NOM
North Fork of Clear Creek ..... NFCC
Quality assurance/quality control ..... QA/QC
Scanning electron microscopy ..... SEM
Scanning/transmission electron microscopy ..... STEM
Single particle inductively coupled plasma-mass spectrometry ..... spICP-MS
Single particle inductively coupled plasma-high resolution mass spectrometry ..... spICP-HRMS
Single particle inductively coupled plasma-quadrupole mass spectrometry ..... spICP-QMS
Single particle inductively coupled plasma-time-of-flight mass spectrometry ..... spICP-TOFMS

Time-of-flight ..... TOF

Total organic carbon ..... TOC

Transmission electron microscopy ..... TEM

Turbiscan Stability Index ..... TSI

U.S. Geological Survey ..... USGS

Water treatment plant ..... WTP

Zeta potential ..... ZP

ACKNOWLEDGEMENTS

I wish to express gratitude to the following individuals:

Dr. James Ranville, thesis advisor, for inviting me into seemingly endless opportunity through research with you and for providing second chances, patience, and for teaching me to embrace spontaneity in science.

Dr. Bettina Voelker, thesis committee member, for getting me started in my graduate school journey, persistently looking out for my best interests, and believing in me.

Dr. Kamini Singha, thesis committee chair, and Dr. Alexis Navarre-Sitchler, thesis committee member, for advice regarding my dissertation research and thoughtful teaching in subjects crucial to my education but previously unfamiliar to me. Never again will I hesitate to try new statistical tests or "think like a modeler".

Dr. Joseph Meyer, for invaluable assistance with data interpretation and for making us all laugh in group meetings, even during challenging times.

My labmates Katie Challis, Angela Barber, Dr. Elizabeth Traudt Middleton, and Jill Murphy, for better research comradery than I could have imagined.

Dr. Manuel Montaño, Dr. Frank von der Kammer, and Dr. Thilo Hoffmann for hosting me for a week of experiments at Universität Wien. Special thanks to Manuel for his company and kind advice during this and our other encounters.

Dr. Marc Benedetti, Dr. Rémi Losno, and Mickaël Tharaud, for hosting me for nine months at Institut de Physique du Globe de Paris. Special thanks to Jialan Wang for help getting oriented in a new lab and new country as well as for much needed companionship.

Mary Boardman, North Fork Clear Creek Superfund project manager at Colorado Department of Public Health and Environment, for providing information on water treatment plant activities during North Fork of Clear Creek field sampling.

Fulbright-France, for funding my research stay in Paris and introducing me to remarkable friends and professional colleagues.

For my brother, Kip.

He cheered me on, made me laugh, and was my strongest base. I will never stop telling our stories and wanting to make you proud.

CHAPTER ONE
INTRODUCTION

1.1 Occurrence of Nanoparticles in the Environment

Nanoparticles (NPs) are generally defined as 1-100 nm sized materials which often exhibit size-dependent properties that differ from the bulk material of the same chemical composition.[1] Advances in their synthesis have rapidly increased their incorporation into industrial applications and consumer products. The rapid growth of nanotechnology implies inevitable engineered NP (ENP) release to the environment, prompting fate and transport, toxicology, and risk assessment studies.[2–11]

The attention directed toward ENPs has been accompanied by recognition of natural NPs (NNPs) formed in nature, which result from both biotic and abiotic mineral crystal growth as well as weathering processes.[5,12–18] Common examples include aluminosilicates, metal (hydr)oxides, and sulfides.[19] NNPs are widespread in the environment and play important roles in environmental processes due to their high surface reactivity, affecting the distribution of dissolved ions and molecules as well as environmental redox reactions.[14,19,20] Researchers have also identified incidental NPs (INPs) as a third NP classification.[5,10,21] These form in the environment as an unintentional byproduct of human activity, making them distinct from both ENPs and NNPs.

NNPs are widespread in the environment.[13,19] Specific examples are amorphous silica, allophane, halloysite, ferrihydrite, vermecular smectite, chlorite, anatase, schwertmannite, and zinc sulfides. Much of the clay fraction (defined as < 2 μm) in soils is nanoparticulate. Release from soils into water is favored by high pH, low ionic strength, and high Na^+ saturation.[22] All minerals growing from seed nuclei go through a nanocrystal stage in their growth.[12,19] Supersaturated waters undergoing sudden changes, such as transfer across a redox boundary, precipitate NPs in high abundance.[13,19,22,23] Microbial respiration can also cause rapid precipitation of NPs given the right conditions. Additionally, rock breakdown from weathering often produces NPs.

The supersaturated formation pathways are the most common in surface waters.[12,19,22] Environments that foster NP precipitation include acidic solutions mixing with circumneutral waters, redox transition zones of lakes and sediments, mixing zones between different

groundwater fluids, evaporation of soil waters, and the introduction of hydrothermal fluids to cold ocean water. One example of INP formation important to this dissertation research (Chapter 3) occurs at the confluence of acid mine drainage (AMD) with stream waters.[19,24] Mine waste contains metal sulfide rich rocks, which oxidatively dissolve to release sulfuric acid, Fe, Al, and other metals. Weathering of mine waste creates runoff with low pH and high metal concentrations. Such drainage waters are often hot (> 40°C) because the metal sulfide oxidation reactions are very exothermic. When these fluids are merge with cool, dilute, oxygenated stream waters, metal solubility drops and oxidation of reduced metals is favored, leading to precipitation of nanoscale metal (hydr)oxides. Microorganisms adapted to these environments, such as sulfate-reducing bacteria, utilize this redox gradient for respiration and facilitate rapid precipitation of mineral NPs that would otherwise be kinetically inhibited.

NPs can form suddenly from rapid changes in water chemistry and being susceptible to redissolution and chemical transformations, they are inherently unstable.[20] Therefore, accurately characterizing the water chemistry (pH, E_h, alkalinity, dissolved O_2, natural organic matter (NOM) content, ionic strength, concentrations of major and trace ions) of a system is crucial to predicting the formation and fate of NPs. Because NPs require specific conditions for formation, changing one variable can dramatically alter stability. For example, since clay NNPs typically have a negative surface charge, the concentration of cations affects their tendency to remain suspended versus aggregating and settling out of the water column.[22] This poses a problem for sampling, since taking a sample out of an open aquatic system alone can alter the NPs of interest within the water.[20] The effects of sample storage on NPs in natural waters are unknown. Development of standard sampling and handling procedures is an area of need for future studies on NPs in natural waters. Theoretical mechanisms of NP stability are discussed further below.

1.2 Historical Development of Environmental NP Research

Although NPs are ubiquitous in the environment, much of their behavior and roles in environmental processes has only become recognized in the last 20 years due to recent advancements in analytical techniques.[12–14] Nanogeoscience is a relatively new field that emerged from environmental colloid chemistry. Colloids are defined as particles less than 1 μm in size, including nanoscale particles.

The foundations of environmental colloid chemistry began in soil science over 100 years ago when surface-reactive phases such as $Al(OH)_3$, $Fe(OH)_3$, and SiO_2 were discovered.[20,22]

Evidence for charged soil colloids then emerged in the 1920's and 1930's. Later in the 1970's, colloidal systems in natural waters were studied by atmospheric scientists and wastewater engineers. It was in this period that the term colloid was coined. Finally in the 1990's, NPs began to receive their own attention separate from larger colloidal particles. Initial growth in the field was slow, partly due to the analytical challenge of accurately separating and characterizing these small particles.[22,25] The traditional use of "dissolved" and "particulate" water fractions in field studies was also a detriment to understanding colloids in natural waters. These are operationally defined fractions, where any components that are able to pass through a 0.45 (or another size < 0.8) µm filter are considered "dissolved", whereas anything that is excluded is considered "particulate". Since these definitions are in the middle of the size regime of colloids, their use can inadvertently allow small colloids and NPs in the "dissolved" fraction. This can result in inaccurate assumptions about the water chemistry, since the behavior of small colloids and NPs is fundamentally different than truly dissolved species.

Interest in colloids grew when it was discovered that they can drastically alter the fate and transport of pollutants in water systems.[13,14,20,25–27] Colloids typically have high surface reactivity, which can cause them to sorb or engage in redox reactions with metal and organic pollutants. The colloids themselves may remain suspended in the water column, settle out, or interact with the soil. This complicates modelling predictions of the eventual fate of ground and surface water pollutants. In some environments, this type of sorption can be significant. In the San Joaquin basin for example, 99% of the Al present in the water is colloidally bound.[14]

The existence of NPs complicates our understanding of mineralogy, since a mineral is normally defined as a crystalline substance with a characteristic, and defined chemical composition.[12] NPs often are not truly crystalline and the size-dependent properties complicate their characterization. Minerals existing in the nano size regime exhibit differences in surface structure, topography, and crystal shape. Hochella, et al. have proposed a differentiation between two types of NPs in mineralogy.[12] Minerals that only exist in the nano size range are termed "nanominerals", whereas "mineral NPs" can also occur in both nano and bulk size dimensions.

1.3 Properties of NPs

NPs have attracted interest due to their unique size-related properties.[12,13] While this has led to exciting innovations in ENP synthesis and applications, the focus of this review will be on those size-dependent properties relevant to environmental behavior. At the nanoscale, chemical

properties are different from the bulk material and vary with size.[12] For example, sphalerite (ZnS) has a different atomic structure at the nanoscale than in the bulk.[28] For this reason, it has been suggested that instead of an arbitrary cap at 100 nm, the upper limit of the NP size range be defined based on where properties no longer differ from the bulk material.[12] This would require developing a NP definition specific to every material of interest. In practice, the 1-100 nm definition is most used and 100-200+ nm particles are often included as well.

Size distribution is always a key aspect of NP studies because of its importance for governing surface area (surface/volume ratio decreases with size),[29] adsorption capacity,[15] and circulation in natural waters.[22] Mean and median particle sizes and the width of the distribution depend on the source, composition, aggregation state, and age of the NPs. For example, NPs resulting from rock weathering often have a very wide size distribution, but NPs developing from crystal growth typically have a narrow size distribution. NP sizes are thought to follow Pareto's Law, which is a mathematical power law stating that the number concentration of particles increases logarithmically with decreasing particle size.[20,22] This implies that there are far more small particles than large particles in the environment. Pareto's Law was developed from observations by aerosol physicists and oceanographers in the 1970's on particles > 1 μm in diameter. Although there are fewer studies investigating its applicability to submicron particles, evidence so far suggests that it is also valid for NPs.

Surface charge is a crucial consideration of environmental NP studies due to its influence on stability and aggregation[29] as well as interactions with other substances.[22] Surface charge is produced by chemical reactions, lattice imperfections, and dissolved ion adsorption. Many NNPs are negatively charged in circumneutral waters, but surface charge cannot be assumed constant, as mineral NPs often have variable surface charge as a function of pH due to protonation and deprotonation of hydroxyl surface groups.[30] NPs in natural waters are often coated by NOM, which is thought to have a stabilizing effect via charge repulsion (produced by carboxylic acid functional groups) and steric interactions.[20,22] However, these phenomena vary across the NOM subclasses. For example, humic-like NOM and rigid polysaccharide fibrils can have opposite effects on stability.[20]

The surface reactivity of NPs can control the distribution of ions and pollutants in the environment.[13,14,19,26,27] Mineral NPs have many sorption sites available for Ni, Co, Pb, Cr, Se, Cd, U, Zn, As, and P. NPs can affect the fate and transport of organic pollutants via sorption and

redox active NP surface groups may alter the speciation and behavior of many dissolved constituents. This may subsequently have ramifications for environmental toxicity of pollutants.

1.4 Stability of NPs

NPs are inherently unstable and susceptible to aggregation, dissolution, and chemical transformations that arise from shifts in water chemistry and physical conditions.[20,22] Like any other colloidal system, NP suspensions tend toward a state of minimized interfacial contact area between phases.[29] In other words, a NP dispersion is thermodynamically unfavorable but surface chemistry effects can impose kinetic stability upon the system, thereby preventing NP aggregation and settling. NP stability, viewed as the total free energy of interaction between two particles, is the sum of the attractive and repulsive energy forces acting upon particle surfaces. This includes van der Waals attraction and electrostatic interactions, but electrostatic forces contribute the most to the total free energy of interaction.

NP stability is promoted by conditions that cause repulsion between particles.[29] Mechanisms for repulsion can be electrostatic, resulting from surface charge, or steric, where the presence of large surface groups spatially inhibits aggregation. In natural waters, the adsorption of NOM typically works to prevent aggregation by steric inhibition.[31–33] Surface charge is determined by both the NP material and the solution chemistry and often varies with pH. Additionally, the ionic strength of the water affects the electrostatic double layer (EDL) that surrounds each NP. The EDL concept is used to describe the ion cloud surrounding charged particles. Ions with the opposite charge of the particle surface inhabit the area closest to the particle, known as the Stern layer. Outside this is the diffuse layer, where a charge excess exists which can be described by Boltzmann's distribution. The nature of the EDL is a crucial factor determining whether NP stability or aggregation is promoted in the system. Particles will be very susceptible to aggregation when surface charge is near zero and the EDL is small. Electrostatic sorption of ions compresses the EDL and makes aggregation favorable. Therefore, an overall increase in ionic strength provokes aggregation. Specific (chemical) adsorption, however, can either increase or decrease surface charge and subsequently promote or prevent aggregation.[34] More detailed discussion of NP stability is presented in Chapters 3 and 4 in the context of the relevant research projects.

1.5 Nanometrology and Single Particle ICP-MS

NP behavior can be explored experimentally with numerous analytical tools, though many do not perform well with complex, environmentally relevant matrices.[8,13,18,35,36] Current tools can determine size distribution, number concentrations, shape, surface charge, and chemical composition, but most instrumentation can only determine 1-2 of these attributes. For brevity, only the techniques relevant to this dissertation research will be summarized here. Electron microscopy (EM) can yield size, shape, as well as number, but translating the observation of NPs over area to a solution concentration is very time intensive.[8,37] While scanning electron microscopy (SEM) can be useful, transmission electron microscopy (TEM) and scanning transmission electron microscopy (STEM) are ideal due to their very high resolution at the nanoscale.[13,38] Energy-dispersive X-ray spectroscopy (EDS) coupled with EM can additionally provide composition information and elemental mapping. Dynamic light scattering (DLS) is a very efficient means to determine NP size from their Brownian motion in suspension, but it is prone to artifacts in complex matrices and when analyzing NPs with high polydispersity (many different sizes).[8] Optical particle sensing provides particle number concentrations and sizes, but only for particles larger 0.5 µm or larger, making the technique more useful for studies on colloids than NPs.

Single particle inductively coupled plasma-mass spectrometry (spICP-MS) merits further explanation due to its importance to each of the projects described in this dissertation.[39,40] Standard mode ICP-MS quantifies an element in an aqueous sample by averaging its signal over the full scan time of data collection. When present only in a dissolved form, the element will generate a steady signal. Particulate samples, however, create a high intensity peak in the signal in proportion to the elemental mass of the particle, which is proportional to size. Given a big enough particle (size detection limit is dependent on the analytical sensitivity for the element of interest) in a dilute enough sample, this peak can be differentiated from the dissolved background and the integrated peak area can be used to determine NP size. Assuming particles are spherical and of known composition (element fraction and density), the corresponding NP size can be calculated for each peak.[41] Counting the peaks allows for the calculation of the sample's number concentration and binning them by size provides the NP number-based size distribution. Because of the element specificity and the low mass detection limit (parts per trillion) of ICP-MS, spICP-MS is a powerful tool that has revolutionized environmental NP

research. The challenges and latest advancements in spICP-MS instrumentation will be discussed further in the context of the research presented in subsequent chapters.

1.6 Motivation and Research Projects

The past decade has seen rapid advancement in environmental NP analysis and many questions in this field are being resolved. However, the majority of published articles are laboratory studies of NPs in artificial media, which are necessary for extracting mechanistic details but reveal little information about NPs in a true environmental system. One of the most challenging issues that prevails is the accurate measurement and characterization of NPs in collected environmental samples. SpICP-MS has been well validated for quantifying NPs in simple and carefully controlled media and shows promise for environmental analysis. This dissertation research focuses on applying spICP-MS to environmental samples and improving our knowledge of NPs in natural systems.

Chapter Two describes a study of sunscreen ENP release in recreational rivers over Labor Day weekend. The first year of sampling in this study examined oxybenzone and Ti-containing NPs in Clear Creek, Colorado with high frequency, automated sampling from September 2-9, 2016. This sampling campaign emphasized temporal variation in order to investigate the variability of sunscreen chemicals and metal NPs during and outside of recreational stream use. The results demonstrate the difficulty of achieving representative sampling and establishing background in a natural system with poorly dispersed NPs.

The second sampling campaign was conducted at three streams simultaneously on September 4-6, 2017, including Clear Creek, Colorado, Salt River, Arizona, and Truckee River, Nevada. The diurnal cycling of sunscreen chemicals and metal NPs previously observed in Clear Creek was reproduced in both Clear Creek and additionally observed in Salt River and, to some extent, Truckee River. The differing water composition, discharge levels, and recreational use of the three streams created situations of varying ENP detectability. Although no ENPs could be conclusively identified in TEM imaging, spICP-MS measured perturbations to the NP populations during recreation.

The multi-site Labor Day sampling campaign was designed and carried out in collaboration with Dr. Paul Westerhoff and Dr. Yuqiang Bi at Arizona State University, and Dr. David Hanigan and Andy Pousti at University of Nevada Reno. Dr. Anthony Bednar at U.S. Army Corps of Engineers was a collaborator in both the 2016 and 2017 sampling campaigns.

The manuscript of this study is not yet submitted for publication and permission for use in this thesis has been obtained from all co-authors.

A study of changes to the Fe-oxide INP population and stability in the North Fork of Clear Creek (NFCC), a mining-impacted stream, is detailed in Chapter Three. In this research, aggregated Fe INPs that had accumulated over many years of AMD release to NFCC were examined using multiple NP measurement techniques before and during remediation of the stream. Changes in the stream INP concentrations were correlated to shifts in water chemistry using multivariate statistical analyses. Comparisons of the aggregation rates to INP surface charge were made using a model Fe INP suspended in filtered NFCC waters collected during the initial stages of remediation. The results indicate a rapid decrease in Fe INP concentrations with treatment that was accompanied by an increase in stability. The transition from an unstable to a stable system occurred along a gradient of decreasing conductivity (a proxy for ionic strength), increasing pH, and increasing dissolved organic carbon concentrations, with conductivity being the most statistically significant predictor of NP behavior. These outcomes are in good agreement with expectations from surface chemistry theory and prior knowledge of AMD INPs, and the study results advance the current state of knowledge of AMD INP behavior during remediation. Additionally, the novel application of spICP-MS to examine AMD INPs in-stream is successfully demonstrated, with accompanying discussion regarding its limitations. This work is in review at the journal *Environmental Science & Technology* and reproduced in this thesis with copyright permission.

The final project of the dissertation research is described in Chapter Four, regarding the ability to measure NP aggregates using spICP-MS with different mass analyzers. Because aggregation of released ENPs is likely to occur in the environment, the ability to quantify aggregates using spICP-MS would greatly advance the applicability of the technique to environmental studies. Most ICP-MS instruments use a quadrupole mass analyzer, but instruments have also been developed to have high resolution (HR) using a magnetic sector or the ability to measure multiple elements near-simultaneously with a time-of-flight (TOF) mass analyzer. The advantages and disadvantages of these instruments for measuring size and concentration of aggregated CeO_2, goethite, and kaolinite NPs was examined with the intent of developing methods to determine the extent of NP aggregation. Non-uniformity of NP pulses measured per second of analysis time, as well as shifts in the size distributions, were found to be

potentially useful indicators of aggregation. However, attempts to quantify heteroaggregation of NPs with the multi-element capability of TOF were less successful due to the higher size detection limits of that instrument.

While further work will be needed to perfect the use of spICP-MS in environmental NP investigations, the projects comprising this Ph.D. thesis are an important contribution to this research area and signify an advance in analytical capabilities.

CHAPTER TWO

QUANTIFYING TEMPORAL AND GEOGRAPHIC VARIATION IN SUNSCREEN AND MINERALOGIC TITANIUM-CONTAINING NANOPARTICLES IN THREE RIVERS DURING RECREATIONAL WATER USE

L.N. Rand,[1*] Y. Bi,[2] A. Poustie,[3] A.J. Bednar,[4] D.J. Hanigan,[3] P. Westerhoff,[2] J.F. Ranville[1]

2.1 Background and Previous Studies

TiO_2 and ZnO engineered nanoparticles (ENPs) are effective UV filters[42–44] and their use in commercially available sunscreen products is increasing, generating research into the life cycle and release of these products.[45–48] The photocatalytic properties of TiO_2 easily lead to the production of reactive oxygen species, causing toxicity via inflammogenic, oxidative, and genotoxic effects.[48–51] TiO_2 toxicity has been found to increase with decreasing size, implying particularly detrimental effects from nanoscale particles.[49,51] To mitigate this toxicity for use in sunscreens, TiO_2 ENPs are surface coated with Al oxide, Si oxide, organic polymers, or some combination thereof.[49] These surface coatings additionally aid in keeping the ENPs dispersed throughout the lotion and upon application to skin. However, the surface coatings have been shown to readily break down upon release to environmental media.[47,52] The rate and extent to which the coating degradation occurs would vary depending on the specific product formulation and environmental conditions, but loss of protective coatings is likely and could result in ecotoxicity. This motivates research into the fate and transport of these sunscreen ENPs upon environmental release.

Increasing prevalence of ENPs in consumer products has generated research into environmental release and fate of a broad range of ENPs.[2–11]Various research studies have attempted to examine release of sunscreen ENPs to natural water bodies as a result of recreational activities.[53–56] In scenarios involving expected sunscreen release into a natural water body, it proves very challenging to determine whether Zn or Ti detected is anthropogenic.[54–56] This is a direct consequence of the presence of natural nanoparticles (NNPs) containing these elements and the expected low amounts of ENPs released. A prior study of Clear Creek in

*Primary author, [1]Colorado School of Mines, [2]Arizona State University, [3]University of Nevada Reno, [4]U.S. Army Corps of Engineers

Golden, Colorado found that elevated Ti and oxybenzone concentrations did coincide with peak recreational activity.[55] However, simultaneous elevation of Fe and Al concentrations suggested that the Ti increase may result from natural particle resuspension from bed sediments. This is a consequence of the very shallow depth (< 1 m) of Clear Creek, and the fact that wading is a major activity. Additional evidence of resuspension came from the magnitude of the increase in Ti, which was roughly an order of magnitude higher than the oxybenzone concentrations.

A limitation of the prior ENP release studies is the reliance on total mass concentration measurements and lack of particle-specific analyses.[53–56] Regardless of the analytical method however, the ENP number or mass concentration must be high enough to generate a quantifiable signal within the sample measurement time. Most studies rely on some type of ICP-MS analysis for detecting ENPs.

Perhaps the most common analytical approach is to compare the sample mass concentration of the primary ENP element to that of a reference sample. In the prior Clear Creek study, this involved examining upstream samples as well as the samples from the recreational area.[55] This approach has been repeated in the current study. Unlike oxybenzone, Ti is present in the stream naturally and will thus be present in samples both upstream and downstream of recreation. In a study of CeO_2 ENPs, a single soil was spiked with CeO_2 and the results compared to the non-spiked soil.[57] This study quantified how much CeO_2 was needed to be detectable above the natural Ce level in that specific soil. Another approach is to compare the elemental ratios of mass concentrations.[17,36,54] The addition of an ENP containing a specific ratio of elements, if they are different than the NNPs present in the reference, should result in a change in the element ratio of the sample containing ENPs.

Alternatively, ENPs may be observed directly with a particle-specific analysis technique, rather than inferred from total mass concentrations.[8,18,40] This could be the detection by ICP-MS in single particle mode of a uniquely-sized particle or the observation by electron microscopy (EM) of a unique morphology that is characteristic of the ENP. Single particle ICP-MS (spICP-MS) is especially useful because it can rapidly determine nanoparticle (NP) number concentrations and size distributions in addition to the total mass concentration for the element of interest in the sample.[39,40] An ENP input to a natural water could be detectable using this method based on changes to the number concentration or size distribution of NNPs in the reference sample.

As a NP suspension is ablated in the plasma during spICP-MS analysis, dissolved species generate a stream of ions that the detector registers as a steady signal, while NP species generate a packet of ions that produce a brief, high intensity pulse.[39,40] The NP pulses are separated from the background signal (either by manually setting a threshold or using a 5σ statistical algorithm to filter the data), integrated, and counted. The integrated peaks can be converted from signal intensity to NP sizes if the elemental composition and density of the NP, as well as the percentage of sample uptake to the plasma (referred to as transport efficiency), are known.[41] These calculations assume that the NPs analyzed are spherical. The technique is challenging to apply to samples with high dissolved concentrations or complex matrices that result in a high background signal.[58,59] Additionally, the assumptions regarding elemental composition can result in experimental artifacts when the actual composition of the sample NPs is unknown. This limitation may be overcome with the development of multi-element detection capabilities (time-of-flight and dual element quadrupole mass analyzers), but such instrumentation is not widely available. Nevertheless, spICP-MS has revolutionized NP studies due to its ability to generate element specific size distributions at very low (ng L^{-1}) concentrations.

The use of EM allows for detailed characterization of sample NPs, including size, number, morphology, and even elemental composition if coupled with energy-dispersive x-ray spectroscopy (EDS).[8,37] Visualization of NPs is best done with transmission EM (TEM), which has higher resolution than scanning EM (SEM).[13,38] The major drawback to using EM is the time and labor required to examine enough NPs under the microscope for an accurate size distribution and number concentration. Additionally, drying the NPs and examining them under vacuum may produce artifacts for aqueous NP suspensions. However, it can be the most accurate and provide the most NP characterization information in samples of unknown compositions. For the analysis of ENPs in natural waters, an increase in the number of ENPs identified by their characteristic morphology or elemental composition in the suspected anthropogenically impacted sample compared to the reference could be a means of detection and perhaps quantification.

Especially when a distinguishing ENP signature (specific size, elemental composition, and morphology) is lacking, all of these approaches rely on one major consideration: the need to know not just the concentrations and sizes of the NPs, but the variability within the sampling in order to detect a significant perturbation from background. For the most part, this has been minimally-investigated in prior research and the sampling is often infrequent and done without

replicates. Because the uncertainty of sample representativeness may be a serious concern, it has been chosen as the main focus of this study. Observing an elevated level of the NP-associated element, or change in elemental ratio, in any given sample as compared to a single sample of the reference is not sufficient. Concentrations in the sample of interest must significantly exceed the range of values observed in the to support the argument the ENPs are present. Although this is most apparent for ICP-MS analysis, it is true for EM measurements as well. In fact, due to the time investment of characterizing hundreds of NPs under the microscope, it may be more problematic in EM to assure that a statistically viable NP measurement is captured. Understanding these uncertainties is key to determining what amount of ENP input to natural systems would be detectable.

These questions motivated a follow-up study on sunscreen ENPs in Clear Creek, Colorado that would more heavily emphasize sampling variability and particle-specific methodology. Additionally, collaboration provided opportunity for sampling to be extended to two additional recreational streams: Truckee River in Reno, Nevada and Salt River near Phoenix, Arizona. The study was designed to investigate several sources of variation: temporal variations at different time scales (minutes, hours, days), sampling reproducibility, and geographic differences. This investigation was facilitated by proposing several hypotheses to be tested: 1) Ti and oxybenzone concentrations during periods of recreational activity are statistically different from naturally occurring background concentrations. 2) The elevated Ti observed during Clear Creek recreation also occurs in other streams with similar recreation use. 3) Ti increases associated with recreation are caused by the resuspension of bed sediments.

The approach for testing the first hypothesis, regarding differentiation between recreation and non-recreation concentrations, is to compare samples impacted by recreation with samples having little to no human impacts. The hypothesis would be supported if differences are observed in weekend versus weekday samples, as much greater recreation occurs on the weekends. Similarly, comparing samples collected in the morning, prior to people using the stream, and afternoon when people are observed in the stream would test the hypothesis. Differences between samples collected at a location downstream of human activity and samples from a location upstream of activity during recreation times would also support the hypothesis. Finally, taking samples a few minutes apart during the recreation times would provide an

uncertainty estimate on the measured Ti and oxybenzone concentrations during the times of recreation.

The second hypothesis, that other recreation-use streams will exhibit elevated Ti and oxybenzone during human activity, is tested by comparing measurements made simultaneously in several different streams. Days and times of recreation and non-recreation were examined, as well as comparison of background and impacted sites. This hypothesis is supported if multiple streams produce concentration differences during versus outside of recreation that exceed the uncertainties in the analysis.

The approach to test the final hypothesis, that elevated Ti results from bed sediment resuspension, is to characterize the NPs in recreation and non-recreation samples using spICP-MS and TEM-EDS. Bed sediment NPs would be expected to be larger than the NPs already suspended in the water column, so a shift in the size distribution toward larger Ti NP sizes would support this hypothesis. TEM-EDS may detect mineralogical or morphological differences in NPs from bed sediments, and the identification of TiO_2 ENPs from sunscreen may also be possible.

The use of total mass concentrations and particle-specific analyses together with sampling schemes that examine variability across different timescales and locations allows for a more comprehensive investigation than previous studies, and more certainty as to differentiating anthropogenic and natural signals.

2.2 Materials and Methods

This section describes the sampling procedures in the 2016 and 2017 sampling campaigns and the methodology used in all laboratory analyses.

2.2.1 2016 Sampling Protocols

Sampling of Clear Creek in Golden, Colorado was conducted from Friday September 2 to Friday September 9, 2016. Automated ISCO™ samplers were placed at the bridge site, 1.5 km upstream from the main recreational areas, and at the downstream site, just upstream of the beach where people using flotation tubes leave the creek (see map in Figure 2.1 on page 18). In the intermediate reaches of the stream, where the water is very shallow (< 1 m), wading is a popular activity. The ISCO™ samplers were programmed to withdraw samples at the variable intervals that are described subsequently. The sampler intake was positioned ~10 cm below the water surface. Water samples were stored in HDPE plastic bottles within the ISCO™ sampler

until being transferred into sample splits in HDPE bottles for refrigerated (4°C) storage and laboratory analyses.

Both ISCO™ samplers were programmed to take up samples at high, medium, and low frequency depending on the amount of recreation use in stream, with the goal of achieving better temporal resolution of chemical peaks associated with bathing. High frequency sampling: during peak bathing periods (2-5 pm Saturday, Sunday, and Labor Day Monday), a 1 L sample was taken every 10 min. Medium frequency sampling: during daytime hours with no/low bathing on Saturday, Sunday, and Monday, a 1 L sample was taken from the creek every hour. Low frequency sampling: during Friday 9/2, at nighttime Saturday, Sunday, and Monday, and all day each of the following weekdays, a 250 mL sample was withdrawn at every hour and combined with the next three 250 mL samples to make up 4-hour composite samples that were 1 L in size.

The bridge site was intended to serve as a reference and had been used in the previous study by Reed, et al.[55] However, in the 2016 study described here, many bathers were observed entering the creek directly above the bridge site during recreation times. This prompted the collection of additional grab samples on Saturday, Sunday, and Monday from a site 2 km upstream from the bridge site. These additional samples help to establish the natural background during recreation but provide limited temporal information. These samples are denoted as upstream (as opposed to bridge) samples.

2.2.2 2017 Sampling Protocols

This sampling campaign was designed to explore sampling reproducibility and geographic variability. Three locations were sampled simultaneously on Sunday September 3 through Wednesday September 6, 2017: Clear Creek, Colorado, Salt River, Arizona, and Truckee River, Nevada. All three streams are described later in section 2.3.1, with maps indicating the downstream (recreation) and upstream (reference) sampling sites at each. Water pH, conductivity, and alkalinity of the river water were measured on site during sampling.

Grab samples for metals and NPs analysis were collected in triplicate in 250-mL HDPE bottles. Sample times were at 8 am and 4 pm on each day of sampling, at both upstream and downstream locations. Grab samples for oxybenzone analysis were collected in triplicate, 500-mL amber glass bottles. Since prior results have shown no oxybenzone present at non-recreational times, samples were collected at 4 pm at only the downstream location.

At the 4 pm sampling times each day, the number of people currently in the water were counted at each river.

2.2.3 Sample Processing, Shipping, and Laboratory Analyses

In 2016, the 1-L samples collected by the ISCO samplers were transferred into the following sample splits: 500 mL into amber glass bottles for oxybenzone analysis, 10 mL into HDPE Falcon™ tubes for total metals analysis, and 250 mL HDPE bottles for NPs analysis and archiving. The subsequent storage, shipment, and analyses of these samples was identical to the 2017 campaign and is described below.

In 2017, all 250 mL grab samples for metals and NPs analysis were shipped to Colorado School of Mines in order to process and analyze them as soon as possible, generally within 24 hours of the final sample collection. Sample bottles were shaken, then 10 mL was poured into 15-mL Falcon™ tubes. Then 30 mL was withdrawn via polypropylene syringe and filtered through a 0.02 µm (Anotop) filter, discarding the first 20 mL and collecting the remaining 10 mL filtrate into a 15-mL Falcon™ tube. All samples were stored under refrigeration until shipment and/or analysis.

All 10 mL unfiltered and filtered sample splits were acidified with several drops of concentrated nitric acid prior to shipment at room temperature to the U.S. Army Corps of Engineers lab for total metals analysis. The metals concentrations were determined using ICP-AES or ICP-MS, as appropriate for expected concentration ranges, following EPA methods 6010C and 6020A.[60] These analyses were conducted using a PerkinElmer Optima 8300DV ICP-AES and a PerkinElmer NexION 300D ICP-MS with NIST-traceable standards (SPEX CertiPrep and CPI International). Quality control utilized Sc, Ge, Y, Rh, Tb, and Hointernal standards, which were required to vary less than 15% during the analysis. Continuing calibration verification and independent second source verification standards were also analyzed regularly during each batch and each analyte was within 10% of the certified value.

The 500-mL samples for oxybenzone analysis were bubble-wrapped and shipped on ice overnight to the U.S. Army Corps of Engineers lab. Samples were first pre-concentrated by solid phase extraction, then analyzed for oxybenzone via high performance liquid chromatography (HPLC) with UV absorbance detection at 315 and 365 nm as described by Peck, et al.[61] This

analysis was carried out on an Agilent 1200 HPLC with a Phenomonex Synergi 4u Hydro-RP 80A column with standards purchased from U.S. Pharmacopeia.

Selected samples were shaken and analyzed for ^{49}Ti NPs using a PerkinElmer NEXIon 300D ICP-MS operated in single particle mode with 100-µs dwell times. The nano application module in the PerkinElmer Syngistix software determined the cutoff for separation of NP pulses from background signal via the 5σ statistical algorithm, calculated NP sizes assuming the mass and density of TiO_2, and generated NP number concentrations and size histograms.

The 2017 samples from Salt River, Truckee River, and Clear Creek downstream Monday afternoon (9/4/2017) were characterized for particle morphology, size, and elemental composition by TEM-EDS. After sonication for 30 min, 50 mL of collected river samples were directly centrifuged onto 200 mesh carbon type B (Ted Pella) TEM grid for 2 hours at ~3000 g as described previously.[62] TEM grids were placed on the flat bottom of 50 mL centrifuge tubes and a swinging bucket rotor was used (Eppendorf Centrifuge 5810). The applied centrifugation conditions were designed to result in a total removal of 20 nm sized particles from the water column of 5 cm height for 20 nm TiO_2 NPs. After the supernatant was poured off, the grids were collected and dried under ambient conditions. The TEM grids were washed afterwards in a drop of distilled water to remove the dissolved components. The TEM samples were then transported to ASU for analysis on a JEOL 2010F TEM operated at an acceleration voltage of 200 kV coupled with energy dispersive X-ray spectroscopy (EDS). The obtained TEM images were examined by ImageJ software for statistical analysis. The error bar of the particle size is reported as ± 1 standard deviation.

All statistical calculations on total mass and NP concentrations were carried out in OriginPro 2018, with the add-in app "Post-hoc Analysis for Non-parametric Tests".

2.3 Results and Discussion

The following sections describe the field observations from each sampling campaign and study site, the measured metal and oxybenzone concentrations, and results of the particle-specific analyses including spICP-MS and TEM.

2.3.1 Field Site Descriptions and Stream Characteristics

Clear Creek enters the town of Golden, Colorado from an alpine watershed. The section of the creek utilized for recreational bathing and tubing has been modified from its natural state, with areas lined by concrete. Large boulders have been placed to provide areas of fast water for

kayaking. Throughout the study area, there is a predominance of cobbles and coarse gravels among the bed sediments, with a low abundance of sand or fine sediment. Recreation use is very mixed, with many people tubing and wading as well as some kayaking. The stream depth is shallow (< 1 m) and discharge is low (~2 $m^3 s^{-1}$) under the baseflow conditions encountered during the study. However, summer thunderstorms can more than double the stream flow and the 2016 sampling campaign was affected by a storm that occurred the Thursday night before sampling began. This resulted in elevated streamflow that gradually returned to baseflow over the weekend (Figure 2.4a). Alkalinity in Clear Creek water is low, ~20 mg L^{-1} as $CaCO_3$, and there are moderately high levels of background metals (resulting in a typical conductivity of 200 µS cm^{-1}) due to extensive weathering of minerals and abandoned mines in the upper reaches of the watershed.

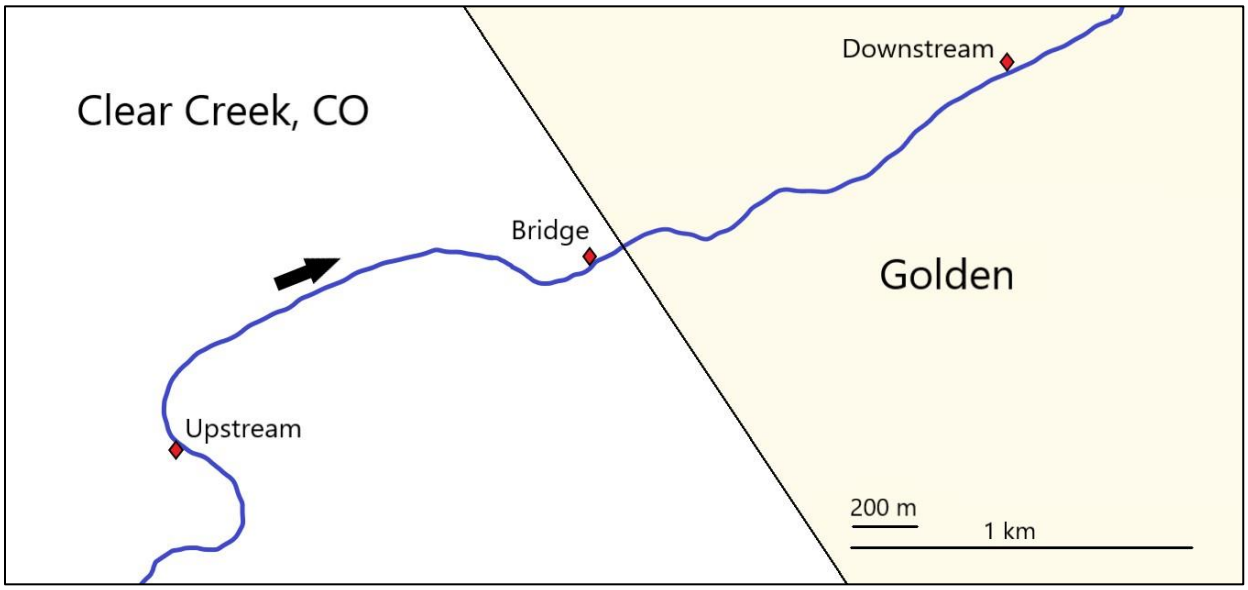

Figure 2.1 Site map of Clear Creek, Colorado showing upstream and downstream sampling locations (used both sampling years) and the bridge sampling location (used in 2016 only) and approximate city limit of Golden. The stream flows in the northeast direction, as indicated by the arrow.

Approximately 160 km east of Phoenix, the Salt River is formed by the confluence of the Black and White Rivers. The river flows west through a series of dams and reservoirs that provide water and power to the Phoenix metropolitan region. Recreation use at the Lower Salt River Recreation Area is almost entirely tubing. The river depth is similar to Clear Creek (~1.5

m) with a sandy bed. The average discharge is much higher (~30 m^3 s^{-1}) than the other stream systems in this study. The water chemistry of the Salt River is characterized by slightly high pH (7.69-8.11), high alkalinity (> 100 mg L^{-1} as $CaCO_3$) and high background metals and ionic strength resulting in typical conductivity readings of 1700 µS cm^{-1}.

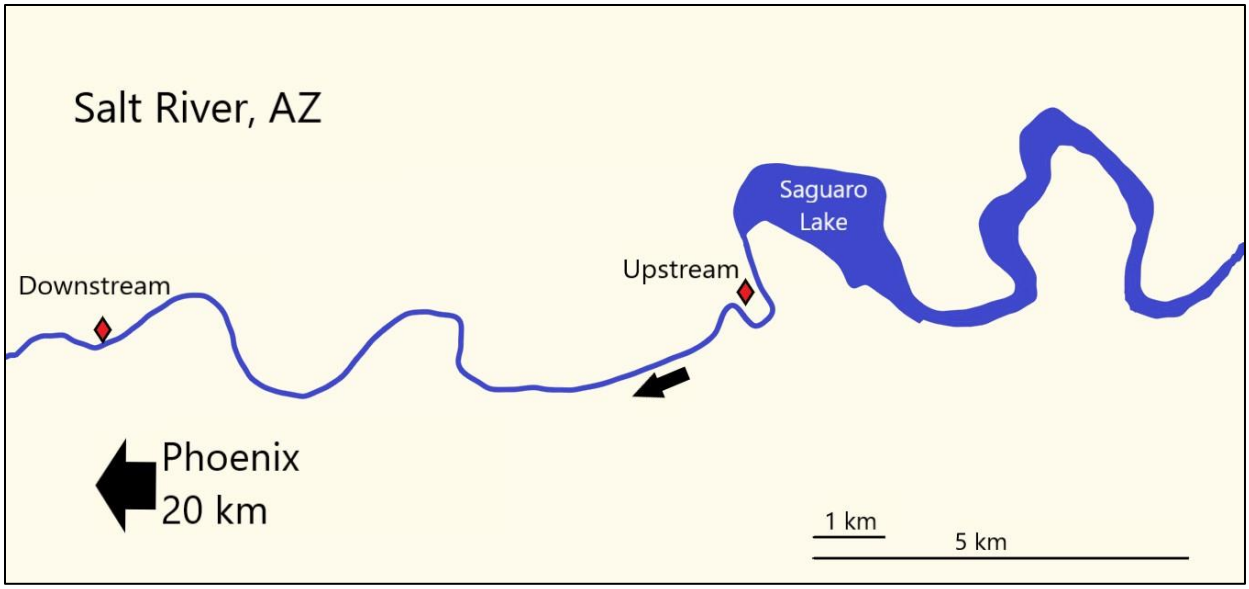

Figure 2.2 Site map of the Salt River, Arizona sampling locations in the 2017 sampling campaign. The upstream sampling location is ~1 km west of Saguaro Lake and the downstream location is approximately 20 km east from the city of Phoenix

Truckee River enters Reno, Nevada from the Sierra Nevada Mountains after originating from Lake Tahoe 76 km upstream. The stream section utilized recreationally in Reno has been completely reengineered as a kayaking and tubing park. Consequently, the stream bed is made up of concrete and large boulders and has little sediment. Recreation in Truckee River is shared between kayakers, tubers, and swimmers and Lake Tahoe is used for swimming and boating. The river depth of 1.4 m and discharge of 11 m^3 s^{-1} were higher than average during the study due to heavy precipitation that year. Alkalinity is moderate (40 mg L^{-1} $CaCO_3$) and the dissolved ion concentrations are low, producing conductivity readings around 90 µS cm^{-1}.

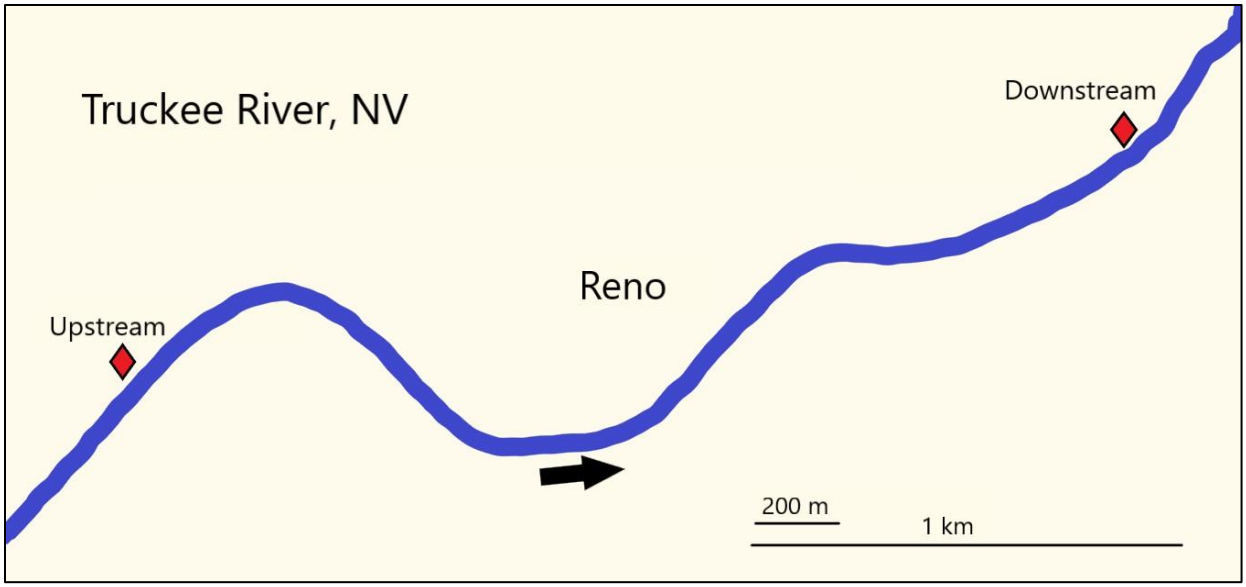

Figure 2.3 Sampling map of Truckee River in downtown Reno, Nevada. The river flows west to east with the upstream sampling site approximately 3 km from the downstream site.

2.3.2 Temporal Variability of Metal and Oxybenzone Concentrations

The diurnal variations of Ti and Al mass concentrations that were observed at an hourly frequency by Reed, et al.[55] were reproduced in both the 2016 and 2017 sampling years in Clear Creek (Figures 2.4 on page 21, 2.5 on page 22, 2.7 on page 28). In contrast there is no evidence of diurnal variation in Na and Ca (Figure 2.4 on page 21). In 2016, a higher background of Ti and Al was noticeable outside recreation periods in the first few days of the study (Figure 2.5 on page 22). This is likely related to a storm which occurred immediately prior to the study and caused the mean daily discharge to increase to 4 m^3 s^{-1} on Thursday August 31 and gradually return to 2.5 m^3 s^{-1} over the following week. This storm likely flushed additional sediments into the creek, resulting in higher concentrations of natural particulate metals, as has been seen in other field studies.[63] Even with this higher background however, samples collected downstream during recreation (2-5 pm on Saturday, Sunday, and Labor Day Monday) contained Ti and Al at as much as three times their morning concentrations. Simultaneous increases in oxybenzone concentrations were observed during recreation, whereas most oxybenzone measurements outside of recreational hours were below the detection limit. Greater than 50% of the oxybenzone samples were lost due to bottle breakage during shipment to the U.S. Army Corps of Engineers lab, resulting in fewer oxybenzone observations than for metals concentrations.

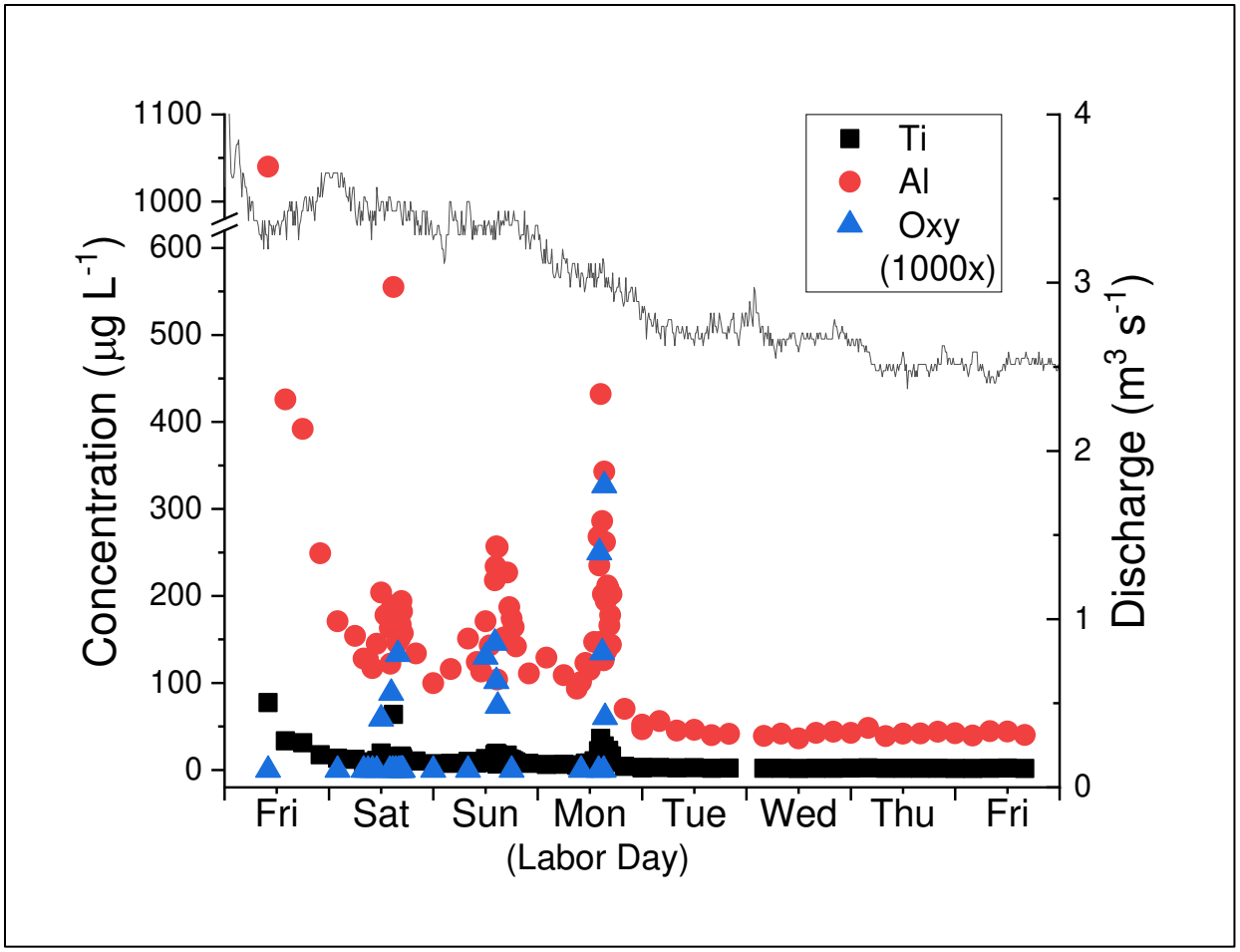

Figure 2.4 Downstream unfiltered concentrations of Ti (black squares), Al (red circles), and oxybenzone (blue triangles) and USGS flow rates measured at 15-min intervals (black line, right y-axis) in Clear Creek 9/2 – 9/9/2016. Oxybenzone data are shown at 1000 times the measured concentrations for ease of comparison to metals concentrations. The weekend metal concentrations were affected by a storm at the beginning of the study.

The collected data were analyzed at various temporal scales (Figure 2.6 on page 26) to answer several questions as to the impact of variability on the results of any given measurement. To do this assessment the downstream data are grouped by site, day, and recreation use. Because of differences between morning and afternoon samples over the weekend, comparing data on a daily basis is clearly not sufficient. The recreation periods were defined as 2-5 pm Saturday, Sunday, and Monday based on the times that most people were observed entering the stream. The bridge data, which included human impacts during recreation, are in two groups: “all bridge” and “bridge without both Friday and recreation”. The “bridge without Friday and recreation” group includes all the bridge data except those collected on Friday 9/2 (to avoid the

immediate effects of the storm) and the recreation times in attempt to establish a control group with a large sample size. The upstream data (all during recreation) are shown as a single group.

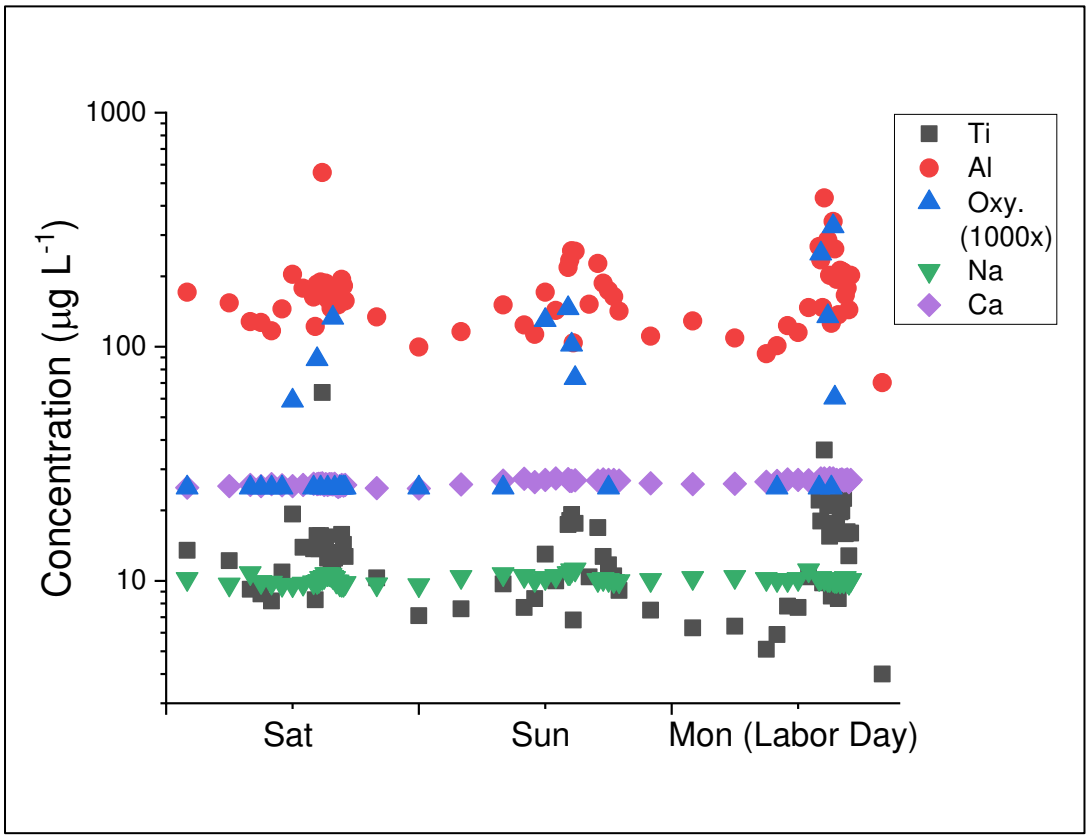

Figure 2.5 Downstream Clear Creek 2016 unfiltered concentrations of Ti (black squares), Al (red circles), oxybenzone (blue triangles), Na (green inverse triangles), and Ca (violet diamonds) over the holiday weekend, log scale. Oxybenzone data are shown at 1000 times the measured concentrations for ease of comparison to metals concentrations. Samples with no detected oxybenzone are shown at half the detection limit. Diurnal cycling during recreation is only visible for metals that are particle-associated, rather than dissolved.

The Friday Ti and Al mass concentrations are extremely elevated and have a wide distribution width, resulting from the sharp decrease over the day (Figure 2.5). As Friday was cool and overcast, and no bathers were observed in the stream, the elevated Ti and Al were likely produced by the storm on the previous day. On 9/2, the median (shown as the middle line in the Figure 2.6 boxes on page 26) was 32 and 400 µg L^{-1} for Ti and Al, respectively. The mean for non-recreation periods decreases steadily to below 10 and 200 µg L^{-1} for Ti and Al over Saturday, Sunday, and Monday.

Several bathers were present during the early afternoon samples that were included in the Saturday, Sunday, and Monday non-recreation groups. This would account for the occasional

elevated oxybenzone and may have impacted the Ti and Al during those times as well. However, the storm preceding the study could be largely responsible for the higher Ti and Al signal in the weekend (9/3-9/5) non-recreation times. The decreasing discharge shown in the hydrograph in Figure 2.5 on page 22 suggests that the stream did not return to normal flow conditions until the middle of the following week. The gradual decrease in non-recreation Ti levels over the weekend tracks with this decrease in discharge, supporting that it could be a lingering by-product of the storm.

Statistical analyses ($\alpha = 0.05$) were conducted to evaluate the differences between recreation and non-recreation periods at the downstream site as well as bridge and upstream site data. First, each group of data in Figure 2.6 on page 26 was tested for normality using the Shapiro-Wilk test. For Ti and Al, normality is rejected for "downstream Saturday recreation" and for both bridge groups. Most groups of oxybenzone data are either non-normal or do not have enough observations to test for normality. The oxybenzone data were not examined further due to the limitations of the small number of observations. The Ti groups were then tested for equivalence using Kruskal-Wallis ANOVA. The same was done for the grouped Al data. In both tests, the null hypothesis (that the Ti/Al groups come from the same population) was rejected. Dunn's test for equality of means was subsequently conducted to determine which groups differ significantly from one another. The analyses were repeated on Ti loads instead of concentrations and resulted no major changes (see Appendix A). The following discussion applies to both Al and Ti concentrations, as Dunn's test flagged the same groups in each dataset.

Major findings from the Dunn's test results (Table 2.1 on page 24) are that: a) the downstream Saturday and Sunday non-recreation groups are different from "downstream weekday non-recreation", b) the downstream Saturday, Sunday, and Monday recreation groups were each different from "downstream weekday non-recreation" and "bridge without Friday and recreation", and c) "downstream Monday recreation" differs from both "upstream recreation" and "downstream Monday non-recreation".

The significantly elevated Ti and Al in "downstream Monday during recreation" is strong evidence that recreation exerts an anthropogenic effect on particulate metal concentrations in Clear Creek. However, proving an anthropogenic effect on Saturday and Sunday afternoons is difficult due to the question of establishing a clear background signal from which to compare, which is a consequence of the storm-elevated background.

Table 2.1 Matrix of Dunn's Test p-values comparing Ti data grouped by sampling location, day, and recreation (R) versus non-recreation (NR). Significant p-values ($\alpha = 0.05$) are shaded green while results indicating non-significant p-values are shaded yellow.

			Downstream								Bridge		Upstream
			Fri	Sat		Sun		Mon		Wkdy	All	No Fri	All
			NR	NR	R	NR	R	NR	R	NR	All	NR	R
Downstream	Fri	NR		1	1	0.337	1	0.0372	1	6.26E-07	0.277	0.00255	0.0710
	Sat	NR	1		1	1	1	1	1	2.38E-05	1	0.288	1
		R	1	1		0.946	1	0.056	1	6.12E-13	0.181	7.73E-06	0.201
	Sun	NR	0.337	1	0.946		1	1	0.115	0.00257	1	1	1
		R	1	1	1	1		0.222	1	1.35E-07	1	0.00609	0.434
	Mon	NR	0.0372	1	0.0563	1	0.222		0.00521	0.758	1	1	1
		R	1	1	1	0.115	1	0.00521		1.20E-15	0.00428	3.99E-08	0.0328
	Wkdy	NR	6.26E-07	2.38E-05	6.12E-13	0.00257	1.35E-07	0.758	1.20E-15		2.23E-11	5.87E-03	1
Bridge	All	All	0.277	1	0.181	1	1	1	0.00428	2.23E-11		0.00308	1
	No Fri	NR	0.00255	0.288	7.73E-06	1	0.00609	1	3.99E-08	0.00587	0.00308		1
Upstream	All	R	0.0710	1	0.201	1	0.434	1	0.0328	1	1	1	

The downstream Saturday, Sunday, and Monday non-recreation samples were intended to serve as a baseline from which to compare the recreation samples collected on the same day. Although recreation did result in elevated Ti and Al, the differences between same-day recreation and non-recreation are only enough to be statistically significant on Monday. The storm may be partially responsible for the difficulty in discerning a difference between same-day recreation and non-recreation groups, since most non-recreation data were obtained in the morning before sampling and elevated natural Ti and Al from the storm would be expected to decrease alongside the discharge decrease over the course of each day. Additionally, some bathers entering the creek early could have caused some sediment resuspension before the main recreation time period.

The "downstream weekday non-recreation" group (whose samples were collected when the effects of the storm were more worn off) could be considered the true background, but it differs significantly from both non-recreation and recreation during the weekend. This makes it unsuitable as a control against which to measure recreation effects, but highlights the importance of the storm in affecting background concentration.

The upstream grab samples were collected during weekend recreation above all human activity in the creek, making them most representative of the natural background during recreation. As seen in Figure 2.6 on page 26, the "upstream" Ti and Al groups have narrow concentration ranges and no oxybenzone was detected. The Ti and Al medians in the "upstream" group are ~8 $\mu g\ L^{-1}$ and 110 $\mu g\ L^{-1}$, respectively, which is lower than "downstream Saturday non-recreation" and "downstream Sunday non-recreation", but not as low as "weekday non-recreation" Ti and Al. This could be because the upstream grab samples were collected when the stream had not yet recovered from the storm. The only group that "upstream" differs from significantly is "downstream Monday recreation".

Therefore, while there is strong statistical evidence of an anthropogenic effect on particulate metals on Monday afternoon, Saturday and Sunday are more uncertain. Clearly the definition of a background signal is important for gauging environmental contamination. When the background source is altered, either naturally (i.e. the storm preceding Friday) or unnaturally (i.e. bathers and tubers in the water near the bridge sampling location), it is more difficult to establish certainty in an anthropogenic effect.

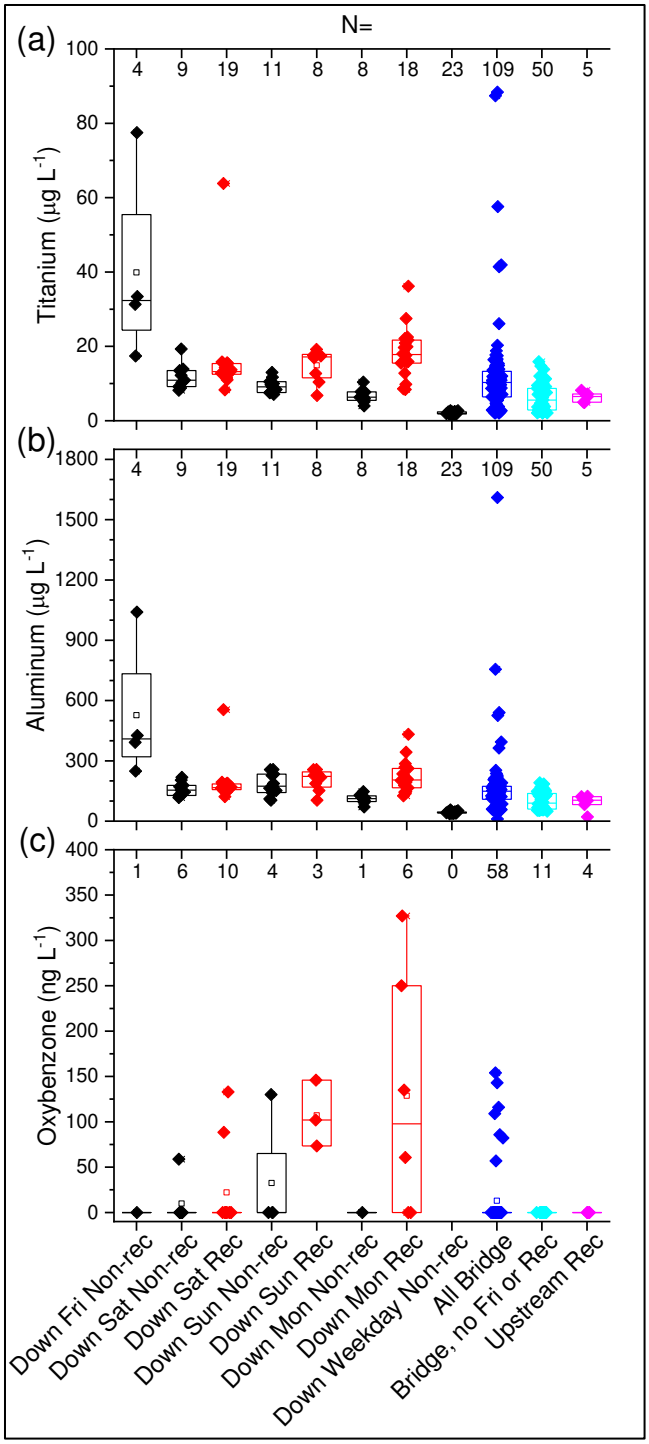

Figure 2.6 Ti (a), Al (b), and oxybenzone (c) concentrations from Labor Day week, 2016. Downstream data are grouped by day and recreation use at the time of sampling (black, non-recreation times; red, recreation times). Bridge data are grouped together (blue) and together minus Friday 9/2 and recreation times (cyan). Upstream data (magenta) include up to four samples collected Saturday, Sunday, and Monday only. Top x-axis indicates the number of observations in each group. "Downstream Monday recreation" is significantly different from "downstream Monday non-recreation" and "upstream recreation".

The high frequency automated sampling in 2016 showed a high degree of variability among the 10-min samples taken from Clear Creek during recreation hours. These groupings show wide ranges for Ti, Al, and oxybenzone levels during recreation (Figure 2.6 bright green, cyan, and olive series on page 26). While many samples within the recreation groups had elevated concentrations, many were similar to non-recreation times. Saturday, Sunday, and Monday non-recreation groups mostly had narrower ranges than the recreation groups. The distributions of the "downstream weekday non-recreation" data are particularly narrow, implying minimal natural variation occurred after the effects of the storm passed. Apart from Friday 9/2, the effects of human activity on Ti, Al, and oxybenzone concentrations appears to cause far more variation than is naturally present in the stream. Additionally, this variability between samples collected only 10 min apart from each other was only observed in concentrations of metals expected to be particle associated, while dissolved metals, such as Na and Ca, were nearly constant across the study and within recreation hours (Figure 2.5). A possible explanation is that the particles from recreation, either released ENPs or resuspended bed sediments, are poorly dispersed. The ramification of non-uniform NP dispersion is that grab samples are less likely to accurately represent the system. Some NPs may or may not be captured in a given sample and the sample NPs may not resemble the composition of that stream section as a whole. Future environmental NP studies attempting to capture accurate representations of a non-uniform stream particle population with high timescale resolution should consider integrated sampling methods. Although we did not investigate small-scale spatial variability at any specific site, future studies should consider examining samples of discharge-weighted volume and integrated across multiple lengths and depths of the stream cross section.

2.3.3 Geographic Variability of Metal and Oxybenzone Concentrations

Data were collected at the three streams described in section 2.3.1 to investigate the third hypothesis that multiple recreational use water systems will show similar concentration trends during recreation. The recreation-associated elevation of Ti and oxybenzone observed in Clear Creek was also visible multiple rivers in the 2017 sampling (Figure 2.7 on page 28). Of the three streams, Clear Creek exhibited the highest peaks in oxybenzone and Ti. Clear Creek oxybenzone and Ti concentrations were higher on Sunday than Monday afternoon while Salt River's maximum oxybenzone concentrations occurred on Monday afternoon and maximum Ti concentrations occurred on Sunday afternoon. Elevated concentrations were not observed on

Tuesday or Wednesday, consistent with the low counts of people in the streams. Two people were observed in both Salt and Truckee Rivers at the time of sampling and no people were observed in Clear Creek on those days.

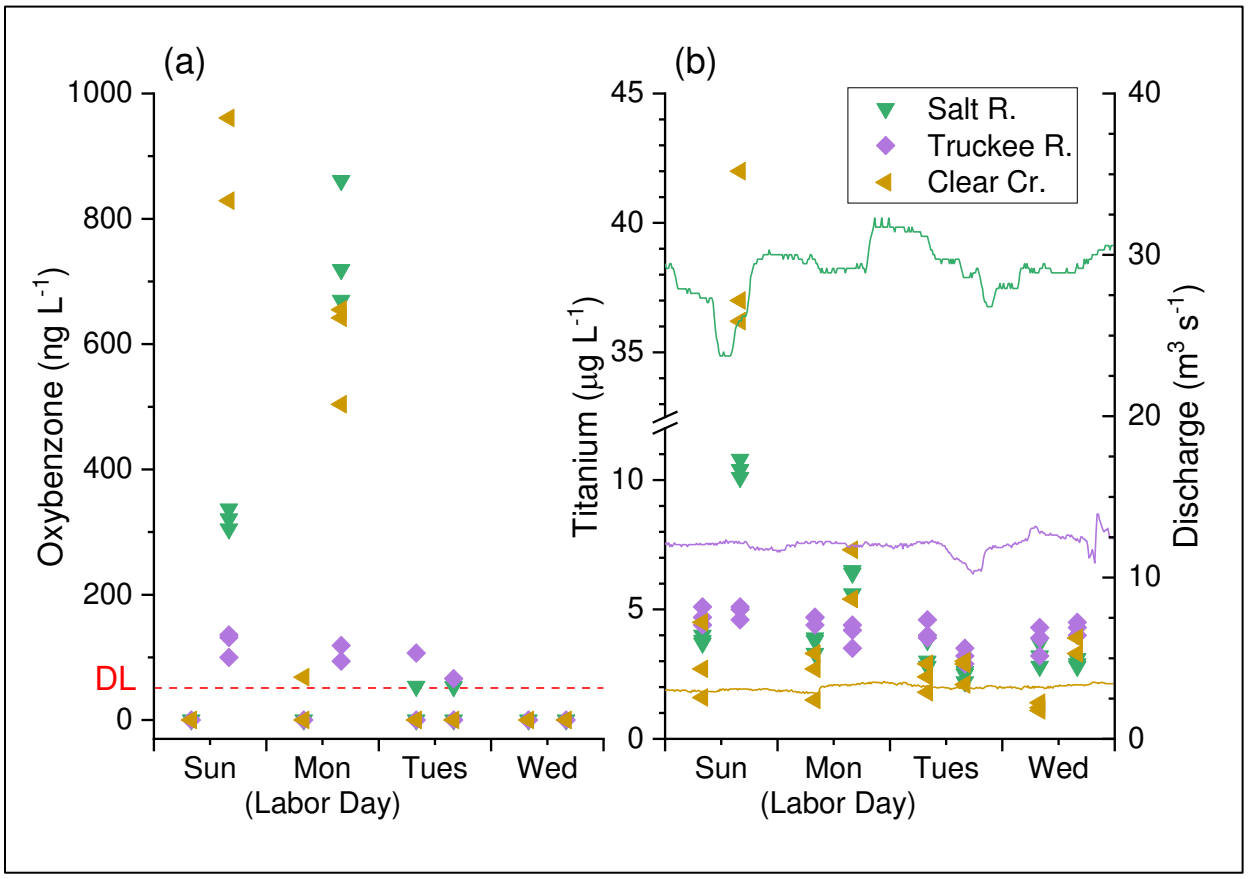

Figure 2.7 Downstream oxybenzone (a) and Ti (b) concentrations in the Salt River (green inverse triangles), Truckee River (violet diamonds), and Clear Creek (gold left triangles) during the week of Labor Day, 2017. The discharge of all three streams is shown in (b), right y-axis. Individual triplicates are shown at morning and evening sampling times. Oxybenzone was elevated during recreation (Sunday and Monday afternoons) in all three streams, but only just above the detection limit (DL) in Truckee River. Only Salt River and Clear Creek exhibited elevated Ti during recreation.

Truckee River's Ti and oxybenzone concentrations on Sunday and Monday were low relative to the other study sites, with oxybenzone only increasing just above the detection limit during recreation and no elevated Ti. The lack of change in Ti in Truckee River is unsurprising, given the evidence that the majority of the Ti measured in these studies is believed to be from sediment resuspension and Truckee's reengineered stream bed has resulted in very little loose bed sediment.

Due to the small sample sizes, comparing data grouped into separate days as was done in 2016 study was not possible for this dataset. Instead, the data for each river were grouped into a recreation versus non-recreation category and compared using a two-sample Kolmogorov-Smirnov test ($\alpha = 0.05$). The oxybenzone in all rivers, including Truckee, was significantly different in recreation versus non-recreation. The Ti concentrations, however, were significantly different during recreation only for Salt River and Clear Creek, not Truckee River.

The collection of triplicate samples in the multi-river study allowed for another examination of sampling variability. Moderate reproducibility within the triplicate samples was observed, with Ti relative standard deviations of 4-15% in Salt and Truckee Rivers and 8-50% in Clear Creek. The absolute standard deviation of the Ti triplicates is greater during recreation than non-recreation times in all streams. This finding, like the 2016 observations of recreation versus non-recreation measurements, suggests that Ti concentrations during human activity are more variable than the natural stream background.

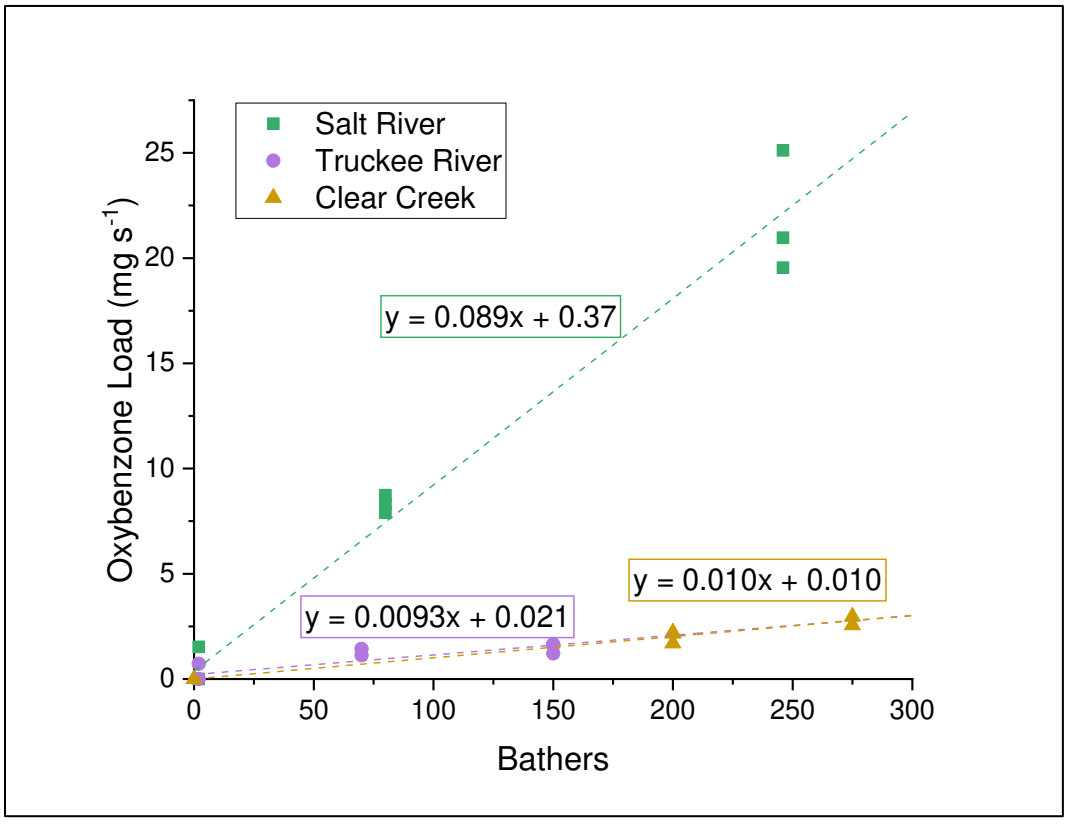

Figure 2.8 Downstream oxybenzone loads in Salt River (green squares), Truckee River (violet circles), and Clear Creek (gold triangles) as a function of the estimated number of bathers. The greatest amount of oxybenzone release was observed in the Salt River, especially on Monday, suggesting that Arizona bathers apply more sunscreen than at the other sites.

In all systems, the afternoon oxybenzone loads correlate with the amount of river use, as estimated by the bather counts (Figure 2.8 on page 29). However, the magnitude of oxybenzone release as a function of bathers is different for each river. Based on the linear regression slopes, Salt River, Truckee River, and Clear Creek each respectively had 89, 9.3, and 10 µg oxybenzone released per bather per second. The Truckee River and Clear Creek slopes are substantially lower than Salt River, but still statistically different from a slope of zero ($\alpha = 0.05$). This may suggest that bathers in Salt River apply much more sunscreen than in Truckee River and Clear Creek.

2.3.4 NP Size Distributions from spICP-MS

The preceding sections discuss using differences in concentration to detect the presence of anthropogenically-introduced NPs. One of the alternative approaches is to use spICP-MS to determine if the naturally occurring NP size distribution of the stream is perturbed by recreational activities. Two samples in the 2016 Labor Day Clear Creek study were selected for spICP-MS analysis: downstream 3:30 pm Sunday (recreation time/location) and bridge 12 am Sunday (non-recreation time/location). The mean sizes (computed as TiO_2) and NP number concentrations, respectively, were 86 nm and 1.4 x 10^5 particles mL^{-1}, and 80 nm and 1.5 x 10^5 particles mL^{-1}. The size distributions were examined using a two sample Kolmogorov-Smirnov test for equivalence ($\alpha = 0.05$), which found that they are not significantly different. In light of the discussion of total Ti and Al mass concentrations in section 2.3.3, which found Sunday recreation concentrations not to be significantly elevated and weekend non-recreation samples affected by a high background post-storm, it is unsurprising that the Ti NP population in these two samples do not appear significantly different.

In the 2017 three river study, Ti NPs in the triplicate samples collected downstream Sunday morning and afternoon, upstream Sunday morning and afternoon, and downstream Wednesday afternoon were analyzed with spICP-MS. Only the downstream Sunday afternoon samples were collected during recreation, so all others were expected to serve as controls and generate identical distributions of background-only NPs. For simplicity, only the downstream Sunday morning and afternoon spICP-MS results are shown in Figure 2.9 on page 31. All other size distributions are shown in Appendix A. The size distributions of each stream were tested for equivalency using one-way Kruskal-Wallis ANOVA, followed by Dunn's test for non-parametric pairwise comparison of means ($\alpha = 0.05$).

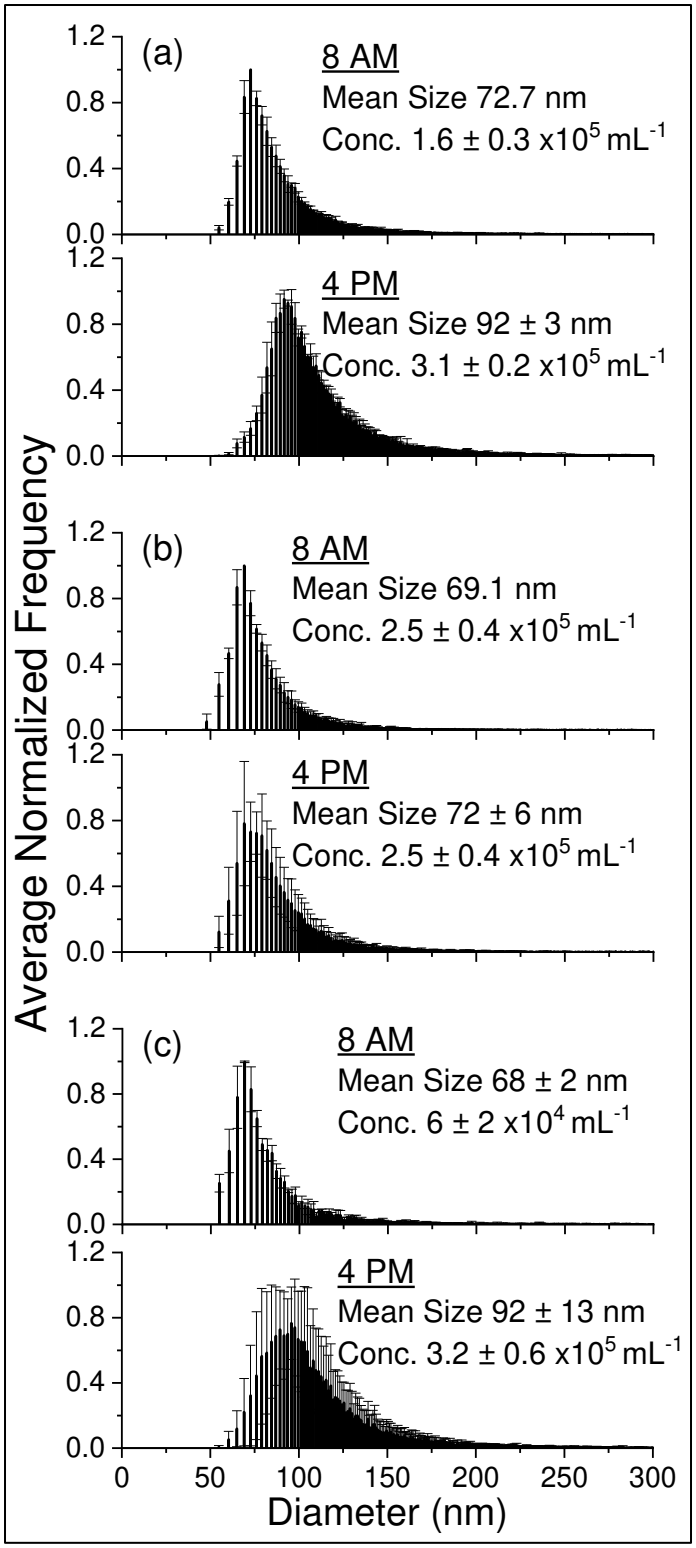

Figure 2.9 ^{49}Ti NP size distributions in (a) Salt River, Arizona, (b) Truckee River, Nevada, and (c) Clear Creek, Colorado in the morning (top graphs) and late afternoon (bottom graphs) on Sunday September 3, 2017. Changes to NP size distributions during afternoon recreation were only significant in Salt River and Clear Creek.

The mean size of downstream Salt River Ti NPs increased from 72.7 nm Sunday morning to 92 ± 3 nm during recreation (Figure 2.7a on page 31). Downstream Sunday NP concentrations also doubled, from 1.6 ± 0.3 to 3.1 ± 0.2 x 10^5 particles mL^{-1}. These NP distributions are significantly different from each other, suggesting that an increase in Ti NP size and concentration is statistically supported. However, all other samples expected to be background-only (and therefore identical) also differed from each other significantly (see Appendix A). A possible explanation is that the natural Ti NP population in the river is too variable outside of recreation use for an effect during recreation to be observable. This seems counter to the relatively consistent trends in Ti mass concentrations during and outside of recreation (Figure 2.5 on page 22), but those measurements with standard ICP-MS do not account for the number or size of particles making up the overall mass concentration.

The Truckee River Ti NPs were 69.1 nm downstream Sunday morning and 72 ± 6 nm Sunday evening, with a number concentration of 2.5 ± 0.4 x 10^5 particles mL^{-1} at both times (Figure 2.9b on page 31). These samples are statistically the same, as were the other samples from upstream Sunday morning and afternoon and downstream Wednesday afternoon. Consistent with the Ti mass concentrations observed (Figure 2.7b on page 28), recreation did not appear to affect particulate Ti in Truckee River.

Downstream Clear Creek Ti NPs increased from a mean size of 68 ± 2 nm Sunday morning to 92 ± 13 nm during afternoon recreation and the NP number concentration increased by an order of magnitude (Figure 2.9c on page 31). The difference between these two is statistically significant and in fact, the downstream Sunday afternoon sample was statistically different from all four background-only samples. This shows a change in the Ti NPs that only occurs during recreation, supporting the hypothesis of an anthropogenic effect.

2.3.5 TEM Characterization of NPs

The 2017 multi-river sampling campaign utilized TEM-EDS as a particle-specific analysis technique complimentary to spICP-MS. Due to the time requirements needed to generate quantitative (concentration and size distribution) data for the NP population of one sample, a comprehensive comparison between NPs during and outside of recreation (as was done using the other methods previously discussed) was not feasible. However, the in-depth characterization of individual NPs within a sample using this method can potentially allow identification of NNPs and ENPs.

An example NP visualized with TEM from each site is shown below in Figure 2.10. In the downstream Sunday samples from all three sites, the morphology of the inorganic particles were diverse and highly branched aggregates were often visible. Amorphous, sheet-like particles were commonly found in the mixture of particles of all three rivers. EDS showed the common presence of Si, Al, K, Fe, and Mn elements, suggesting that phyllosilicate clay minerals were the dominant mineral components of the collected particles. Several instances of amorphous SiO_2 were observed. The results agree with previous studies showing that most aquatic NNPs are composed of mixture of inorganic materials, mainly Fe and Mn oxides, and clays.[19] From their size, chemical composition, and morphology, these clay-rich nanophases are interpreted to most likely be (hydr)oxides, but further NP analysis with high-resolution TEM and selected-area electron diffraction would be needed for structure confirmation. No clear differences in mineralogy between three locations were found.

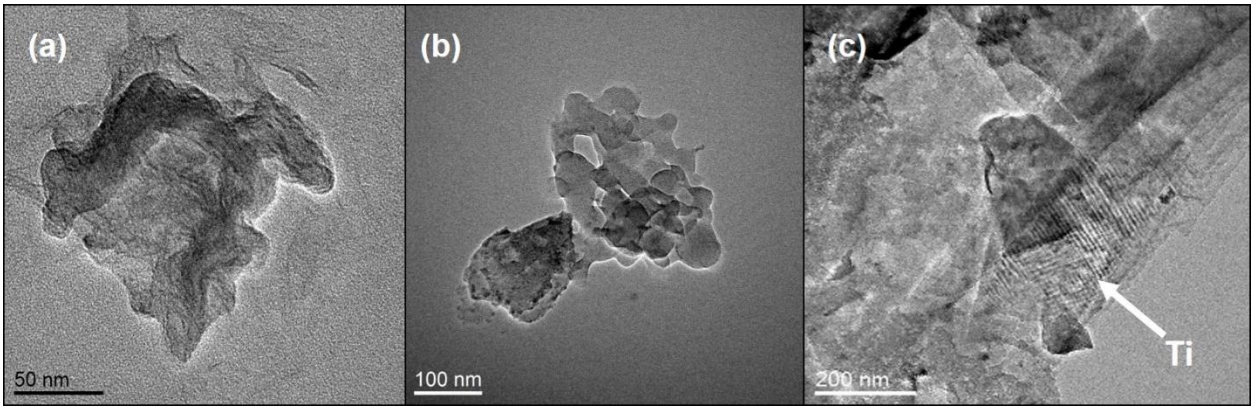

Figure 2.10 TEM images of NPs collected from (a) Salt River, Arizona, (b) Truckee River, Nevada, and (c) Clear Creek, Colorado. The NPs observed in all three rivers ranged from amorphous to crystalline and included both spheroids and sheets. Most Ti detected by EDS was present in trace amounts with clay and Fe oxide NPs.

In most cases, Ti was found coexisting with Fe oxides and clay NPs (Figure 2.10c). However, one instance of standalone TiO_2 was found in Clear Creek (Figure 2.11 on page 34). At 300 nm in one dimension and nearly 1 µm in another, it is significantly larger than the average Ti-containing NP size reported by spICP-MS. The spICP-MS sizes are likely underestimates because the equivalent TiO_2 size is calculated from Ti mass measured in individual NPs, which may often be present as a trace element of clay NP. It should be noted that this TEM technique is rather limited given the sampling size. While clay particles predominate

natural waters, as was represented in these TEM-EDS analyses, the comparatively few TiO_2 ENPs may not have been captured from 50 mL water sample. It is also possible that TiO_2 ENPs deposited on the TEM grids were not identified during the analysis due to the complexity of the particle mixture.

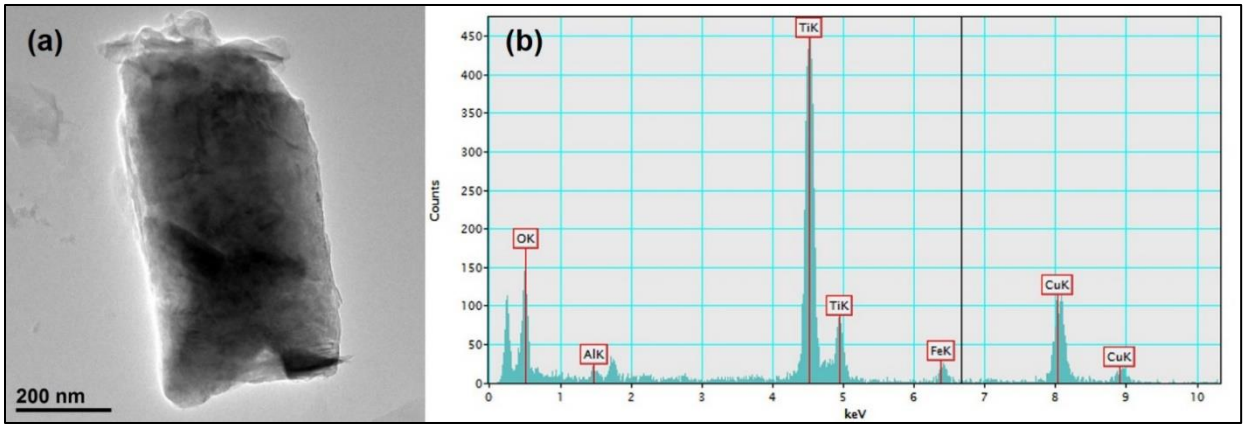

Figure 2.11 (a) TEM image and (b) EDS elemental spectrum of TiO_2 particle collected from Clear Creek, Colorado.

2.4 Conclusions

The hypothesis that Ti and oxybenzone concentrations during recreation differ from the natural background was supported by both 2016 and 2017 sampling campaigns. The data obtained in the 2016 Clear Creek sampling campaign, emphasizing temporal variability and sampling frequency, allowed day-by-day statistical analysis showing strong evidence of an anthropogenic effect during Labor Day Monday's recreation. While Saturday and Sunday afternoons were likely also affected, a higher non-recreation background likely resulting from a storm rendered it more difficult to differentiate recreation concentrations. This suggests the importance of determining background signal in future environmental NP studies in order for an ENP input to be observable. The wide range of concentrations measured in high frequency samples during recreation also casts doubt on the use of grab samples to represent an entire stream section. Future studies examining NPs within poorly dispersed systems should consider sampling schemes that integrate across multiple times, depths and widths in the stream cross section if an accurate snapshot of the stream section as a whole is desired.

The 2017 multi-river sampling campaign supported the second hypothesis that oxybenzone and particle-associated metals occur in multiple recreational stream systems. The

data collected during recreation showed significantly elevated concentrations of oxybenzone in all three rivers, and significantly elevated Ti in Salt River and Clear Creek, but not Truckee River. This further substantiates an anthropogenic effect on stream concentrations of oxybenzone and particle-associated metals, and that this could be generalizable to other recreational streams.

The final hypothesis that recreation is caused by the resuspension of bed sediments was evaluated using spICP-MS and TEM in addition to total mass concentrations. The lack of elevated Ti during recreation in Truckee River, which lacks bed sediments, supports that the strong Ti peaks that occur in the other two streams result from natural particle resuspension. The Clear Creek Ti spICP-MS sizes increased significantly and Ti number concentrations increased by an order of magnitude during recreation only, as would be expected from sediment resuspension. Salt River Ti NP sizes also increased and number concentrations doubled during recreation, but there were also significant differences between the four non-recreation samples analyzed. This demonstrates that high background variability can be problematic for detecting anthropogenic changes in single particle data, not just mass concentrations, and that establishing background needs to be emphasized with all methodology. Truckee River Ti NPs were statistically identical, showing little background variability but also no significant change during recreation. This is consistent with the previously discussed lack of change in Truckee River's Ti mass concentrations. Comparatively little information was gleaned from TEM, other than mineral NNP composition and confirmation of the lack of TiO_2 ENPs. Although EM is invaluable for a full NP characterization on a single particle basis, obtaining enough quantitative data for statistical testing proved to be much more useful in this study. SpICP-MS arguably combines the best of both analytical worlds by providing particle-specific quantitative data that lends itself well to statistical hypothesis testing.

CHAPTER THREE
CHARACTERISTICS AND STABILITY OF INCIDENTAL IRON OXIDE NANOPARTICLES DURING REMEDIATION OF A MINING-IMPACTED STREAM

Modified from the journal article submitted to *Environmental Science & Technology*.

Copyright 2019 American Chemical Society. Logan N. Rand*, James F. Ranville.

3.1 Background and Previous Studies

Acid mine drainage (AMD) generates elevated metal concentrations that can pose long-term ecotoxicological and public health risks.[64–72] This study provides insights into the processes of stream recovery that follow the remediation of AMD inputs. Fe- and Al-oxides, formed by AMD, are commonly nanoparticulate (< 100 nm) but rapidly aggregate and settle in receiving streams.[4,13,19,24] AMD-generated nanoparticles (NPs) are classified as incidental NPs (INPs) as they form as an unintentional byproduct of mining activities.[5,10] There are few instances of *in situ* examination of INP behavior in natural waters.[12,14,19,24,26,31,33,34,73] The characteristics and stability of Fe INPs in AMD-contaminated and remediated surface waters are important, because sorption to Fe-oxide INP surfaces affects the fate and bioavailability of toxic metals.[26,64,69,70,74–78]

AMD Fe INPs have been underexamined due largely to prior analytical constraints.[19] Historically, NPs were not distinguished from colloids, often defined by an ability to pass through a 0.45-or 0.22 µm filter.[4,14,22,71] In addition, analytical techniques capable of characterizing NPs and performing mechanistic particle stability studies were limited.[35] Development of single-particle ICP-MS (spICP-MS), has generated many laboratory studies of engineered NPs but the technique has not been used to examine INPs generated in mining-impacted streams.[13,14,35,39,40,58,79]

Mining exposes metal sulfide minerals to weathering, producing runoff (AMD) rich in sulfuric acid and toxic metals and creating extensive Fe-oxide stream bed coatings.[64,66–70,72,74]

*Primary author

Corresponding author: James F. Ranville. Direct correspondence to jranvill@mines.edu. Department of Chemistry, Colorado School of Mines, 1500 Illinois St, Golden, Colorado 80401.

Because AMD can be generated indefinitely and source-control measures are often unfeasible, effluent treatment is typically needed.[65,67,68] Most often, water treatment plants (WTPs) use lime (Ca-oxide) to increase the pH, precipitate metals, and concentrate them into a sludge for disposal.[68,80,81] Resulting changes to stream water chemistry during treatment may alter the stability of previously deposited INPs.

NP stability can be predicted using Deryagin-Landau-Verwey-Overbeek (DLVO) theory, which provides a mechanistic model of the net interaction energy between NPs.[29] Instability occurs when attractive forces (van der Waals attraction) exceed repulsive electrostatic (surface charge) forces. Zeta potential (ZP), the electrical potential of the shear plane in the electrical double layer (EDL), is commonly examined in stability studies.[82] The isoelectric point (IEP) is the pH at which ZP is zero. Dispersed NPs are most susceptible to aggregation near the IEP and/or when the EDL is compressed by high ionic strength. Laboratory experiments show that DLVO stability models can rigorously predict stability of simple NP dispersions within artificial media,[73,83–92] but may require modification for complex, environmental systems.[32,33,93–96] Classical DLVO models do not include the effects of specific (chemical) adsorption, which can greatly alter surfaces.[29,34]Additionally, DLVO theory is not applicable to situations of high NP concentration, high surface charge,[94] or involving polydisperse aggregate interactions.[33,97]

Mechanistic modeling studies have successfully adapted DLVO to include humic acid,[33,93,98] multivalent electrolyte ions and surface counterions of varying size,[34,84,92,98–102] but the resulting models become specific to the system of study. Electrolyte composition, pH, and specific adsorption of charged species have a strong influence on surface charge.[30,34,82,101,103,104] For specific adsorption on Fe-oxides, experiments with Cu and sulfate binding suggest that while Cu adsorption does not alter goethite ZP, sulfate adsorption decreases goethite ZP when pH < IEP.[105] Surface coating by natural organic matter (NOM) decreases aggregation, likely via both steric inhibition and contribution of negatively charged surface groups.[31–33,82,98,104,106] The large number of variables affecting NP surfaces make NP behavior very susceptible to changes in environmental conditions. A quantitative, environmentally relevant and generalizable mechanistic model for predicting NP stability is likely not feasible.[33,95] However, the lessons of these mechanistic studies can be used to evaluate the agreement of environmental NP observations with theoretical expectations.

Our approach to understand AMD INP stability is to measure water chemistry variables associated with INP stability, create an amechanistic statistical model via multiple linear regression (MLR) for quantitative predictions of stability, and qualitatively compare the outcomes to mechanistic expectations. While this approach only permits a qualitative verification of likely mechanisms at work, it can generate a rationale for understanding NP behavior in a natural system.

We examined the impact of water chemistry changes in an AMD-contaminated stream on the stability of Fe-oxide INPs, before, during, and after AMD remediation. We hypothesized that in addition to removal of previously accumulated Fe INPs from the stream bed via physical scouring, enhanced particle stability from altered water chemistry could further mobilize Fe INPs. We (a) monitored the Fe- and Cu-containing INPs and water chemistry during the early stages of WTP operation, and (b) explored resultant changes in particle stability with laboratory aggregation experiments. Water chemistry changes were related to INP concentration as well as aggregation rates. We demonstrate a complex interplay of several parameters that control stability of Fe INPs in the seasonally-variable and remediation-altered water chemistry, qualitatively consistent with expectations from results of laboratory studies of Fe NPs.

3.2 Materials and Methods

This section describes the experimental details of the study, including descriptions of the study site, field sampling protocols, and laboratory work.

3.2.1 Study Site

The North Fork of Clear Creek (NFCC) near Black Hawk, Colorado, USA is contaminated by AMD from two principal sources, the National Tunnel and Gregory Incline.[64,70,74,107] In 1983, the Clear Creek-Central City Superfund site was designated, with the remediation goals of restoring aquatic life and enabling water use.[64,107] Construction of a lime-based WTP was completed early in 2017, with intermittent operation beginning in March and full-time operation in September.[108] The discharge and water chemistry of NFCC is highly influenced by increased runoff in the spring and early summer months followed by low baseflow in fall and winter.

3.2.2 Field Sampling and Measurements

Sampling was conducted 1-2 times per month from March 9, 2017 to August 29, 2017. Two reference sites upstream of the AMD contamination, and four sites downstream were

sampled. For simplicity, only data from the reference sites and downstream site #6 are shown, unless otherwise noted. Water velocity varied considerably across the stream at the sampling location, due to the very shallow depth (< 0.5 m) and the rocky bed. We report only the maximum water velocity (HACH FH950 flow meter). Stream discharge was obtained from the USGS stream gauge (06718550). Temperature and conductivity were measured in-stream using a VWR field meter and pH was measured in-stream using a Beckman field meter with an Orion Ross electrode. Alkalinity and Fe(II) were measured on site using HACH™ field kits. Grab samples (~1 L) were collected in polyethylene bottles and splits were taken for water chemistry and NP analysis and for aggregation experiments.

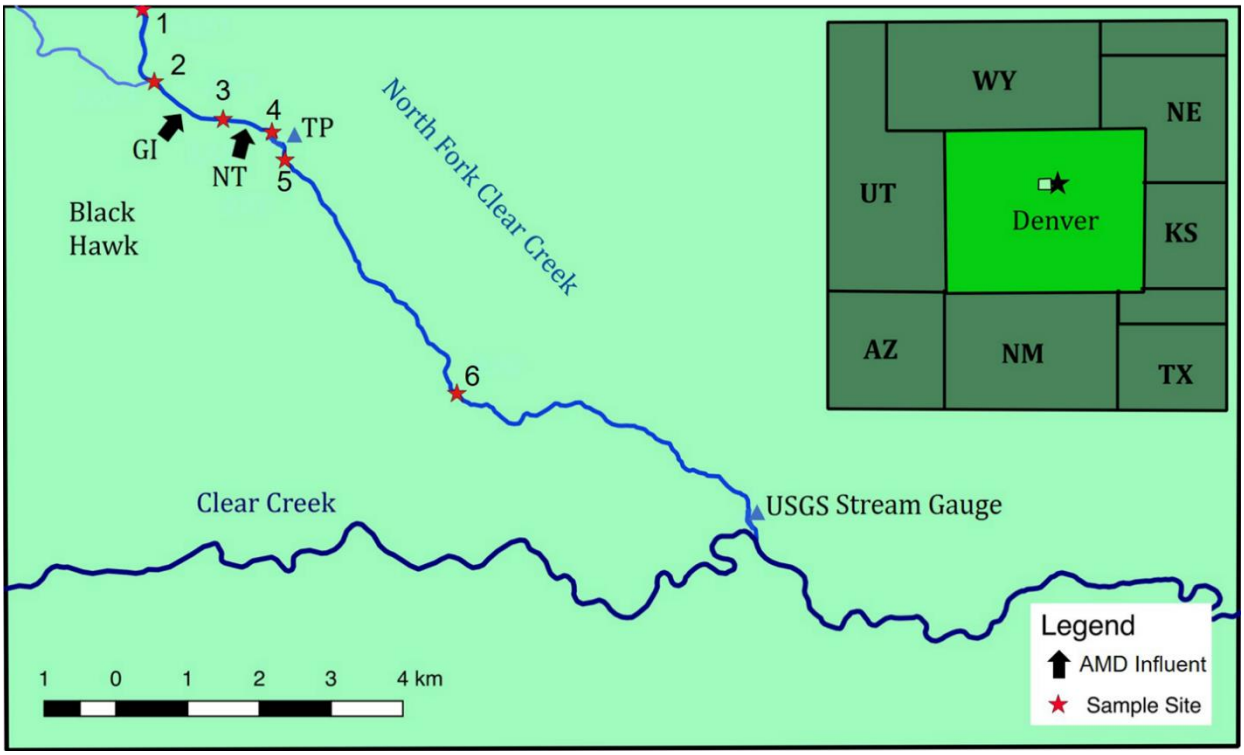

Figure 3.1 Map of the North Fork of Clear Creek and its confluence with the main stem of Clear Creek, with Gregory Incline (GI) and National Tunnel (NT) AMD point sources, water treatment plant (TP), USGS stream gauge 06718550 where discharge data was collected, and sampling locations (red stars). Sites 1 and 2 correspond to "reference 1 and 2" and site 6 corresponds to "downstream" in the text.

Duplicate 10 mL sample splits were taken in 15 mL Falcon tubes for chemical analysis. Unfiltered and filtered (Ahlstrom 0.45-µm syringe filter) samples were analyzed for cations, anions, and organic carbon. Cation samples were acidified on-site with several drops of

concentrated nitric acid (Fisher Trace Metal grade). Samples for dissolved organic carbon (DOC) and total organic carbon (TOC) were acidified in the lab with several drops of concentrated hydrochloric acid (BDH Trace Metal grade). All samples, including the remaining ~500 mL of the grab samples (used for nanoparticle analysis), were transported back to the laboratory and stored under refrigeration (4^{o}C).

Table 3.1 Timeline of sampling and treatment plant events. *Denotes dates when particle analyses were conducted (including spICP-MS, optical particle counting, and hematite zeta potential and aggregation).

Sampling Date	Water Treatment Plant (WTP) Status
*3/9/2017	No AMD source diversion or treatment yet
*3/23/2017	Gregory Incline AMD diverted to WTP, no treatment yet
*5/4/2017	Gregory Incline AMD treated, WTP effluent not flowing at time of sampling
*5/16/2017	Gregory Incline AMD treated, WTP effluent flowing at time of sampling
*6/1/2017	Gregory Incline AMD treated, WTP effluent flowing at time of sampling
*7/19/2017	WTP offline since 6/10, WTP began collecting and holding Gregory Incline AMD again on 7/18 but no treatment or effluent release until 7/25
8/4/2017	Gregory Incline and National Tunnel AMD treated, effluent flowing at time of sampling
*8/29/2017	Gregory Incline and National Tunnel AMD treated, effluent flowing at time of sampling

3.2.3 Laboratory Analyses

Unfiltered and filtered cation concentrations were measured with a PerkinElmer Optima 5300 DV ICP-AES. All samples were analyzed in duplicate with a Sc internal standard. Immediately after calibration, after every 10 samples, and at the end of the run QA/QC check samples were analyzed including DI water blanks (Barnstead Nanopure system) with 2% trace metal grade nitric acid and certified continuing calibration verification (CCV) standards (PerkinElmer). NIST certified standard reference materials 1640a and 1643e73 were also analyzed at the beginning and end of each sample run. Criteria for passing QA/QC checks were that Sc internal standard concentrations did not deviate more than 20% from the known

concentration and deviation of CCV standards of no more than 10% from the known concentrations. Any samples analyzed within failed QA/QC checks were reanalyzed. Detection limit ranges in µg L^{-1} for the elements of interest during this study were Cu 1.1-2.9, Fe 0.3-1.6, S 0.1-7.2 (equivalent to 0.3-21.6 SO_4). Filtered anion concentrations were measured using a Dionex ICS-900 ion chromatograph. A Shimadzu TOCV-TNM-LCSH was used to analyze total and dissolved organic carbon (TOC and DOC).

Cu- and Fe-containing INP mass and number concentrations were measured with a PerkinElmer NexION 300D quadrupole ICP-MS using 100-µs dwell times. The PerkinElmer Syngistix nano application module separated particle-generated pulses from background signal and provided NP sizes and number concentration. The spICP-MS transport efficiency was determined using a 60-nm NIST Au-citrate NP standard.[41] Cu-containing INP number concentrations in the samples were determined from ^{63}Cu pulses. ^{56}Fe was measured in dynamic reaction cell mode with ammonia gas, and particle sizes were calculated assuming the elemental composition and density of ferrihydrite. Scanning/transmission electron microscope images of pre-treatment (October 28, 2016) INPs and synthesized hematite were generated using an FEI Talos F200X 200keV field emission STEM, and elemental maps were created with its integrated energy-dispersive X-ray spectroscopy (EDS) system. Colloidal particle sizes and number concentrations were measured in triplicate on an Accusizer Optical Particle Sizer Model 770 before and after 10 min of sonication in a water bath, with 10- or 100-fold dilution as needed. Serial filtration was also conducted for comparison to the above particle analyses. Water samples collected on May 4, 2017 from sites 2 (reference), 3, 4, and 6 were filtered sequentially in triplicate through 0.45-µm and 0.02-µm filters with sample splits removed for analysis before and after each filtration step.

3.2.4 Stability Experiments

In mildly acidic AMD-impacted streams, ferrihydrite is a dominant phase, with goethite secondary in importance.[23,72,109] However, synthesized hematite (Figure 3.2 on page 42) was chosen as a model Fe-oxide INP for aggregation experiments.[110] Hematite is relatively monodisperse, roughly spherical, and mineralogically stable, which allowed for more reliable and reproducible dynamic light scattering size measurements than would be likely for ferrihydrite. The hematite was suspended in 0.22-µm filtered (Millipore) field waters at concentrations of 55.5 µg L^{-1}. After 10 min of sonication in a water bath, hematite size was

measured for 10 s every 10 min for up to 3 h using a Malvern Zetasizer Nano. Size calculations utilized a refractive index of 4.5 and an absorption coefficient of 0.6. Any size data that did not meet quality criteria (non-uniform size distribution or poor correlation function) were discarded. Aggregation rates were calculated from the slope (nm h^{-1}) of the first hour of size measurements. At the completion of each aggregation experiment, the suspension was transferred to an electrophoretic mobility cell for three consecutive ZP measurements with automatic measurement duration and using the Smoluchowski equation. Descriptive statistics were calculated in OriginPro 2018 and multivariate statistical analyses were carried out using Stata V. 14.

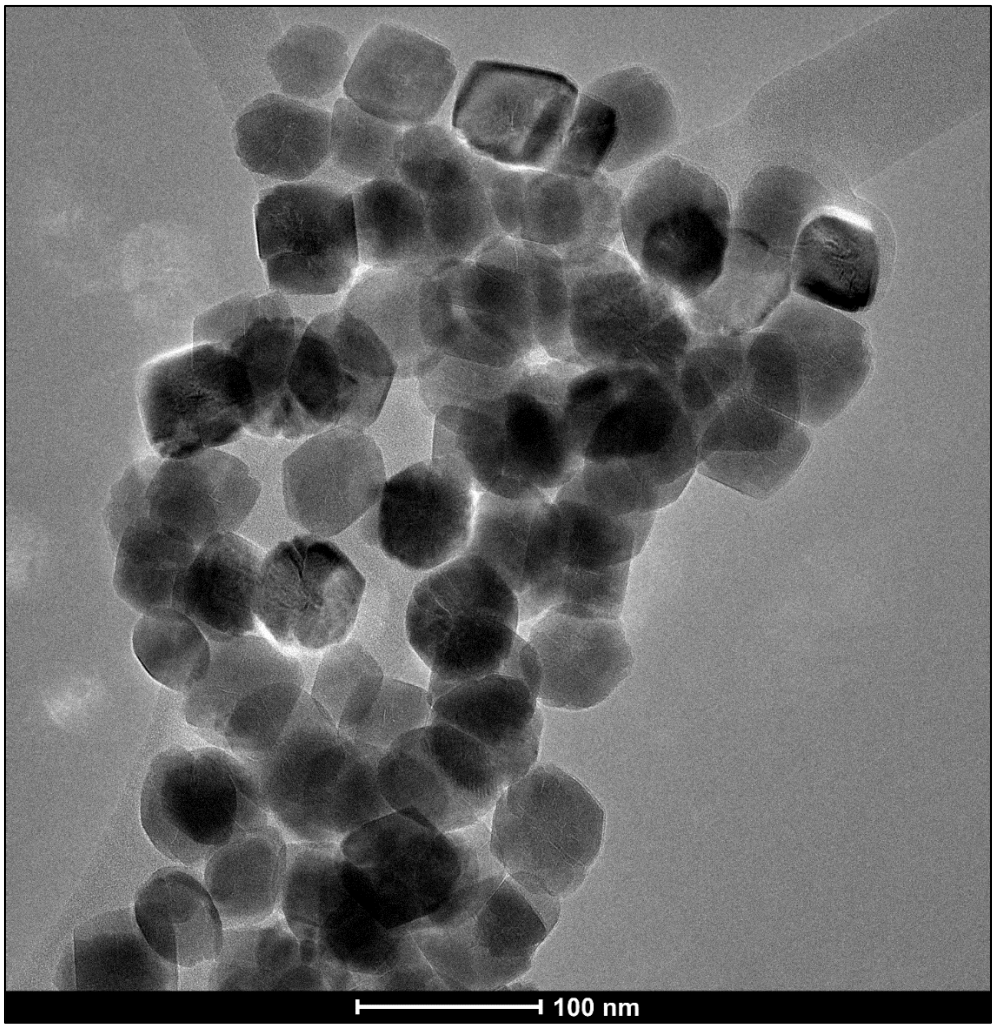

Figure 3.2 TEM image of synthesized hematite used in the model INP stability experiments.

Hematite stability was modeled using unmodified DLVO Theory for comparison to the aggregation results. Graphs of total energy of interaction between NPs were generated using the DLVO calculator contained in the open-source Excel workbook created by Steven Abbott and Nigel Holmes to accompany the book *Nanocoatings: Principles and Practice* (DesTech Publications 2013). Ionic strength (calculated in Visual Minteq using measured water composition) and ZP data from individual samples in were used as model inputs. Other variables were fixed at the following values for all calculations: temperature 20°C, radius 60 nm, Hamaker constant 2.9 $x10^{20}$ J, Flory-Huggins constant 0.3, density 5.26 g cm^{-3}. It was assumed that no coatings were present on the particles.

3.3 Results and Discussion

The stream hydrology and chemical composition of the water observed during the study as well as the INP characteristics are described in the following sections. We observed that INPs and INP aggregates in NFCC stream water decreased in size and concentration over the course of water treatment. Additionally, the stability experiments with model and NFCC INPs showed that a transition from an unstable to a stable system occurred.

3.3.1 Hydrology and Water Chemistry

Treatment of Gregory Incline began several months before spring runoff and was intermittent until late summer, when the National Tunnel was also diverted and WTP operations stabilized. To consider the effects of both treatment and stream hydrology, the study can be divided into three major time periods: spring (March – April), when the creek was pre-remediation and low flow; early summer (May – June), when AMD inputs were partially remediated and streamflow increased from snowmelt; and late summer (July-August), with near-complete remediation and decreasing flow (Figure 3.3a on page 44). Due to the timing of snowmelt, both treatment and dilution from runoff affected the stream simultaneously. Discharge ranged from an average base flow of 0.1 m^3 s^{-1} to a peak during snowmelt of 2.1 m^3 s^{-1}. Physical scouring from the force of accelerated water velocity (ranging from 0.4 to 1.8 m s^{-1}) would likely have promoted INP removal during peak runoff. The visual changes to NFCC during the three periods were dramatic (Figure 3.3b on page 44).

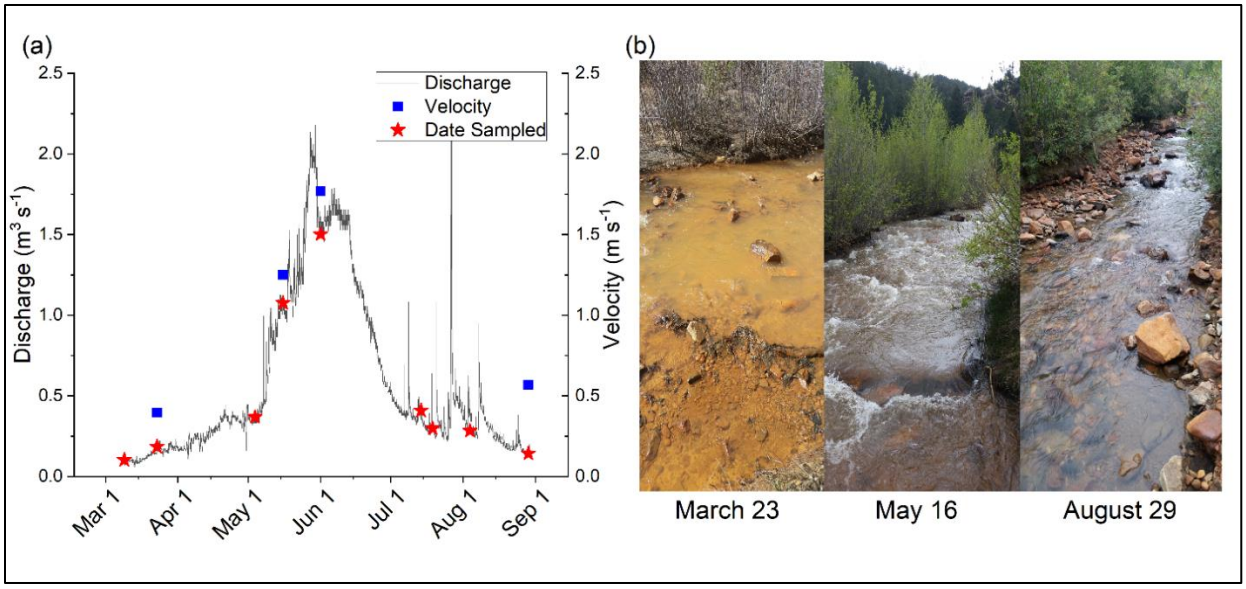

Figure 3.3 Discharge, stream velocity (a) and visual appearance (b) of NFCC downstream. Discharge (black line) data are from USGS stream gauge 06718550 (Figure 3.1). Red stars denote the discharge on dates sampled and blue squares indicate water velocity. Loss of Fe-oxides from the stream bed and water column is visible.

Both treatment and snowmelt runofff affected the parameters suspected to be important for particle stability. Downstream of the mining inputs, the stream initially had a pH ~6, which gradually increased by about 2 pH units over the treatment period (Figure 3.4a on page 45). Although the AMD inputs are more acidic (pH < 5), some buffering occurred even before AMD treatment. The upstream site pH varied by about ± 0.6 units around an average of about 7.2, with the highest three values occurring at the end of the study period. The increase in pH at the reference site is likely due to snowmelt, as this has been observed seasonally in multiple years of sampling (Figure 3.5 on page 46). In NFCC, remediation resulted in only a small shift in pH.

Conductivity remained low and relatively constant at the reference site throughout the study (Figure 3.4b on page 45). At the beginning, conductivity was about 5-fold higher downstream than at the reference site, reflecting the input of the AMD. Downstream conductivity decreased substantially during runoff, then rebounded in late summer when the stream approached base flow. This seasonality in conductivity can be attributed to the dominance of sulfate and major cations (Ca, Mg), which are not removed in the lime treatment process and were only diluted by snowmelt.

DOC concentrations were similar at the upstream and downstream locations on all sampling dates (Figure 3.4d). DOC concentration doubled during peak runoff in the early summer. This seasonal pattern is often seen in alpine streams because of flushing of soil-derived organic matter during snowmelt.[111–114] Changes in surface runoff from snowmelt in the alpine watershed strongly impacted dissolved concentrations as well as particles during the study.

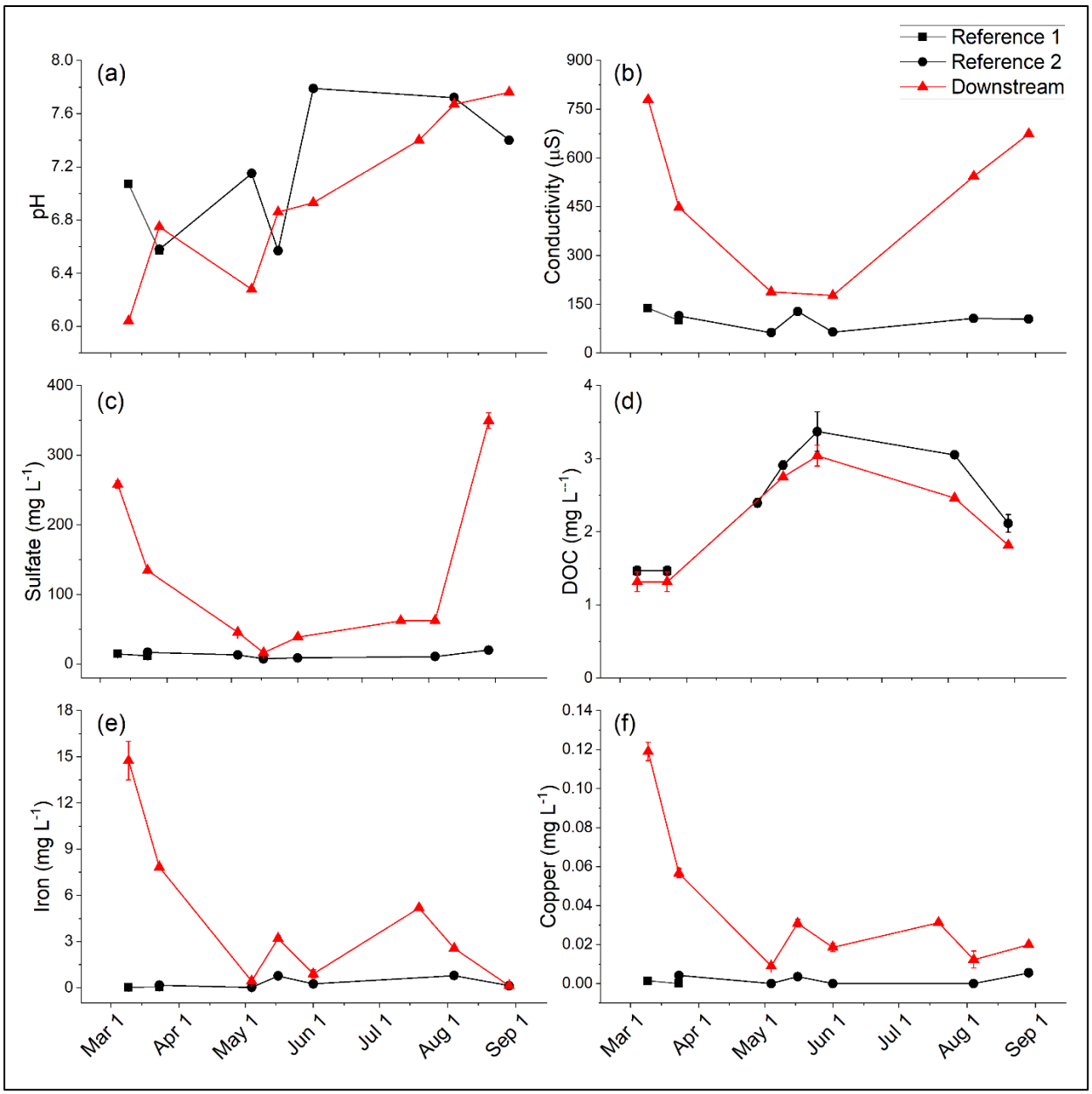

Figure 3.4 Measured pH (a), conductivity (b), sulfate (c), DOC (d), total Fe (e), and total Cu (f) at the NFCC reference (black) and downstream (red) sites. Single values of pH and conductivity were obtained, while error bars in panels c to f are ± 1 standard deviation of duplicate samples.

The input of AMD and its subsequent treatment and dilution by runoff dramatically affect dissolved and particulate metal concentrations. At the beginning of the study, total Fe and Cu concentrations downstream were 100-fold higher than at the reference site (Figure 3.4e and f on page 45). During early summer, the combined effects of dilution and partial-treatment of the AMD resulted in much lower metal concentrations. Unlike sulfate (Figure 3.4c on page 45), Cu and Fe did not return to pre-treatment concentrations as discharge approached base flow in the fall. This clearly shows successful metal removal from the AMD as a result of treatment. Water chemistry data over an entire year (fall 2016 to fall 2017), including alkalinity and Fe(II) concentrations, are presented in Figure 3.6 on page 47.

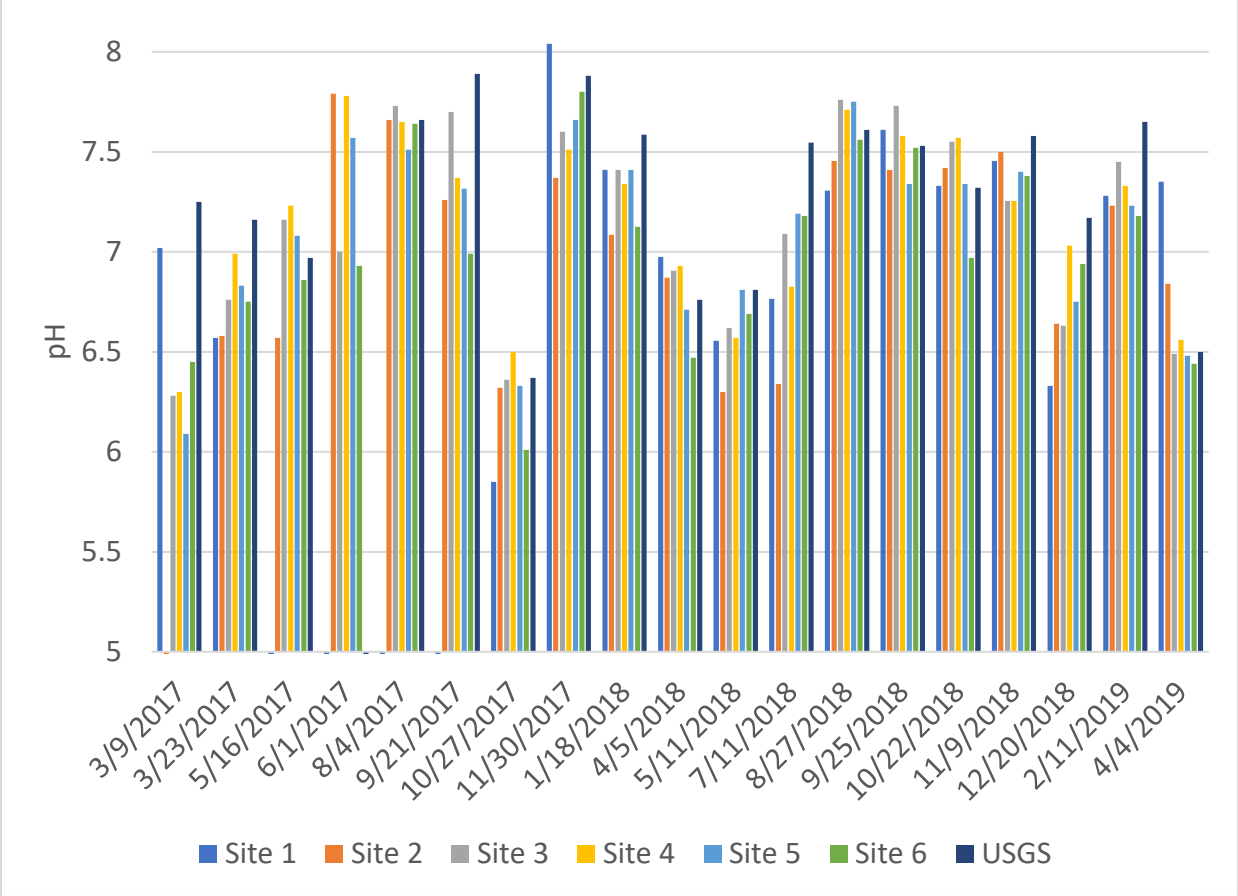

Figure 3.5 The pH of NFCC from March 9, 2017 to April 4, 2019 at all sampling sites and the USGS stream gauge location. An increase of 0.5-1 pH unit at all sampling sites during the summer months was observed in both 2017 and 2018. This is likely related to the seasonal changes to the stream that occur during peak snowmelt.

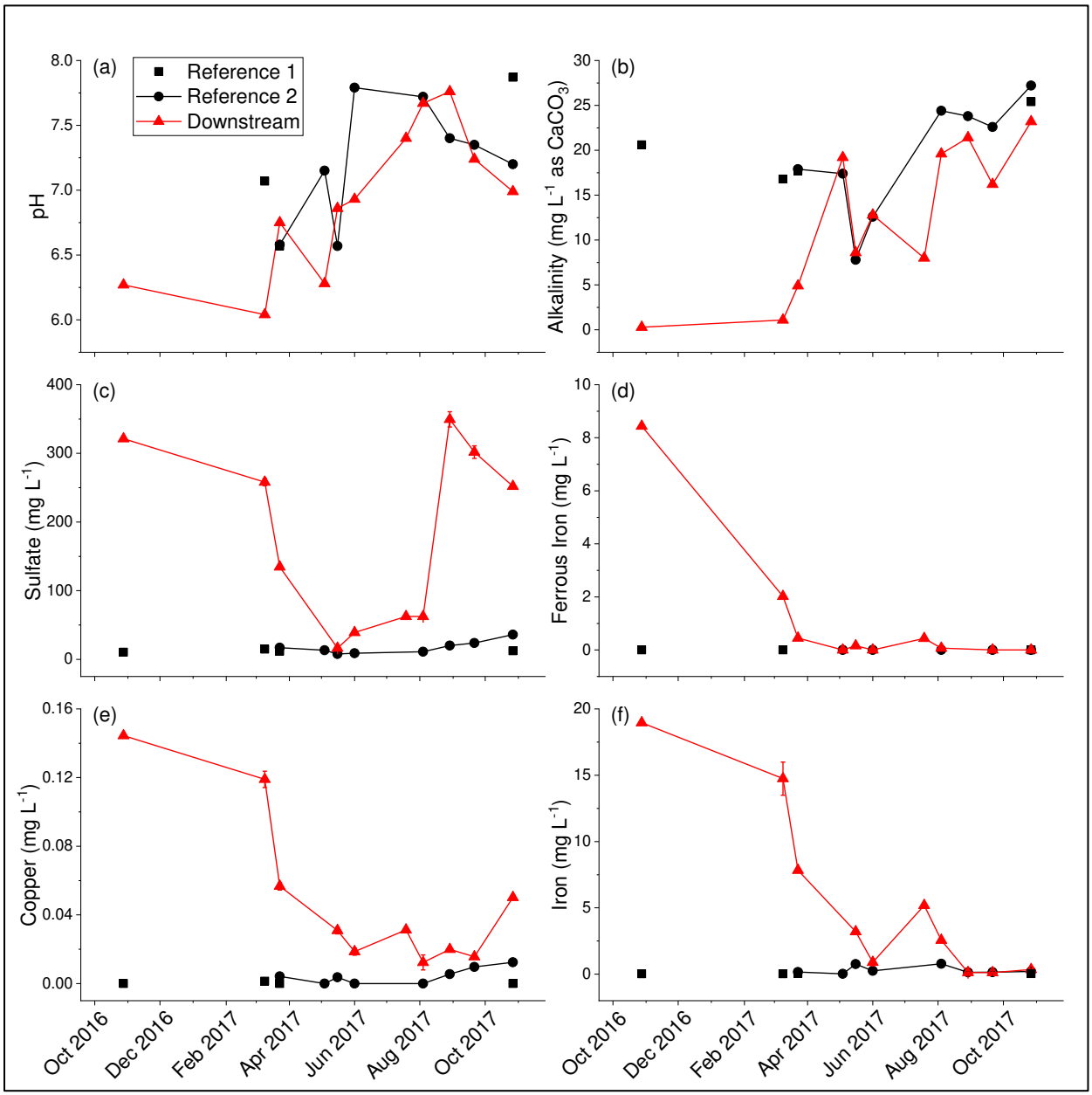

Figure 3.6 NFCC water chemistry spanning one year starting five months before treatment began, including pH (a), alkalinity (b), sulfate (c), Fe(II) (d), Cu (e), total Fe (f). Single values of pH, alkalinity, and Fe(II) were obtained; while error bars in panels c, e, and f are ± 1 standard deviation of duplicate samples.

3.3.2 NFCC INPs Analysis

The chemical composition of the remediated water was no longer conducive to precipitating Fe-oxide INPs. The spICP-MS results support that the INPs that had previously accumulated on the streambed were mostly removed during the early summer runoff (Figure 3.7a). Fe and Cu INP number concentrations downstream decreased by several orders of magnitude during the study period, ending with late summer downstream concentrations similar to the reference concentrations. The Cu NPs detected likely represent Cu sorbed to Fe oxide INPs, with thecorrelation between Cu and Fe number concentrations showing approximately 4 Cu INPs counted for every 100 Fe INPs (Figure 3.6b, m = 0.0364; R^2 = 0.786). The lower number of Cu-containing INPs compared to Fe-containing INPs results from the lower content of Cu than Fe in the INPs and consequently, smaller Fe INPs likely contained insufficient Cu to register as a pulse in the spICP-MS analysis.

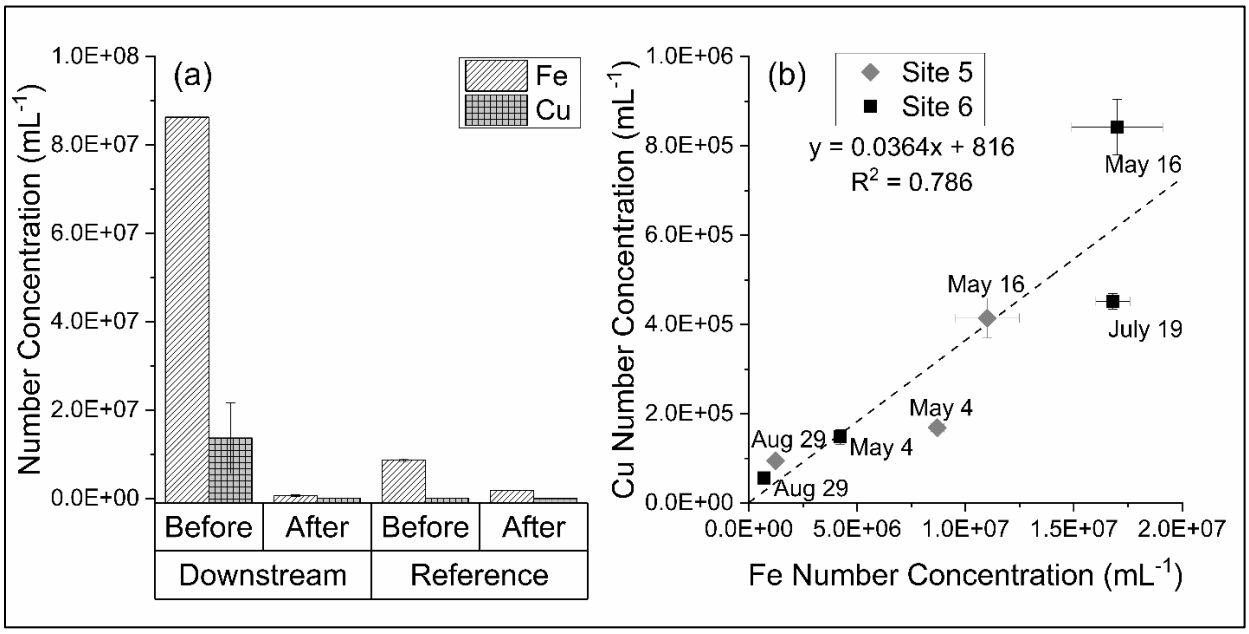

Figure 3.7 Overall decrease in spICP-MS-measured INP concentrations in NFCC following AMD treatment. (a) INP number concentrations of Fe (light diagonal hashed bars) and Cu (dark cross hashed bars) in downstream and reference samples at the beginning and end of the study period. (b) Correlation between Cu and Fe number concentrations in downstream sites 5 (gray) and 6 (black) (Site map in Figure 3.1); m = 0.0364; R^2 = 0.786.

Based on masses measured by spICP-MS, the calculated mean size of Fe-oxide (as $Fe(OH)_3$) INPs in downstream water before treatment was 180 nm (s.d. = 6 nm; n=3) (Figure

3.8). We suspect this size distribution is in part composed of small aggregates. Indeed, pre-treatment streambed particles examined with STEM included loose aggregates of 2-5 nm poorly crystalline Fe INPs (Figure 3.9 on page 50) that could be ferrihydrite or amorphous $Fe(OH)_3$. We also observed Fe INP aggregates with needle-like morphology resembling goethite (Figure 3.10 on page 51). After treatment, spICP-MS Fe number concentrations were too low to provide sufficient counting statistics for an accurate mean NP size but qualitatively, the NPs in the histogram appear smaller (Figure 3.8).

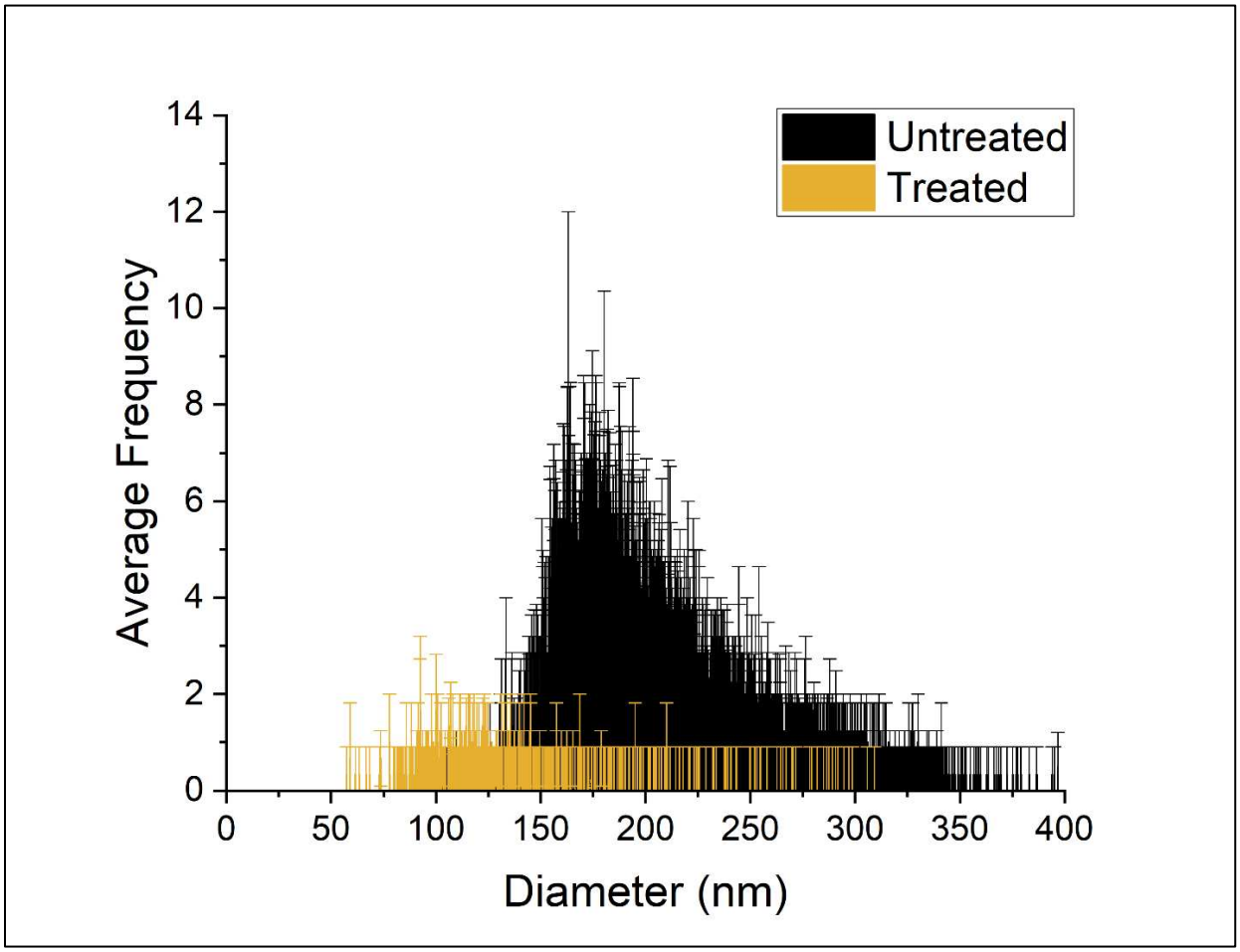

Figure 3.8 Size histograms of downstream Fe INPs without (black) and with (gold) treatment on July 19 and August 29, respectively. The modal size in the untreated histogram is 180 nm (s.d. = 6 nm, n = 3). Post-treatment spICP-MS Fe number concentrations were too low to provide sufficient counting statistics for an accurate modal or mean NP size, but qualitatively the NPs in the post-treatment water appear smaller than in the pre-treatment water.

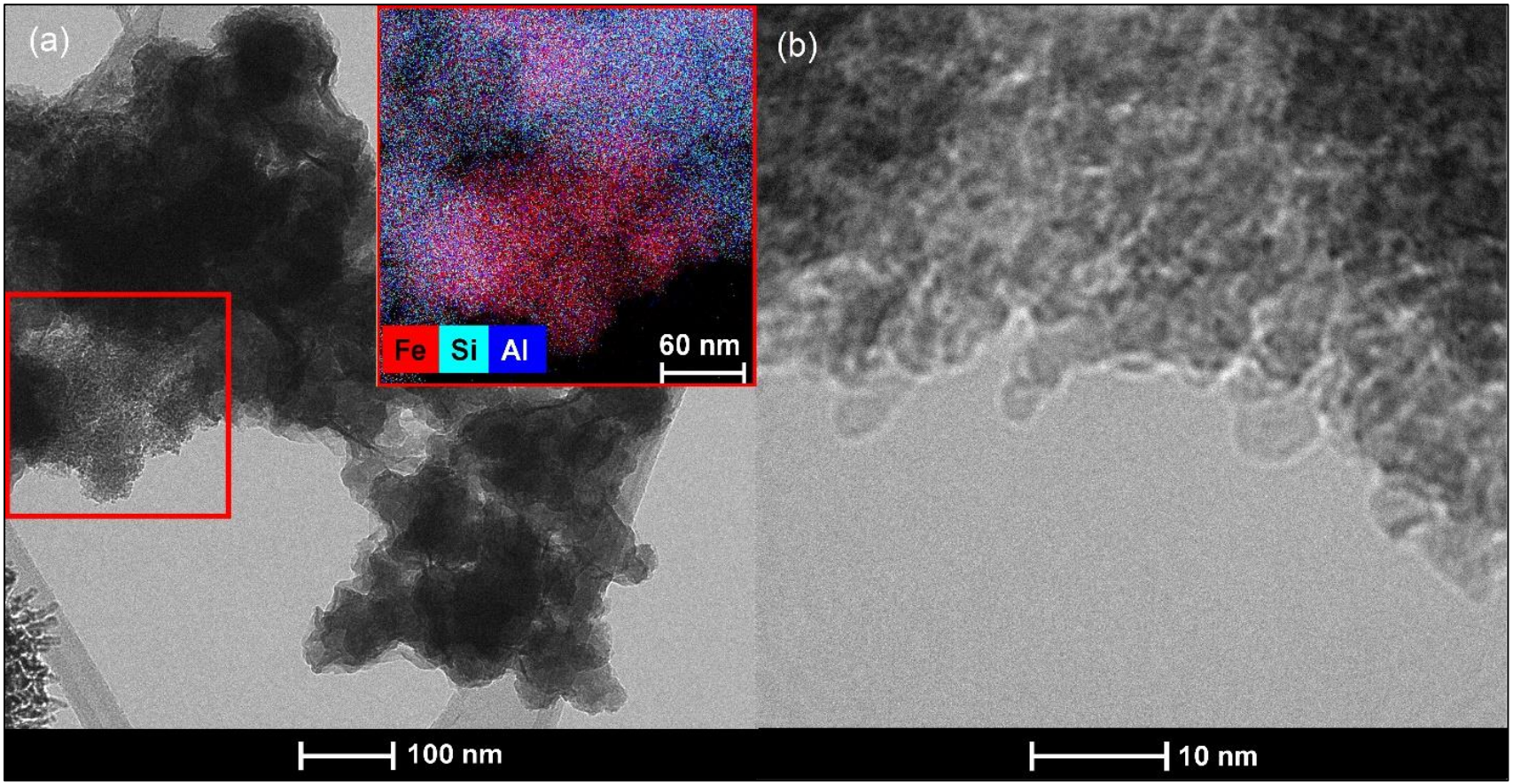

Figure 3.9 STEM imaging and elemental mapping of pre-treatment INPs in NFCC. (a) Fe-rich INP aggregate attached to aluminosilicate, with inset showing Fe (red), Si (cyan), and Al (blue) in an EDS element map of area within red box. (b) High magnification view of Fe INPs.

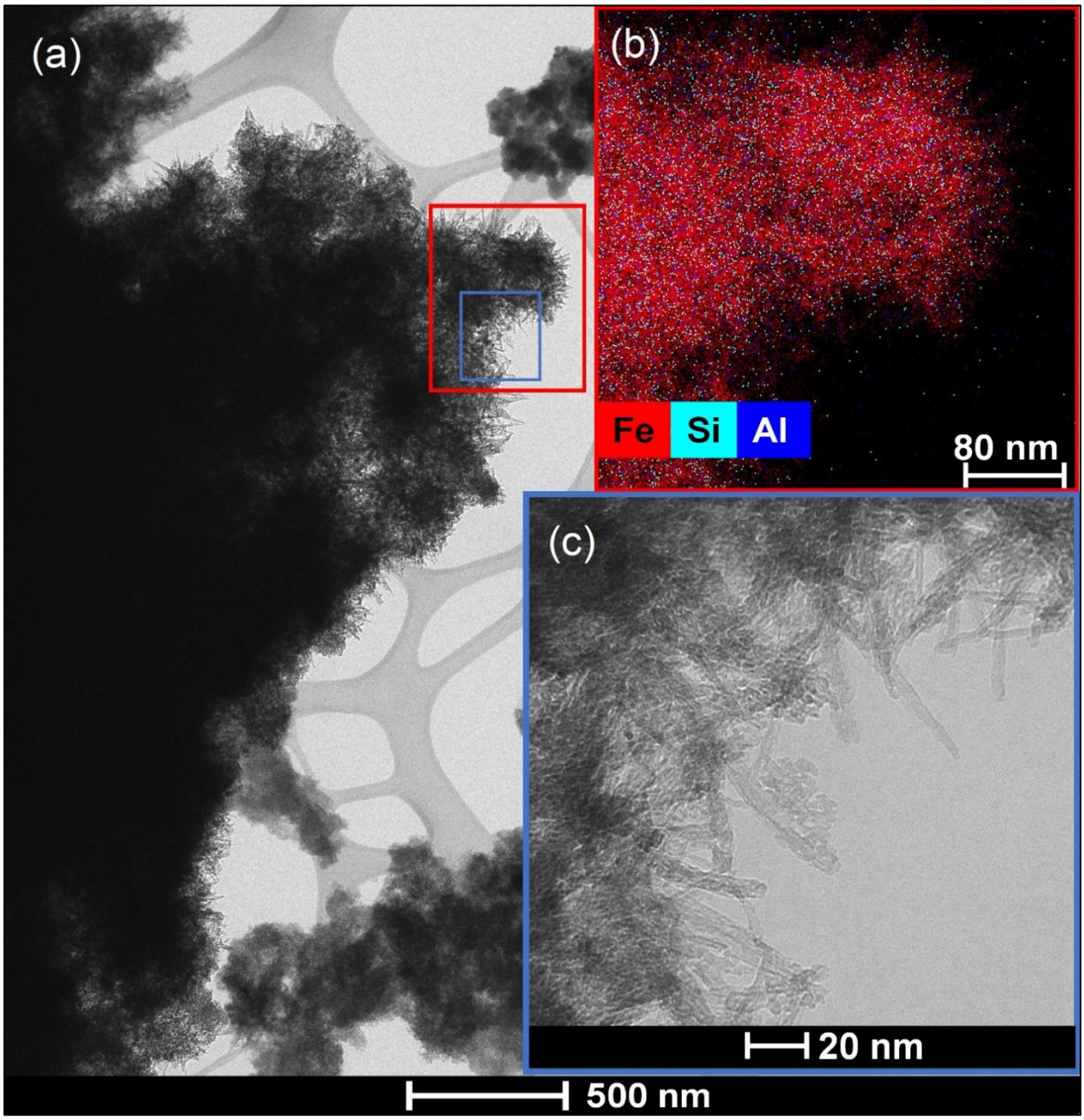

Figure 3.10 STEM images of needle-like particles in sediment sample collected from the Site 6 streambed in NFCC on October 28, 2016. (a) Large-scale image of large aggregate of needle-like particles. (b) Energy-dispersive X-ray spectroscopy elemental mapping of area boxed in red. (c) Enlarged view of needles in blue box. The predominance of Fe over Si and Al and morphology suggests these Fe oxide INPs may be goethite.

Several alternative particle analyses were conducted for comparison to spICP-MS and these cross validations appear to corroborate the SP results. Optical particle counting measurements of colloidal particles greater than 0.5 µm (detection limit of the instrument) showed similar number concentration trends (Figure 3.11) and an increase in small colloids due to sonication supports that particles were aggregated in the pre-treatment conditions (Figure 3.12 on page 53). Additionally, serial filtration of spring samples indicated notable amounts of Fe in the colloidal and nano size fractions – but only in the AMD-affected waters (Figure 3.13 on page 54).

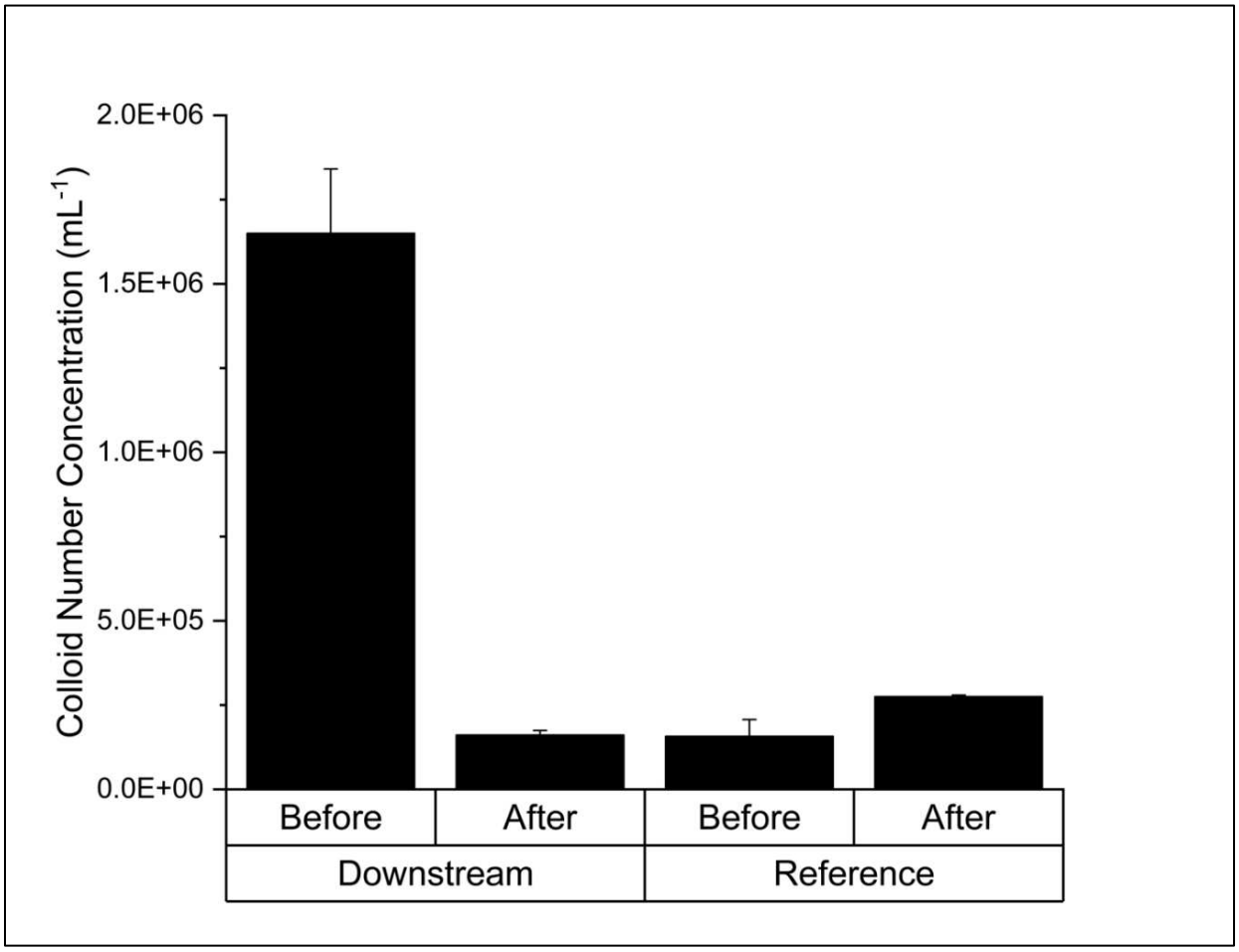

Figure 3.11 Number concentrations of colloid particles downstream (site 6) and at reference site 2 before (March 23) and after (August 29) treatment measured with optical particle counting. Particle counts decreased by over an order of magnitude at the downstream site after treatment.

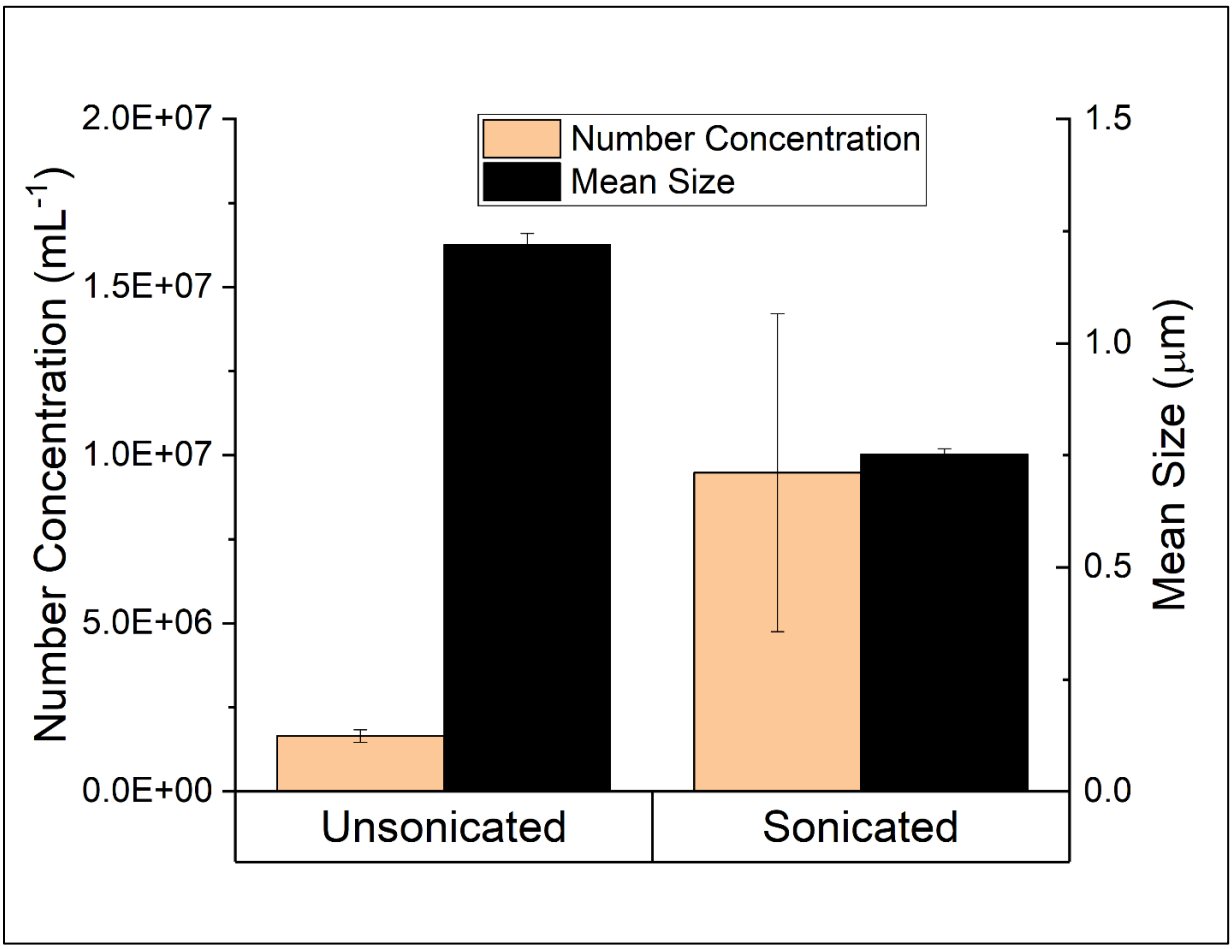

Figure 3.12 Colloid particle concentrations (left y-axis) and sizes (right y-axis) in downstream water (Site 6) on March 23, before and after sonication, measured with optical particle counting. Sonication increased particle concentrations while decreasing mean size, likely due to disaggregation of aggregated INPs and small colloids.

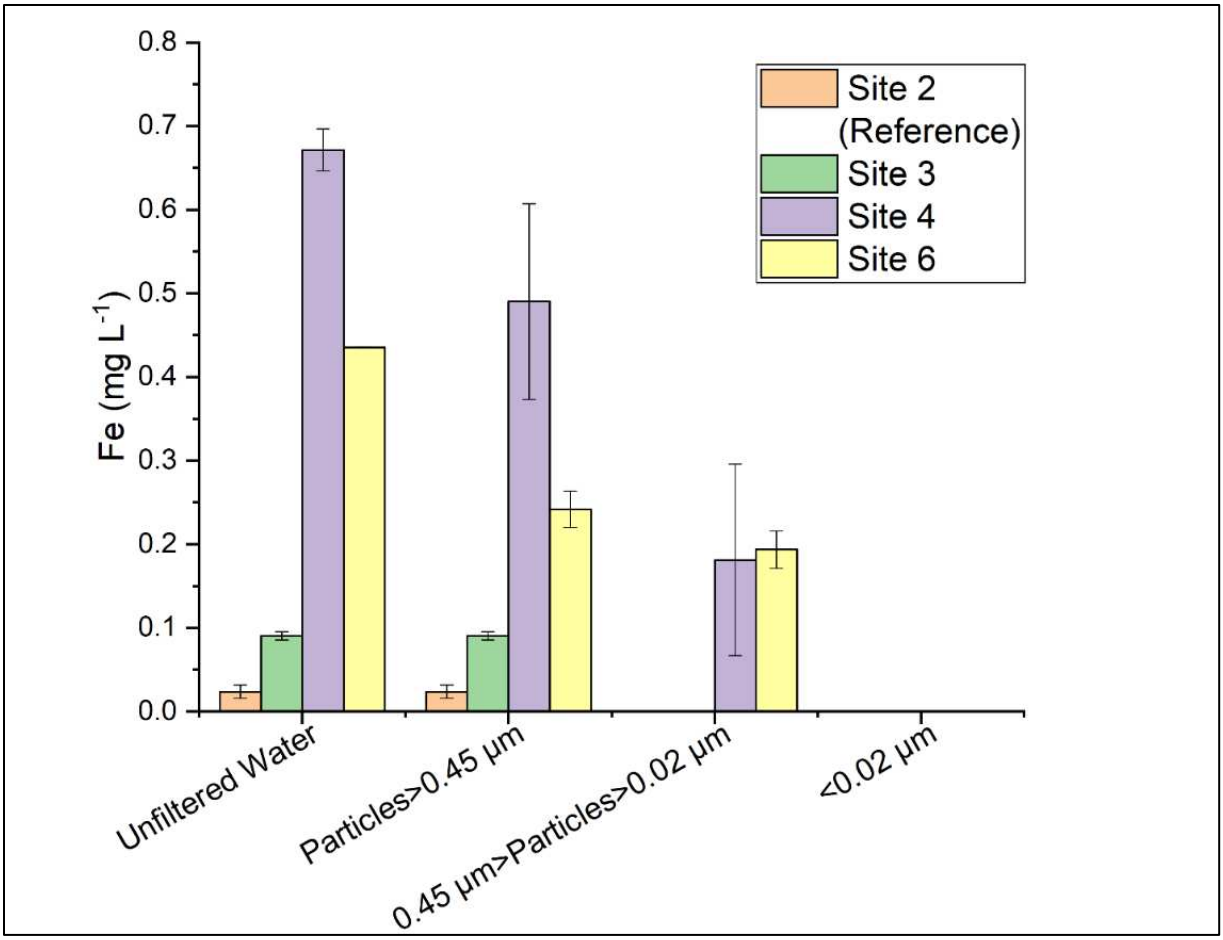

Figure 3.13 Iron fractions NFCC waters on May 4, separated by serial filtration. Site 2 (reference) and site 3 (remediated by date sampled) only contained large particles (greater than 0.45 µm) in mass concentrations less than 0.1 mg L^{-1}. Sites 4 and 6 (both AMD-contaminated) contained particles larger than 0.45 µm, and particles between 0.45 µm and 0.02 µm. The Fe concentrations in the 0.02-µm filtrate, which operationally can only contain truly dissolved species, were below the instrument detection limit in all samples.

The spICP-MS results provide evidence that NFCC INP number concentrations and sizes decreased during treatment, though we remain cautious about the potential for artifacts and overinterpretation during data processing. ^{56}Fe is challenging to measure in natural waters with quadrupole ICP-MS due to isobaric interference with ArO^+ and CaO^+. Even with the addition of a reaction gas, the size detection limit for Fe INPs in this study was approximately 55 nm. The pre-treatment INP size distribution (Figure 3.8 on page 49) is likely unimpacted by the relatively high detection limit because the measured diameters were large, likely due to the presence of aggregates. However, the post-treatment conditions, which favored disaggregation, would have likely resulted in many INPs smaller than the size detection limit.

The loss of large particles during treatment and runoff also creates difficulty in distinguishing NP-generated pulses from the (dissolved) background signal during data analysis. This issue was especially problematic in the June 1 dataset, in which high stream velocity and high discharge from runoff likely counteracted each other, resuspending bed particles into the water column but diluting the particle concentrations closer to the ICP-MS mass detection limit. False-positive NP signals could not be eliminated from the dataset on this date, either by manual manipulations or with the Syngistix statistical algorithm for background determination; therefore, we excluded June 1 data from Figure 3.7 on page 48.

3.3.3 Surface Chemistry and INP Stability

The influence of the changes in stream water chemistry on INP surface charge and stability were demonstrated in the laboratory experiments with hematite. Reference water induced the most negative hematite ZPs during the entire study period (Figure 3.14a on page 56). The strongly negative ZPs coincide with near-zero aggregation rates in the reference water (Figure 3.14b on page 56). Aggregation and ZP varied much more in downstream water than in reference water. The near-zero ZPs seen in the spring, pre-treatment, pre-runoff downstream water indicate that pH was near the hematite IEP. This coincided with the most rapid aggregation observed. During early summer (runoff), the downstream hematite ZP became more negative and aggregation rates decreased sharply, becoming more similar to hematite in the reference waters. Finally, during the late summer (post-treatment, post-runoff), the ZP became slightly less negative, but did not return to pre-treatment values. In the high conductivity post-treatment downstream water, aggregation rates remained low, in contrast to the earlier spring samples that had similar conductivities (Figure 3.14b on page 56). The strong correlation between ZP and aggregation rate suggests that surface charge controls stability in the system, with the transition from instability to stability occurring around -12 mV (Figure 3.15 on page 57).

Calculations with unmodified DLVO theory predict the formation of a repulsive energy barrier in samples which had a ZP of -15 mV or more negative. No repulsive energy barrier was present in the contaminated pre-treatment conditions (10/28/16 site 6), making aggregation highly favorable. The interaction energy increases over the course of treatment and during the runoff period, resulting in a repulsive energy barrier of 7 kbT at 5 nm from the surface on 5/16/17. After runoff, the interaction energy decreases once again as a result of the increase in ionic strength and zeta potential. These findings support the observed stability in the aggregation

experiments. However, there is less repulsion than would be expected in samples where slow or zero aggregation was observed, suggesting that there are repulsion mechanisms that are not included in the DLVO modeling. This is unsurprising, given the many factors that were not considered in this simple calculation, especially steric repulsion from DOC coatings.

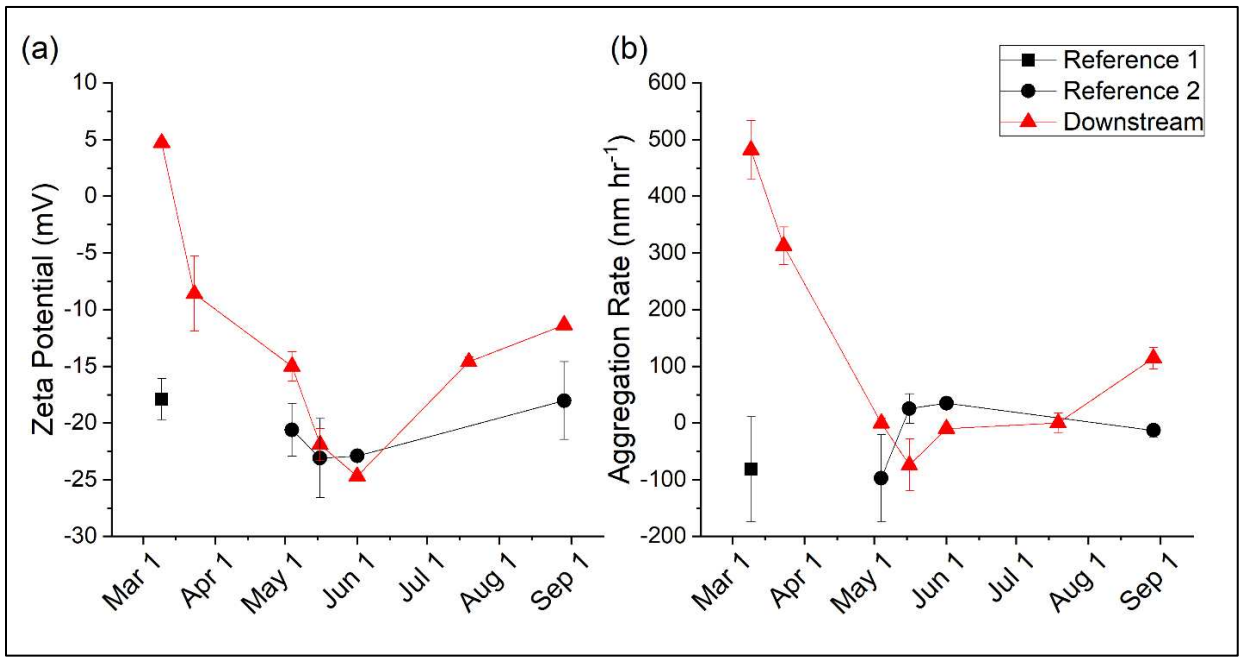

Figure 3.14 ZP (a) and aggregation rate (b) of hematite suspended in filtered water from the reference (black) and downstream (red) sites on NFCC. Negative aggregation rates are a reflection of the difficulty in quantifying a near-zero slope in a regression of average particle diameter versus time, and are not statistically different ($\alpha = 0.05$) from 0 nm h^{-1}.

Rapid aggregation and ZPs near zero occurred in water with high conductivity, low pH, and low DOC, which were the downstream conditions in the pre-treatment period (Figure 3.16 on page 58). Conversely, greater stability and increasingly negative ZPs occurred along a gradient of decreasing conductivity, increasing pH, and increasing DOC. These observations, as well as the overall dependence of stability on surface charge, are in good agreement with expectations. High ionic strength, indicated by conductivity, compresses the EDL, thus decreasing particle-particle repulsion and decreasing stability.[29]

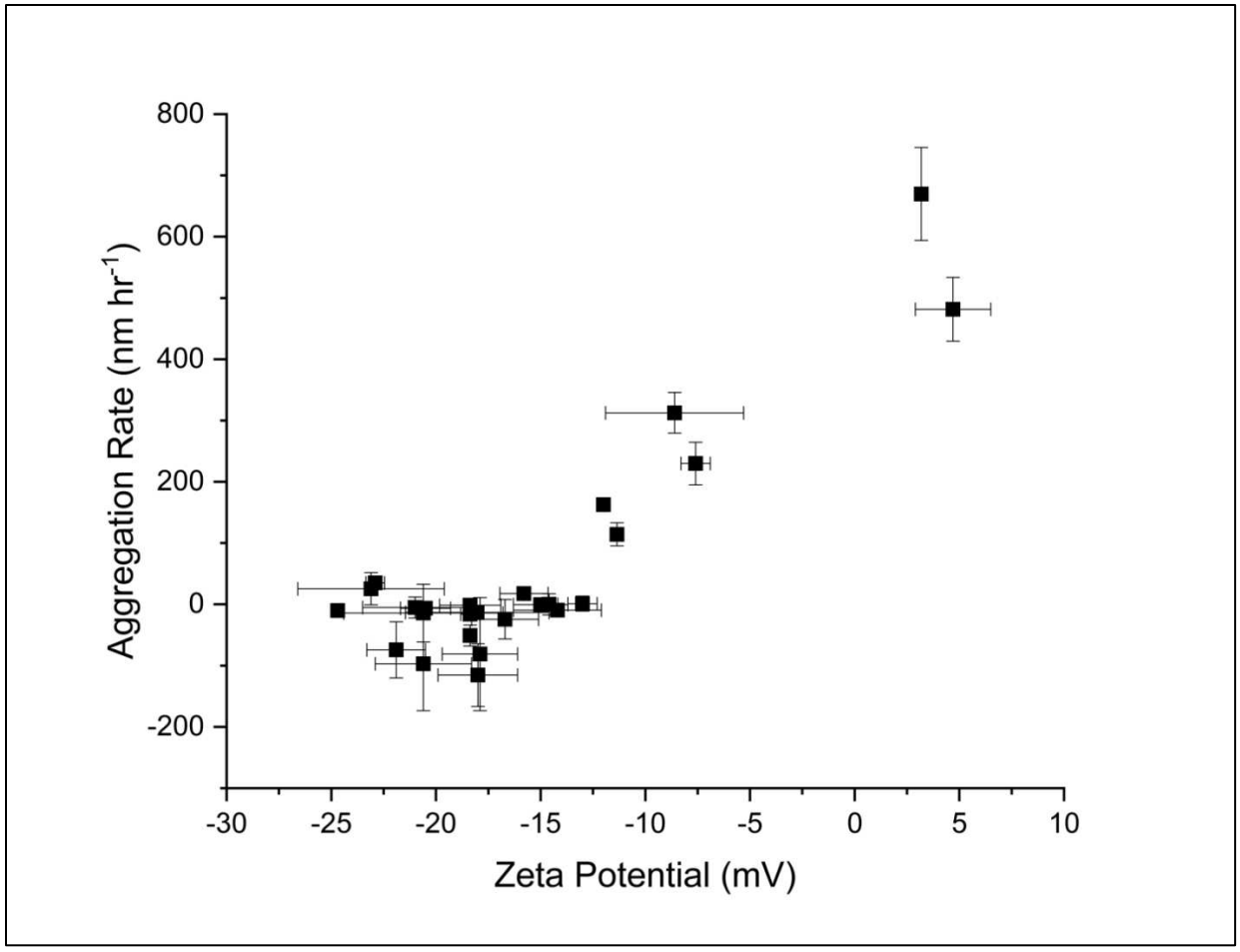

Figure 3.15 Aggregation rates and corresponding zeta potentials for all hematite stability experiments in water from NFCC, including samples from sites 1-6 on various sampling dates during the study period. The transition from a stable system (aggregation rate not statistically different from 0 nm h^{-1}) to an unstable system (aggregation rate greater than 0 nm h^{-1}) occurs at a zeta potential of -10 to -15 mV.

The dependence of hematite stability on pH agrees with expectations that Fe-oxide NPs would be less negatively charged, and possibly positively charged, under acidic conditions.[30,34,103] The occurrence of the IEP near pH 6.5 in these waters is in agreement with reported values in the literature, given the age of the synthesized hematite and the presence of sulfate and DOC.[82,105] Because the hematite NPs were near their IEP in the pre-treatment downstream conditions, the pH increase improved stability by making NP surfaces more negative. The decreasing ZP and aggregation rates with increasing DOC concentration are also consistent with expectations, because DOC coatings can promote stability by contributing negative surface-charge and steric hindrance.[31–33,82,98,106,115]

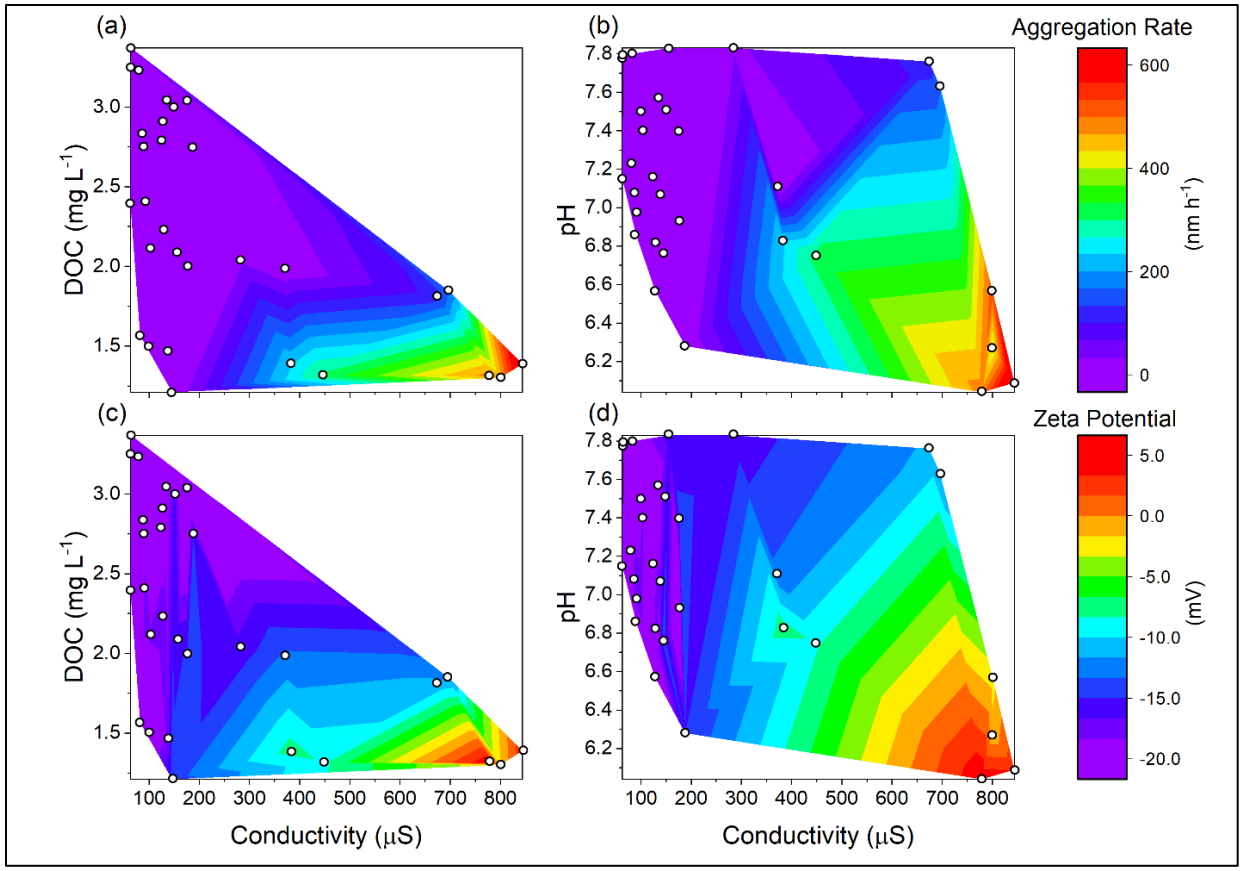

Figure 3.16 Hematite aggregation rates in filtered water from NFCC, as a function of conductivity and DOC (a) or pH (b). ZPs as a function of conductivity and DOC (c) or pH (d). Experimental data from all sampling locations and dates are included. High conductivity promoted fast aggregation and near-zero ZPs, while increases in DOC and pH promoted stability and negative ZPs.

3.3.4 Multivariate Statistics of Variables Influencing Surface Chemistry

Quantitatively determining the extent to which each of the water chemistry variables is responsible for the changes to ZP and aggregation would require mechanistic experiments beyond the scope of this study. After examining correlations between individual water chemistry variables and the ZP and aggregation rate, we performed a multivariate linear regression (MLR) to evaluate which variables are most strongly associated with the observed changes in aggregation and ZP. Based on surface chemistry fundamentals, the most important variables were expected to be pH, which can determine mineral surface charge,[30,34,103] and conductivity, which is a proxy for the ionic strength (Figure 3.17 on page 59) and affects the thickness of the EDL.[29] The role of DOC, which varies 2-fold, was also included in the MLR.

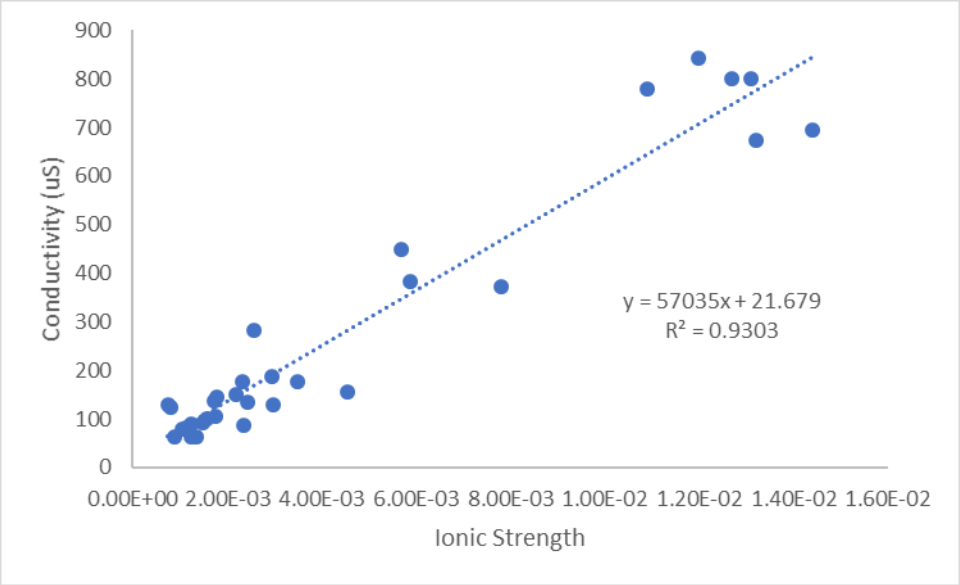

Figure 3.17 Correlation between conductivity (measured in-stream) and ionic strength (calculated in Visual MINTEQ from measured water composition) for NFCC samples.

Data for all variables were determined to be non-normal by Lilliefors' test, and all variables were significantly correlated with one another based on a Spearman correlation matrix ($p < 0.05$). MLRs were constructed using pH, DOC, and conductivity (or sulfate or ionic strength) as independent variables and aggregation and zeta potential as dependent variables. In all cases, models utilizing conductivity performed better than those with ionic strength or sulfate. Transformations to reduce non-normality were attempted for each of the independent variables, including log10, inverse, square root, and squared transformations. However, the untransformed data performed slightly better in the regressions, possibly because transformation of the dependent variables was not possible due to zero's (aggregation rate) and negative values (ZP).

The best model for predicting aggregation rate utilized conductivity (coefficient 0.6021, $p < 0.001$) and pH (coefficient -70.60, $p = 0.040$) and resulted in an adjusted R^2 of 0.812. The best model for ZP included conductivity (coefficient 0.01930, $p < 0.001$), pH (coefficient -3.161, $p = 0.010$), and DOC (coefficient -2.623, $p = 0.011$), with an adjusted R^2 of 0.859.

The MLR suggests that in this study, conductivity is the most statistically significant variable driving Fe NP stability in NFCC stream water. For predicting ZP, pH is weighted slightly more than DOC, but both affect ZP similarly. For aggregation however, only conductivity and pH load significantly into the best performing predictive model. It is surprising that DOC appears to affect ZP as much as pH, but is not significant for predicting aggregation. It

is possible that this is simply a reflection of the greater uncertainty in measuring aggregation rate than ZP, resulting in greater difficulty constraining the model.

While it is surprising that conductivity outperforms ionic strength and sulfate in the predictive models, we can propose several explanations. In NFCC, sulfate contributes heavily to ionic strength but cannot account for all dissolved ions interacting with particle EDL's. Ionic strength calculations require assumptions about the abundance of dissolved versus particulate elements (estimated in this study via 0.45 μm filtration) and the nature of the DOC. These assumptions, as well as the compound analytical error of many measurements, contribute to the uncertainty of ionic strength, while conductivity may be more robust due to its reliable measurability in-situ. The strong correlation between conductivity and ionic strength (Figure 3.17) supports the use of conductivity as a proxy for ionic strength.

Further explanation for stability dependence on water composition would require mechanistic experiments beyond the scope of this paper. Therefore, in this amechanistic, nonparametric analysis, conductivity and pH may be considered the variables driving stability with the possibility of DOC playing an additional role.

Table 3.2 Descriptive statistics for dataset examined with multiple linear regression. N, the number of independent observations, is lower for DOC due to several missing replicates and N is very low for pH and conductivity because only single measurements were made.

	N	Mean	SD	Sum	Min	Max
pH	31	7.11	0.53	220.35	6.04	7.83
Conductivity	31	276	262	8555.1	62.7	844
DOC	83	2.29	0.69	199.31	1.19	3.56
Aggregation Rate	93	84	177	7336.59	0	730.
Zeta Potential	93	-16	7.6	-1365.89	-33	4.72

3.4 Conclusions

The trends in hematite stability compliment the observed occurrence of Fe-oxide INPs in NFCC. Although the ZP of pre-treatment INPs was not measured, the ZP of newly formed INPs in water collected during a WTP shutdown in January 2018 was +0.6 mV (s.d. = 2.1, n = 3), similar to that of hematite in pre-treatment water. The contaminated pre-treatment conditions (low pH and DOC, high sulfate and ionic strength) downstream likely resulted in near-zero surface charge and a compressed EDL, inducing rapid hematite aggregation and settling. This behavior in the stability experiments is consistent with the extensive streambed coatings of Fe-

oxide INPs (Figure 3.2b on page 42), the high concentration of large Fe INPs (Figures 3.7 and 3.8 on pages 48 and 49, respectively), and the large aggregates of Fe-rich INPs observed with TEM (Figures 3.9 and 3.10 on pages 50 and 51, respectively) downstream at the beginning of the study.

Hematite suspended in the downstream water was most stable during the early summer, when higher pH, low ionic strength, and high DOC caused increasingly negative surface charge (Figure 3.14a on page 56) and allowed EDL expansion. These chemistry-induced stability changes prohibited aggregation (Figure 3.14b on page 56) and likely promoted dispersion and disaggregation of the INPs, which may have contributed an additional INP-removal mechanism during the scouring period. Both physical and chemical processes thus could account for the decrease in turbidity and color of the water (Figure 3.2b on page 42) and lowering INP number concentrations (Figure 3.7 on page 48). Snowmelt may have been more important for INP removal than AMD treatment in early summer, due to the dilution and physical scouring from the high discharge and velocity (Figure 3.2a on page 42). However, the co-occurrence of AMD treatment and spring runoff events makes assessment of their relative importance for surface chemistry effects and INP removal difficult.

In late summer, the ZP of hematite in downstream water became slightly less negative (Figure 3.14a on page 56) and aggregation rate increased to ~100 nm h^{-1} (Figure 3.14b). This indicates the downstream water was no longer as stabilizing as it had been during early summer, but it still was not nearly as destabilizing as the pre-treatment conditions. The late summer stability decrease could be attributed to the conductivity rebound (Figure 3.4b on page 45) that occurred as the stream approached base flow (Figure 3.2a), as well as DOC concentration decreasing to pre-runoff concentrations (Figure 3.4d). However, the higher pH (Figure 3.4a) appears to have partially offset the destabilizing effect of the conductivity increase and DOC decrease. These chemistry conditions likely caused more EDL compression than the early summer water but more negative surface charge than in March, resulting in some slow aggregation but overall greater stability of any INPs that remained after scouring.

The authors highlight that no previous publications exist on the in-stream behavior of AMD INPs during remediation and that this may be the first study of its kind. As Fe-oxide INPs are expected to be important vectors for related AMD contaminants (i.e. Cu, Zn, As), the greater scope of their fate and transport warrants consideration. We suggest that the combination of

increased NP stability and increased discharge during early summer caused removal of previously aggregated Fe-oxide INPs from the study area and their transport to the lower reaches of the watershed. These stream conditions could also promote graduate release of AMD contaminants from the hyporheic zone. Indeed, an increase in Cu concentrations was observed in October 2017, after the WTP was treating both major AMD sources 24/7 (Figure S3e). Further monitoring of this potential continued Cu release was beyond the scope of the study presented here, but is of interest for future work. A gradual release of accumulated contaminants from the streambed in the months or years following the onset of treatment could have ecotoxicological impacts downstream of the study area, depending on the resultant concentrations. These hypotheses merit serious investigation in future studies.

This novel application of spICP-MS to an AMD system demonstrates its utility for detecting Fe- and Cu-bearing INPs in AMD waters. However, NP characterization in natural waters remains challenging, even with best practices (i.e. next-day analysis, daily transport efficiency calibration, ensuring sample is dilute enough to not exceed one NP per dwell time, use of a statistical algorithm for setting background cutoff). The high instrument sensitivity and assumptions (particle shape and composition) required for the technique may create experimental artifacts as the analytical limit is approached. Therefore, although spICP-MS is useful for observing INPs in an evolving natural water system, we recommend caution and diligence in the data treatment and interpretation.

Based on results of this initial spICP-MS study of remediated AMD waters, the stability of Fe INPs (and thus their role in the fate of metal contaminants) after AMD enters a receiving water is a complex interplay of chemical parameters that can be quantitively predicted as a function of conductivity, pH, and DOC using an amechanistic, MLR approach. Our predictive model for INP stability is site-specific to NFCC, but the general trends are qualitatively predictable based on previous mechanistic studies. Future field studies should continue to utilize surface chemistry theory and the findings of mechanistic studies to explain and predict NP behavior in the environment.

CHAPTER FOUR

QUANTIFYING MINERAL NANOPARTICLE HETERO- AND HOMOAGGREGATION USING SINGLE PARTICLE ICP-MS WITH HIGH RESOLUTION AND TIME-OF-FLIGHT MASS ANALYZERS

L.N. Rand,[1,2*] M.D. Montaño,[3] M. Benedetti,[2] J.F. Ranville[1]

4.1 Background and Previous Studies

The aggregation of nanoparticles (NPs) is of interest due to its role in environmental behavior .[4,14,19,116,117] The most fundamental effect of aggregation is an apparent increase in particle size, which accelerates gravitational settling described by Stokes' Law and can result in more rapid removal from aqueous systems. Another consequence is a decrease in the surface area/volume ratio which decreases the high surface reactivity of NPs. Aggregation can be classified as homoaggregation, when occurring between NPs of the same composition, or heteroaggregation, when involving interactions between different NP materials.

Engineered NPs (ENPs) are typically manufactured for specific applications and therefore tend to have very consistent compositions and are often monodisperse, having a narrow size distribution.[35,117] Conversely, natural NPs (NNPs) are far more variable and polydisperse, having a wide distribution. The expected uniformity of ENPs could make them easier to distinguish from NNPs, but it is unlikely for them to remain unchanged after entering a natural system. Aggregation is expected to be a common alteration to ENPs after environmental release. Although ENPs can be susceptible to homoaggregation, in natural systems they are likely to heteroaggregate with natural NPs (NNPs) due to the greater abundance of NNPs in the environment.[35,116,118] Heteroaggregation alters the properties of ENPs, including surface charge, reactivity, and interactions with NOM, soil, and aquatic organisms, which in turn affects dissolution/degradation rates, NP transport, and toxicity. Therefore, the ability to measure ENP heteroaggregation is critical to understanding their environmental behavior.

Since the theoretical basis for NP aggregation has already been described in previous chapters (sections 1.4 and 3.1), the emphasis in this chapter shall be on instrumentation and

[*]Primary author, [1]Colorado School of Mines, [2]Institut de Physique du Globe de Paris, [3]Universität Wien

experimental methodology for studying aggregation. Briefly, NP stability is favored by the presence of repulsive forces between particle surfaces that promote separation.[29] Aggregation occurs when attractive forces are greater than repulsive forces. Electrostatic forces typically make the most significant contribution toward stability or aggregation, making surface charge an important consideration. NPs whose surfaces are oppositely charged or near the point of zero charge (PZC) tend to aggregate quickly. Additionally, the ionic strength of the medium in which NPs are dispersed can impact stability by affecting the electrical double layer (EDL) of ions surrounding each NP. The EDL provides another source of interparticle repulsion and at high ionic strength, the EDL is compressed and is therefore less of a barrier for aggregation.

Many experimental studies of NP aggregation rely on time-resolved dynamic light scattering (DLS), which calculates hydrodynamic diameter based on the Brownian motion of NPs measured by backscattering.[8,18,35] A major drawback to the technique is that it works best with monodisperse samples and is very prone to artifacts when analyzing a polydisperse system. However, the technique is non-destructive, fast, and works well at low concentrations, making it highly useful for environmental studies despite its limitation. For example, DLS has been used to determine metal oxide ENP aggregation kinetics in different types of synthetic media and natural waters and examine the impact of pH, ionic strength, and natural organic matter (NOM) on stability.[33,96,98,106,119] These and other studies have used DLS experiments to strengthen mechanistic expectations of NP behavior in response to individual variables, which is important for predictive modeling. However, the technique's inaccuracy for sizing polydisperse NPs in complex media makes it unsuitable for measuring ENP and NNP heteroaggregation in environmental samples.

A new device called Turbiscan can examine both size and settling kinetics. Turbiscan utilizes timed, vertical scans across a 40-mL sample column and records transmittance or backscatter intensity, depending on the particle size and concentration regime.[120] The uniformity of the detected light (180° and 135° from the incident light for transmittance and backscattering, respectively) across the sample column and how it changes over time indicate particle stability. For suspensions with low concentrations (< 0.1 vol %) and/or small particles (< 1 μm), as is the case in this study, the transmittance signal is more suitable to use than backscattering.

An overall increase in transmittance results from NP growth or aggregation increasing the clarity of the suspension at all heights. Settling, however, moves NPs from the top of the sample

to the bottom, causing an increase in transmittance at the top and a decrease in transmittance at the bottom.

One published study has shown Turbiscan to be promisingly useful for examining NP aggregation kinetics.[121] However, Turbiscan requires relatively high concentrations (mg L^{-1} or greater) and both Turbiscan and DLS operate with an inherent assumption that all particles within a sample are the same initial size. Additionally, neither of the methods described in the preceding paragraphs is element specific. These are major drawbacks to stability studies on environmentally relevant systems, which are likely to have polydisperse ENPs and NNPs of varying composition heteroaggregating in dilute concentrations.

Single particle ICP-MS (spICP-MS) is a powerful tool for environmental NP analysis, as explained in the preceding chapters of this thesis, due to its sensitivity and element-specificity. It may be possible to use spICP-MS to quantify the extent of NP aggregation in environmentally relevant conditions. The spICP-MS technique is however, more experimentally challenging than DLS for measuring aggregation kinetics. DLS can non-destructively capture NP size, with time resolution on the seconds to minutes scale, within an evolving system. Minimal sample handing is required and experiments can be carried out within the DLS sample cuvette, as was done in the hematite stability experiments in Chapter 3 of this thesis. SpICP-MS is more involved experimentally, often requiring sample dilution. The advantage of spICP-MS is in its ability to follow the increase in size of the NP of interest by tracking the response of its constituent element(s) on a particle-by-particle basis. Only two studies thus far have attempted to employ spICP-MS in an aggregation study. Kim, et al. examined citrate-Ag NPs in very simple artificial media[122] and Donovan, et al. used spICP-MS in a simulated wastewater coagulation study.[123]

We propose that spICP-MS could be used to quantify the extent of NP aggregation in natural waters, based on changes to number concentrations and size distributions. Although measuring aggregation kinetics may be impractical with this technique, the element specificity, low detection limits, and ability to handle polydispersity would improve the environmental relevance of future aggregation work.

Modifications to the mass analyzer of spICP-MS instruments have made exciting improvements to its use in environmental studies. The most common spICP-MS instruments use one or more quadrupoles (ICP-QMS) to separate elements by mass before reaching the detector, resulting in the measurement of only one isotope in each NP at a mass resolution of 0.07 amu.

High resolution (HR) instruments use a magnetic sector (ICP-HRMS) that is capable of resolving isotopic interferences down to 0.1 amu. This eliminates much of the high background signal that plagues ICP-QMS analysis of environmental samples, allowing for lower mass and size detection limits. Both methods can allow for time-resolved measurements of single-element mass that allow aggregation studies. SpICP-MS could be ideally-suited to studying heteroaggregation if multiple elements could be measured in each heteroaggregate particle. Time-of-flight (TOF) instruments simultaneously quantify all elements in a sample rather than separating them prior to analysis by the mass spectrometer. The development of commercial spICP-TOFMS instruments has generated much excitement in environmental NP research, because of the ability to fully characterize the elemental makeup of unknown NPs in the environment, possibly even distinguishing ENPs from NNPs.[40,57,124,125] The multi-element capabilities of the TOF could also allow for quantification different types of NPs within a heteroaggregate. The trade-off for this advantage however is poorer sensitivity of the TOF over that of the other instruments. A recent publication compared quadrupole and TOF instruments for analyzing ENPs,[125] but a comparative study between HR and TOF instruments would also be valuable.

The main focus of this study is in examining the capability of spICP-HRMS to detect and possibly quantify ENP and NNP aggregates and heteroaggregates. The working hypothesis is that spICP-HRMS can detect NP aggregation based on an increase in measured NP sizes. This was tested by comparing samples of NPs that are either stable or well aggregated, in order to determine if a difference in size distribution between the two is measurable. Artificial media were used to either maximize or minimize aggregation for the given NP system. “Unstable” samples had high ionic strength and a pH near the PZC while “stable” samples had low ionic strength and pH far enough from the PZC that NPs would not aggregate. By starting with the simplest case of comparing two extremes, this important hypothesis test will help determine robustness before moving on to more complicated scenarios in future studies. This work requires that aggregates remain intact through the sample uptake system of the ICP. This was tested by comparing the size distributions obtained through spICP-MS to those obtained from Turbiscan and conventional particle sizing methods.

A second hypothesis is that spICP-TOFMS can detect heteroaggregation between multiple types of NPs by measuring co-occurring peaks of the principal element of each NP. While individual NPs will only produce single-element pulses, heteroaggregated NPs will

produce simultaneous pulses of multiple elements, assuming that each of the NPs used have different compositions. Furthermore, heteroaggregates will result in pulses of greater magnitude, indicating greater size.

The proof-of-concept experiments outlined in this chapter describe the results of testing these hypotheses, with the intent of establishing the basic capabilities of spICP-HRMS and spICP-TOFMS to study aggregates and heteroaggregates. This effort to improve methods for measuring (hetero)aggregation in a natural sample will prove valuable in future environmental studies of NPs.

4.2 Materials and Methods

The following section describes the experimental protocols for CeO_2, goethite, and kaolinite NP aggregations, spICP-MS analyses, and Turbiscan analyses.

4.2.1 Aggregation Experiments

CeO_2 (30 nm, NanoTek CE-6042 from Alfa Aesar) was chosen as a representative ENP for these experiments and goethite (50-70 nm, synthesized, purified, and dried according to Hiemstra, et al.[126]) and kaolinite (< 2 µm, KGa-2 from the American Clay Mineral Society, size separation, wash, and drying described by Guinoisseau, et al.[127]) were chosen as representative NNPs. All NP stock suspensions were sonicated for 15 min in a water bath prior to use for making aggregation samples.

Artificial media in ultrapure milliQ water were formulated in order to maximize or minimize aggregation for the given NP system. “Unstable” samples had high ionic strength due to added $MgCl_2$ (EMD Millipore, analytical grade) and a pH near the PZC while “stable” samples had low ionic strength and pH far enough from the PZC that NPs would not aggregate. The PZC is a material-dependent property and is around pH 6 for CeO_2,[96] pH 4 for kaolinite,[30] and pH 7.5 for goethite.[34] Depending on the expected PZC and desired NP interactions, 10 mM nitric acid (BDH, trace metal grade), MES buffer (VWR, 99.5%), or HEPES buffer (Alfa Aesar, 99%) was added to the solutions to obtain a pH of 2.0, 6.1, or 7.5, respectively.

Samples were prepared with total NP concentrations of 100 mg L^{-1} the day before analysis and allowed to aggregate overnight. The CeO_2 homoaggregation samples were made with 100 mg L^{-1} CeO_2 and 10 mM HNO_3 for stable conditions; or 100 mg L^{-1} CeO_2, 10 mM HEPES, and 100 mM $MgCl_2$ for unstable conditions. Goethite homoaggregation samples were made with 100 mg L^{-1} goethite and 10 mM MES for stable conditions; or 100 mg L^{-1} goethite, 10

mM HEPES, and 100 mM $MgCl_2$ for unstable conditions. Goethite/CeO_2 heteroaggregation samples were made up of 50 mg L^{-1} CeO_2, 50 mg L^{-1} goethite, and 10 mM MES for stable conditions; or 50 mg L^{-1} CeO_2, 50 mg L^{-1} goethite, 10 mM HEPES, and 100 mM $MgCl_2$ for unstable conditions. Goethite/kaolinite heteroaggregation samples were made with 50 mg L^{-1} goethite, 50 mg L^{-1} kaolinite, and 10 mM MES for stable conditions, or 50 mg L^{-1} goethite, 50 mg L^{-1} kaolinite, 10 mM HEPES, and 100 mM $MgCl_2$ for unstable conditions.

4.2.2 Turbiscan Analysis

Turbiscan aggregation experiments were carried out using a Formulaction Turbiscan LAB™ stability and size analyzer with data processing in the computer program Turbisoft 2.0. The analysis method was set to scan the sample at 5 min intervals for the first hour, 10 min intervals for the second hour, then at 60 min intervals after that. Samples were prepared at the concentrations described in section 4.2.1 in 40-mL, glass Turbiscan vials, immediately placed in the sample holder, and the method was initiated as soon as the sample holder lid was closed. After completion, the top height of the scan data was truncated at the sample meniscus and transmission data was selected for processing and interpretation.

4.2.3 SpICP-MS Analysis

SpICP-MS aggregation experiments were carried out on fully aggregated 10-mL samples with the compositions described in section 4.2.1 within HDPE Falcon™ test tubes. After being allowed to settle overnight, the upper 8 mL from the top of the sample test tube was removed and discarded. Any aggregates settled at the bottom were then gently mixed into the remaining 2 mL before removing 100 µL for dilutions. Samples were diluted in triplicate from 10^4 to 10^6 times and mixed very gently by several inversions between each dilution step.

Analysis by spICP-HRMS was carried out on a Thermo Element 2 high resolution ICP-MS, using a flow rate of 0.2 mL min^{-1} and dwell time of 1 ms under medium resolution mode for measuring Fe and low resolution mode for measuring Ce. Dissolved calibration standards for Ce, Fe, and Au at 0, 10, 100, 1000, 10000 ng L^{-1} and triplicate 60 nm 500 ng L^{-1} Au NP standards (BBI) were prepared the day of analysis. Transport efficiency was calculated using the method described by Pace, et al.[41] and was typically around 7%. Spherical particle sizing was determined from the Fe pulses assuming the composition and density of goethite, and from the Ce pulses assuming the composition and density of CeO_2.

Analysis by spICP-TOFMS was carried out on a TOFWERK icpTOF using a flow rate of 0.28 mL min^{-1} and dwell time of 3 ms. The TOF mass calibration was done using the Thermo Tune B solution (1 µg L^{-1} Ba, Ce, In, U, Bi, Co, Li). Dissolved Ce, Fe, and Au calibration standards (trace certified, Sigma) were prepared at 0, 1, 2, 5, 10, 20, 50 µg L^{-1} and triplicate 100 nm Au NP standards (BBI) were prepared at 500 ng L^{-1} on the day of analysis and a transport efficiency of approximately 5% was determined.

4.3 Results and Discussion

The following sections detail the outcomes of the experiments to examine homo- and heteroaggregation using Turbiscan and spICP-MS with HR and TOF analyzers.

4.3.1 Tubiscan Kinetics of Homo- and Heteroaggregation

Turbiscan transmittance scans over the sample height at the programmed measurement intervals indicated that all aggregation systems exhibited both NP growth and sedimentation in the unstable media over 24 h (CeO_2 homoaggregation in Figure 4.1; see Appendix B for all other experimental data). CeO_2 homoaggregation was especially rapid, with complete sedimentation taking place within 4 h based on the global Turbiscan stability index (TSI), which combines transmittance data across the entire sample height. For the experimental systems involving goethite or kaolinite, aggregation was initially fast and then continued slowly. Goethite/kaolinite heteroaggregation, goethite homoaggregation, and goethite/CeO_2 heteroaggregation took approximately 6, 8, and 12 h, respectively for 90% of the total TSI change to occur. The remaining 10% of the total TSI change measured occurred slowly over the remainder of the 24 h period.

The variable kinetics in aggregation systems with goethite NPs could result from the greater heterogeneity of NP surfaces (defects being common on mineral surfaces), causing more variable surface charge and charge-based interactions between NPs. Additionally, the goethite NPs are expected to be more polydisperse, and a wide range of sizes would cause more variable Brownian motion and therefore a greater range in NP collision kinetics. A prior study on hematite stability found that smaller NPs had lower theoretical interaction energy barriers and were also more strongly impacted by changes in ionic strength.[73] It has also been suggested that smaller NP sizes have a higher surface area than large NPs and therefore higher surface energy.[128] Since systems tend toward minimal surface energy, small NPs aggregate more readily

than bigger NPs. The CeO_2 NPs, on the other hand, likely have a narrow size range and more homogenous surfaces which lends them to more uniform collision kinetics.

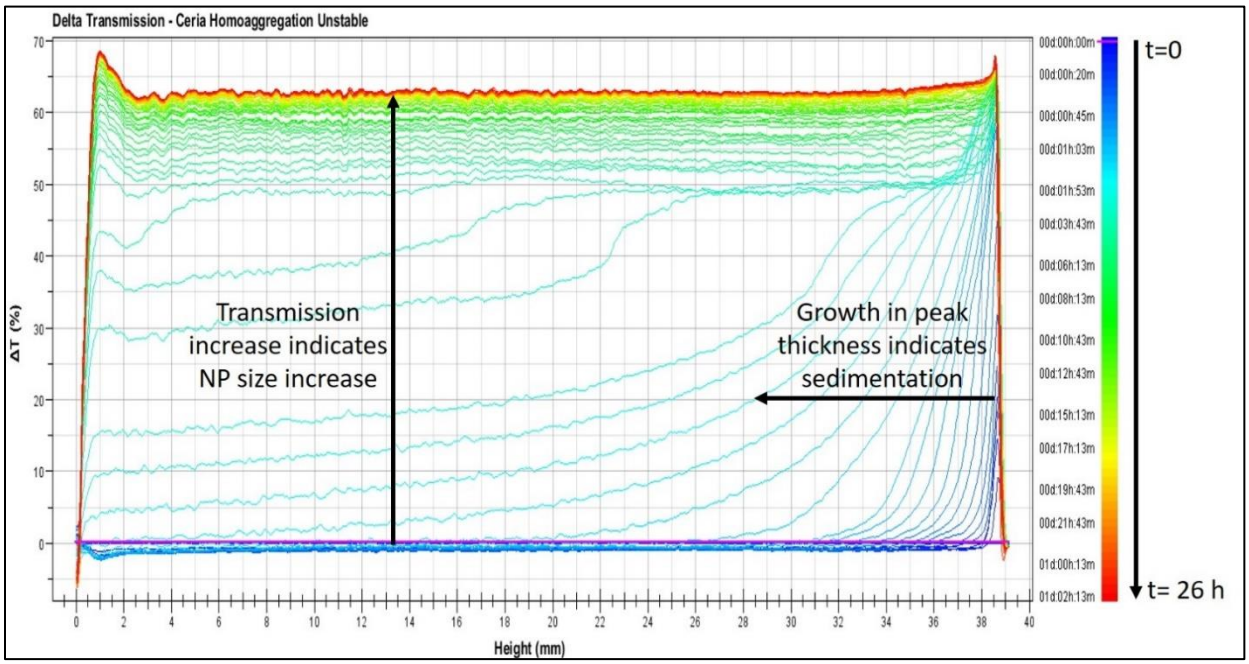

Figure 4.1 Turbiscan change in transmission of CeO_2 NPs suspended in unstable medium, across the entire sample height (x-axis, mm from the bottom of the test tube) at each scheduled timepoint (color bar). Transmission increased over time, particularly in the first 3 h, indicating NP flocculation. A peak appeared immediately at the top of the sample height and then widened rapidly, indicating that NP sedimentation occurred quickly.

The Turbiscan measurements also indicated that some aggregation occurred in the stable samples of goethite, goethite and kaolinite, and goethite and CeO_2 (see Appendix B). This was measured by an increase in transmission across all sample heights, and is consistent with the visual observation of some settled aggregates in the 24 h old stable samples (Figure 4.2 on page 71). While the stable media in the mineral homo- and heteroaggregation experiments restricted aggregation much more than the unstable media, they appear not to have prevented aggregation completely.

4.3.2 Benchtop Observations

The effectiveness of the stabilizing versus destabilizing solution conditions was confirmed visually in a benchtop experiment. Aggregation and sedimentation became visible within hours and was seemingly complete after allowing 24 h of aggregation. NPs suspended in unstable media had settled completely, leaving the media clear with large aggregates at the

bottom of the test tube (Figure 4.2). NPs suspended in stable media remained cloudy and red (if goethite included) or white (if CeO_2 homoaggregation). A few settled aggregates were observed in the suspensions including goethite and kaolinite, but none were observed in the CeO_2 homoaggregation suspension.

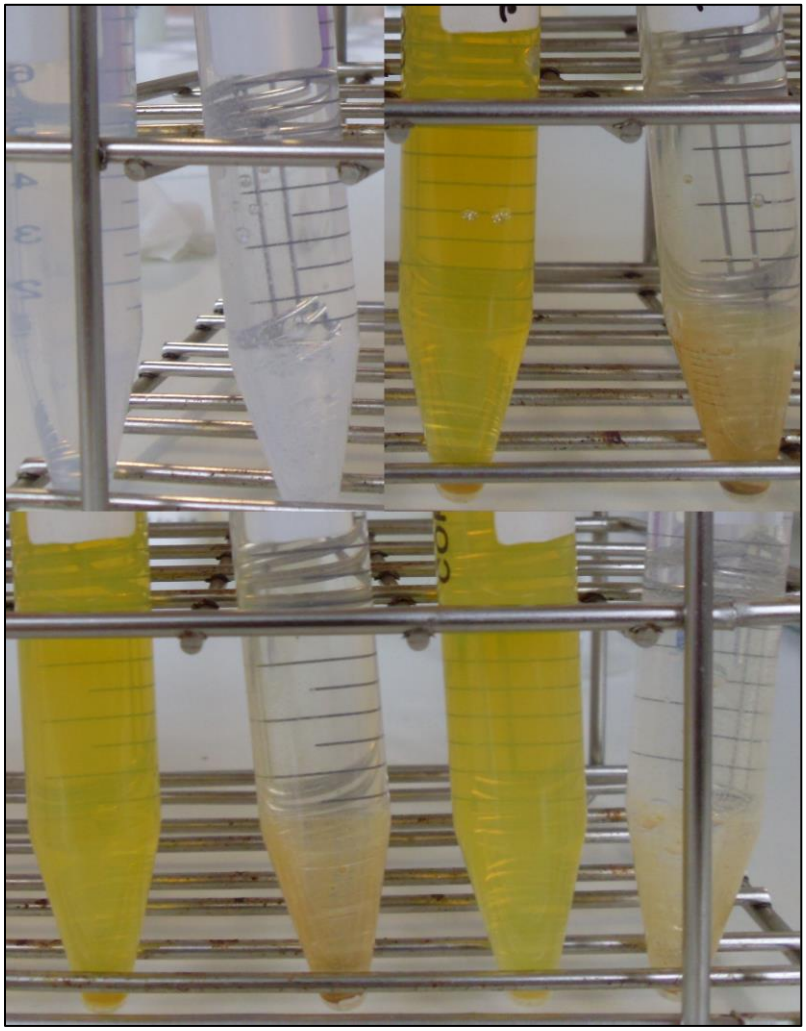

Figure 4.2 NP suspensions after 24 h that had been prepared in stable versus unstable media. From left to right and top to bottom, CeO_2 stable and unstable, goethite stable and unstable, goethite/kaolinite stable and unstable, goethite/CeO_2 stable and unstable. All suspensions in stable media remained cloudy and colored by next day (with some settling occurring in samples with kaolinite and goethite minerals) whereas the unstable suspensions became clear with aggregates settled on the bottom of the test tubes.

4.3.3 Measuring Aggregation with spICP-HRMS

Although limited aggregation may have occurred in some of the stable samples, this section will refer to the NPs in stable media as “non-aggregated” and the NPs in unstable media as “aggregated”. While the upper and lower bounds of NP sizes measured by spICP-HRMS was

similar between both aggregated and non-aggregated samples, the number-based distributions maximum shifted toward larger sizes (Figure 4.3 on page 74) in the unstable samples. The non-aggregated and aggregated mean sizes had overlapping standard deviations, for example, CeO_2 increasing from 23 ± 16 nm to 44 ± 19 nm (Table 4.1). This does not suggest that the particles were very different in stable and unstable media, even though the settling in the unstable media suggest this should have been the case. However, the mean size is a limited metric and much information about the nature of the distribution as a whole is lost in calculating it.

Table 4.1 Means and standard deviations of NP sizes measured by spICP-HRMS in all homo- and heteroaggregation experiments at 24 hours. Most experimental replicates produced significant differences in size distributions between aggregated versus non-aggregated samples (Mann-Whitney U Test, $\alpha = 0.05$). In comparing the amount of pulse clumping in aggregated versus non-aggregated samples, many but not all experimental replicates produced significant differences in clumping variance (Levene's Test, $\alpha = 0.05$) except goethite homoaggregation, which produced no clumping differences in any of the trials. Statistically significant p-values are shaded in green, whereas non-significant p-values are shaded in yellow.

Experiment	**Replicate**	**Non-Aggregated Size (nm)**		**Aggregated Size (nm)**		**p-Value Comparing Size Distributions**	**p-Value Comparing Clumping Variance**
		Mean	**Std Dev**	**Mean**	**Std Dev**		
CeO_2/CeO_2	1	26	16	44	19	<1E-20	1.93E-08
	2	30	17	45	18	<1E-20	3.43E-06
	3	29	16	39	22	<1E-20	4.66E-10
	4	27	15	31	23	0.4484	1.94E-11
Goethite/ Goethite	1	51	24	57	27	0.00141	0.1187
	2	53	25	64	34	1.06E-20	0.31035
	3	55	22	83	36	<1E-20	0.10757
CeO_2/Goethite Fe detection	1	53	23	75	39	3.00E-11	5.40E-08
	2	52	20	65	32	0.21375	1.23E-07
	3	59	24	79	34	<1E-20	0.27315
	4	54	24	72	31	<1E-20	0.98763
CeO_2/Goethite Ce detection	1	29	15	45	19	<1E-20	0.00651
	2	25	14	43	19	8.96E-13	2.50E-09
	3	27	17	50	22	<1E-20	0.11814
	4	25	16	47	22	<1E-20	1.75E-03
Goethite/ Kaolinite	1	60	30	82	44	1.54E-05	0.02195
	2	57	21	76	37	0.00993	2.23E-04
	3	55	25	77	35	<1E-20	0.06031

Although little difference is seen between mean sizes, significant differences are observed in the size distributions. The difference in the shape of the distribution and the most frequent size is particularly striking for the Ce NPs in CeO_2 homoaggregation and CeO_2/goethite heteroaggregation (Figure 4.3a and d on page 73). The most frequent sizes of Fe NPs in goethite homoaggregation, CeO_2/goethite heteroaggregation, and goethite/kaolinite heteroaggregation changed less dramatically, with the main result being a widening of the distribution curve instead of a change in shape (Figure 4.3 b, c, and e on page 73). The Mann-Whitney U-Test ($\alpha = 0.05$) was used to compare all size observations of aggregated versus non-aggregated samples and indicated that their distributions are significantly different from each other in nearly all replicates of the homo- and heteroaggregation experiments (Table 4.1 on page 72). This is strong evidence in support of the first hypothesis that aggregation can be detected with spICP-HRMS.

The assumption that aggregates remain intact during sample uptake to the instrument plasma is important for any future SP applications attempting to quantitatively measure the extent of aggregation. Based on the size distributions obtained in the homo- and heteroaggregation experiments (Figure 4.3 on page 73), it appears that small aggregates up to 200 nm can be transported to the plasma intact. The aggregates formed in the sample were large enough to settle within 24 h however (Figure 4.1 on page 70, Figure 4.2 on page 71), which is not consistent with largest NP sizes reported. Based on Stokes' Law settling calculations, an 80 nm CeO_2 homoaggregate would require 22 days to settle 40 mm and a 200 nm goethite homoaggregate would take 7 days. Clearly larger aggregates must have been formed that were not measured by instrument. Additionally, a number of NPs at or close to the original sizes were measured in all aggregated samples, suggesting disaggregation occurred before plasma ablation. The disaggregation may have occurred during dilutions preceding ICP analysis, though care was taken to mix gently and minimize time between dilution and analysis. It is also possible that aggregates were sheared apart by transport through the sample line and peristaltic pumps prior to injection into the plasma.

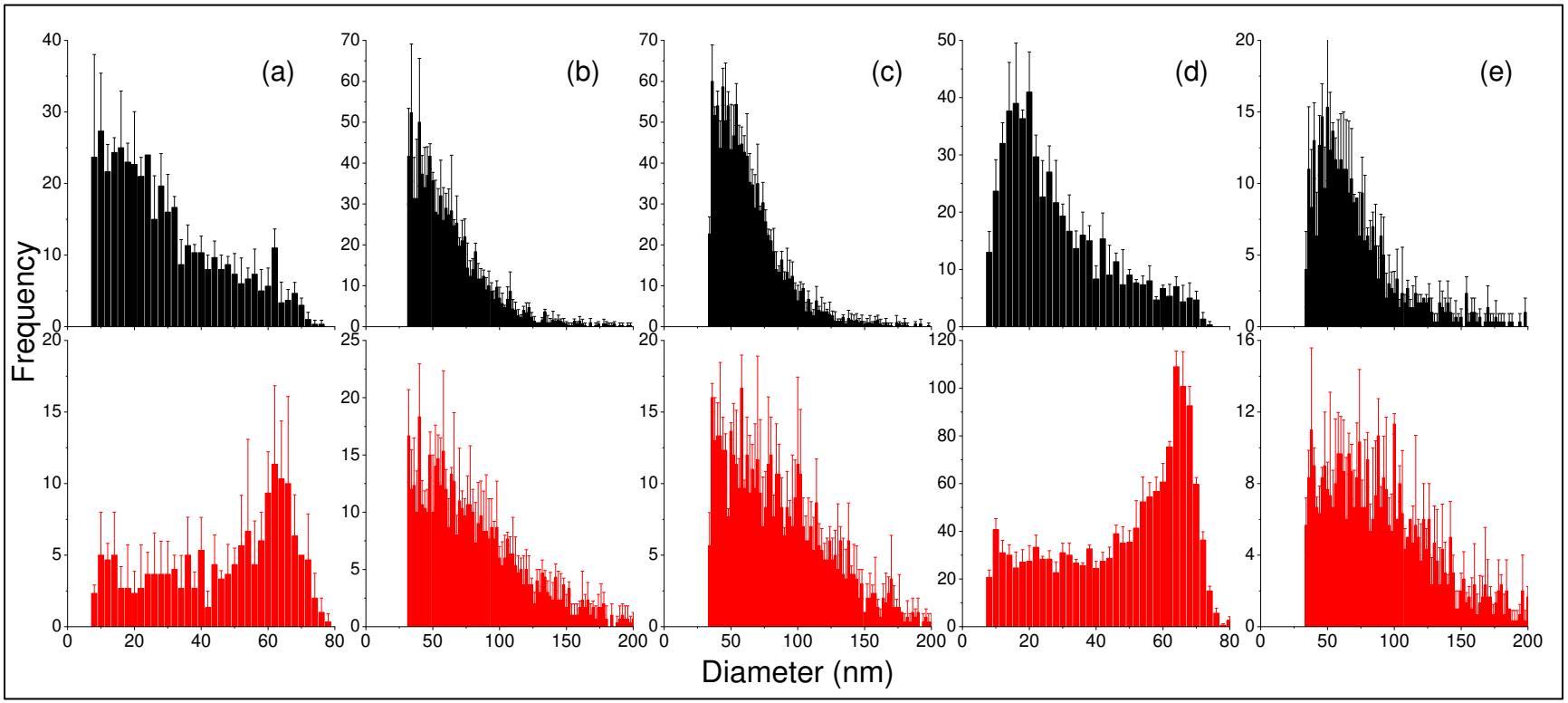

Figure 4.3 SpICP-HRMS size histograms of non-aggregated (top, black) and aggregated (bottom, red) (a) CeO_2, (b) goethite, (c) CeO_2 and goethite with Fe detection, (d) CeO_2 and goethite with Ce detection, and (e) goethite and kaolinite with Fe detection. Error bars represent the standard deviation of triplicate samples Size distributions shift toward larger sizes in aggregated samples and most experimental replicates produced significant differences between aggregated and non-aggregated distributions (Mann-Whitney U Test, $\alpha = 0.05$).

A particularly interesting result of the spICP-HRMS measurements is the observation of signal "clumping" in the raw SP data. A typical SP analysis will show regularly occurring NP peaks spaced evenly across the scan time (Figure 4.4a). In contrast, aggregated NP samples generated peaks that occurred at variable frequencies over the analysis (Figure 4.4b). In order to quantify the extent of clumping in various samples, the number of pulses in each one-second interval were counted, then normalized by the average pulses per second. Non-aggregated samples most frequently produced 3 NP pulses per second, and at most 4.5 pulses per second (Figure 4.4c, Figure 4.5 on page 76). The clumping in aggregated samples however, produced as much as 14 pulses in a 1-second block of CeO_2 homoaggregation scan time. The width of the distribution, resulting from scan data ranging from many to no pulses per second, indicates the range of clumping in the dataset.

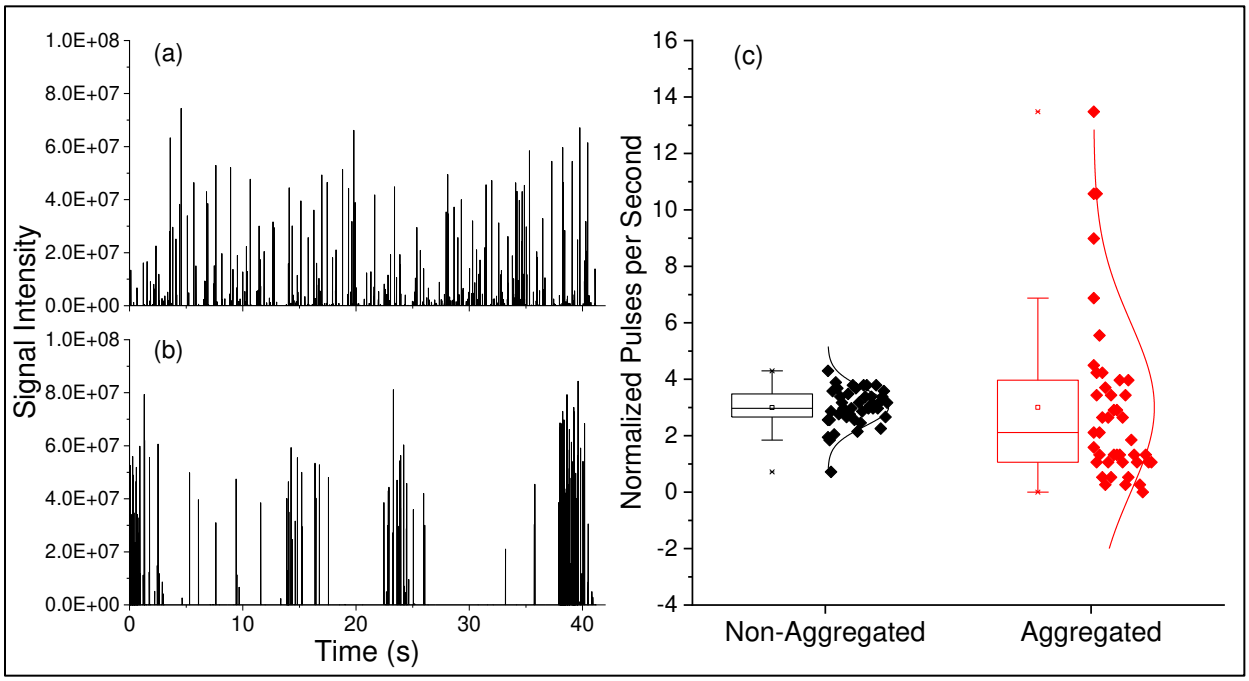

Figure 4.4 Ce signal across 42 s scan time of spICP-HRMS data collection in (a) a non-aggregated CeO_2 homoaggregation sample and (b) an aggregated CeO_2 sample. The clumping effect visible in the aggregated sample could be explained by large aggregates breaking into small aggregates immediately before entering the plasma. (c) The distribution of the number of pulses counted in each second of analysis normalized by the entire scan time average is narrow for the non-aggregated sample (left, black) and wide for the aggregated sample (right, red). Levene's test ($\alpha = 0.05$) indicates that the variances of the aggregated versus non-aggregated samples are significantly different from each other.

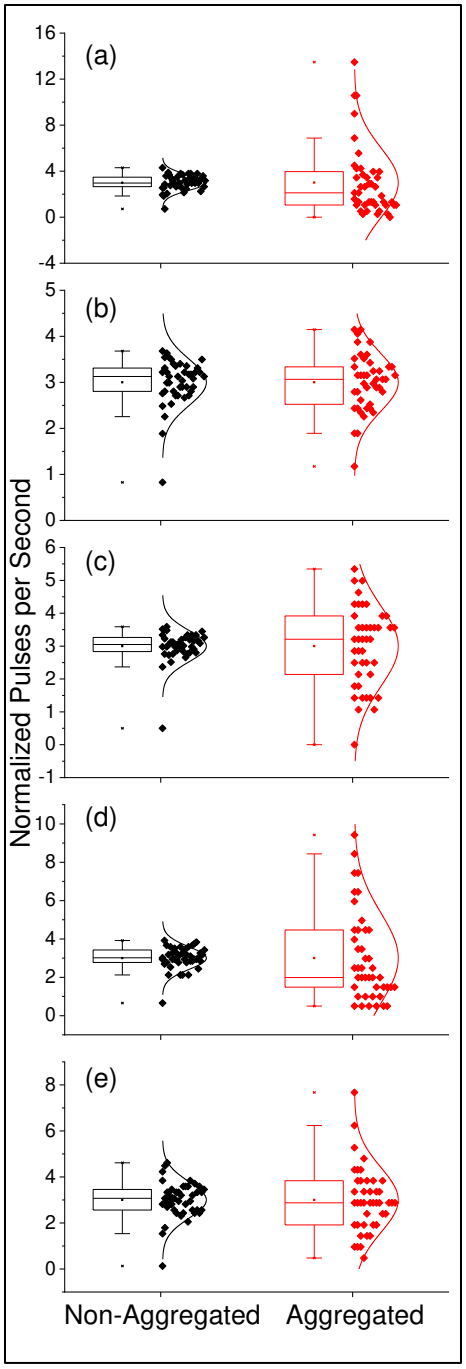

Figure 4.5 Normalized distributions of the number of NP pulses in each second of spICP-HRMS scan time for non-aggregated (black, left) and aggregated (red, right) samples of (a) CeO_2, (b) goethite, (c) goethite and CeO_2 with Fe detection, (d) goethite and CeO_2 with Ce detection, and (e) goethite and kaolinite with Fe detection. In all experiments except goethite homoaggregation (b), aggregated samples produced pulse clumps, whereas non-aggregated samples produced pulses more evenly across the scan time (medians of 3 pulses per second; typical interquartile range of 2.5-3.5 pulses per second). The variances of the aggregated versus non-aggregated samples are significantly different (Levene's Test $\alpha = 0.05$) in each experiment shown here except goethite homoaggregation.

The clumping distributions in Figure 4.5 on page 77 were compared between aggregated and non-aggregated samples in each experiment and tested for equal variance using Levene's Test (Table 4.1 on page 72). This indicates that the phenomenon is particularly pronounced in the CeO_2 homoaggregation experiments, whose aggregated samples have much more NP pulse clumping than the non-aggregated samples and generated p-values < 0.05 for each replicate. Some significant clumping was also observed in goethite/kaolinite heteroaggregation and when detecting Ce in goethite/CeO_2 heteroaggregation, but with less reproducibility between experimental replicates. No goethite homoaggregation experiments yielded detectable differences in clumping between aggregated and non-aggregated samples. Regardless, the clumping occurred in enough aggregated samples that it appears to be a measurable product of aggregation, rather than a one-time anomaly.

A proposed explanation for the clumping effect is that each clump of pulses is produced by a large aggregate that comes apart immediately before entering the plasma, producing a burst of small aggregates and discrete NPs that translate into a series of ion pulses. If the suspension is dilute enough for a second or more to pass between each aggregate introduction, the sample would be expected to produce a scan of irregular pulse clumps such as in Figure 4.4b on page 75. The breaking of large aggregates immediately before entry to the plasma would also explain why more large sizes were not observed in samples that were fully aggregated (i.e. settled) before analysis.

The clumping could be useful as an indicator of aggregation, though it occurred more reliably in CeO_2 aggregation than when goethite was measured. If clumping is produced from aggregates as suggested above, it is unclear why it was not detected in the goethite homoaggregation trials, despite the other indications that aggregation did occur. Mineral NNPs are typically more polydisperse than ENPs, since their formation pathways are less tightly controlled. Perhaps greater NP polydispersity, and subsequently a greater range of aggregate sizes, leads to less discernible clumping in aggregation with NNPs. This speculation requires further investigation to substantiate, but even if it is less useful for NNPs than ENPs, quantifying the raw signal clumping could be a helpful means of detecting the presence of aggregates in spICP-MS analysis.

4.3.4 Detection of Heteroaggregates with spICP-TOFMS

Attempts to repeat CeO_2/goethite heteroaggregation using spICP-TOFMS were met with limited success. The multi-element capability of the TOF mass analyzer allowed for the detection of co-occurring Ce and Fe peaks, providing strong evidence for the formation of heteroaggregates (Figure 4.6). The trade-off for the advantage of multi-element detection however is poorer sensitivity and higher detection limits on the instrument with the TOF mass analyzer. As a result, fewer NPs were detected and very few heteroaggregates were detected, making the estimation of quantitative parameters, such as concentration and size distribution, highly uncertain. Using a cutoff of 10 counts for Fe and 1 count for Ce to separate NP pulses from background, the total number of Ce and Fe peaks were 184 and 93, respectively. Only 23 peaks contained both Fe and Ce, making up 25% of the Fe peaks and 12.5% of the Ce peaks. This suggests the likelihood of a mixture of both homo- and heteroaggregates forming in the goethite/CeO_2 experiment. Furthermore, clumping was not observed on this instrument.

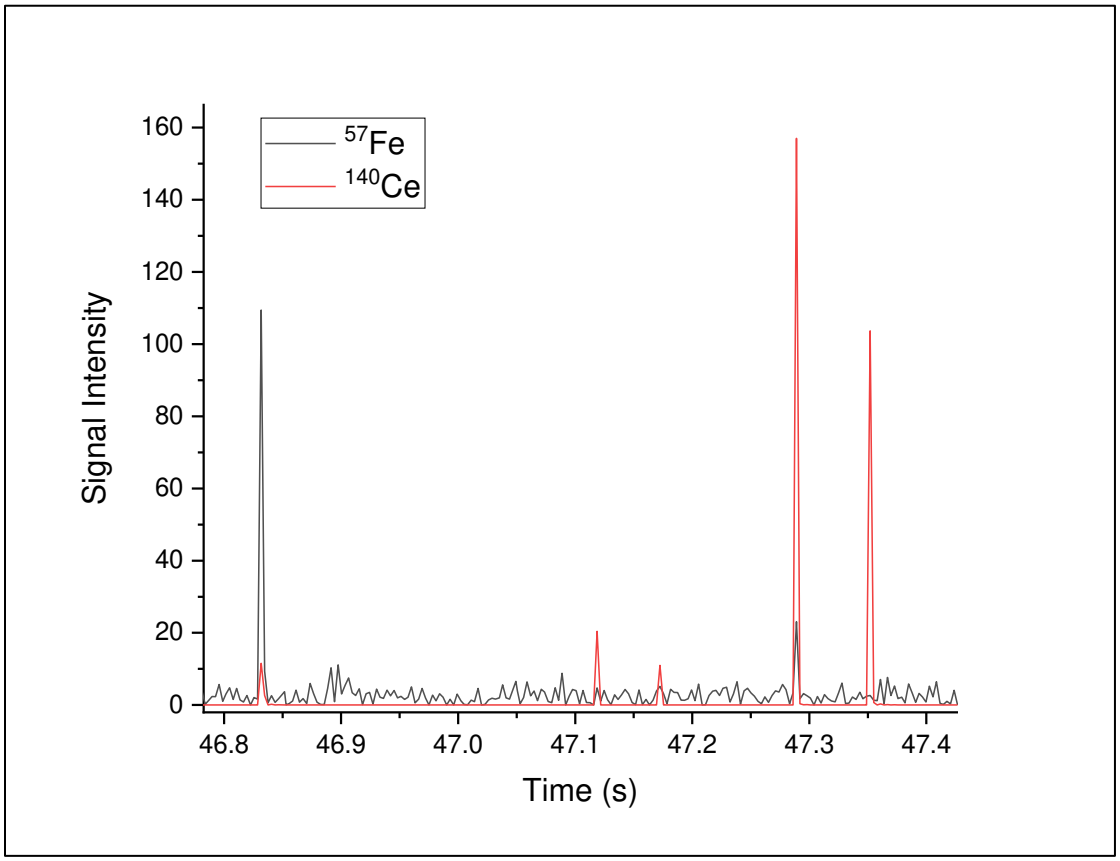

Figure 4.6 ^{57}Fe (black) and ^{140}Ce (red) signal over 0.6 s of spICP-TOFMS analysis time. Two instances where Fe and Ce peaks co-occur are visible at 46.84 s and 47.29 s.

This preliminary study provides proof-of-concept evidence that spICP-TOFMS can be used to measure multiple elements within a heteroaggregate, but more work is need to refine the detection capabilities of this new instrument. Future studies should focus on lowering NP size detection limits and determining optimal run conditions for generating the quality of NP information that should be possible with this instrument.

4.4 Conclusions

This initial study of homo- and heteroaggregation with spICP-MS supports that at least with the HR mass analyzer, the single particle technique is a good candidate for the detection and (in simple scenarios) quantification of aggregates. Significant shifts in size distributions and the regularity of NP pulse occurrence (i.e. clumping) was observed in nearly all trials of CeO_2 homoaggregation, goethite homoaggregation, CeO_2/goethite heteroaggregation, and goethite/kaolinite heteroaggregation.

The data suggest that while small (< 200 nm) aggregates remain intact through spICP-MS sample uptake system, large aggregates are broken apart before entering the plasma. Given that overnight settling was observed visually and via Turbiscan, larger pulses would be expected if aggregates were to remain intact until ablation. Future work should examine the stability of aggregates in ICP sample uptake systems, as the extent to which aggregates are sheared apart in uptake likely varies between the equipment (tubing, peristaltic pumps, nebulizer, spray chamber) and the conditions (flow rate, temperatures, analysis delays) of different laboratory set-ups.

SpICP-TOFMS can detect heteroaggregates by the presence of multiple simultaneous element peaks. Lower sensitivity currently restricted its use in this study, but with larger particles, it could be possible to quantify the amount of different types of NPs within a heteroaggregate. Continued work developing application methods for this instrument will likely resolve these problems.

Future work should also examine the possible use of spICP-MS in aggregation and settling kinetics. In experiments designed with weaker aggregation forces resulting in slow formation of aggregates less than 200 nm, it should be possible to obtain time-resolved size distributions with spICP-MS. A system with strong aggregation and settling should exhibit decreasing NP concentrations in the supernatant with time. These ideas would make for interesting hypotheses to test as the full potential, and limitations, of the technique continue to be explored.

CHAPTER FIVE
SUMMARY AND CONCLUSIONS

5.1 Summary of Dissertation Research Findings

The first research project, Quantifying Temporal and Geographic Variation in Sunscreen and Mineralogic Ti-containing Nanoparticles in Three Rivers During Recreational Use (Chapter Two), tested the following hypotheses: 1) Ti and oxybenzone concentrations during stream recreation differ significantly from those during non-recreation periods. 2) Elevated Ti and oxybenzone concentrations occur in multiple recreational stream systems. 3) Elevated Ti during stream recreation is caused by suspension of natural nanoparticles (NNPs) from bed sediments. This was done in two sampling campaigns, one emphasizing temporal variability over a week of intensive sampling in Clear Creek, CO and the other emphasizing reproducibility at multiple geographic sites and nanoparticle (NP) specific analyses.

Both sampling campaigns supported the hypothesis of significant changes to Ti and oxybenzone concentrations during stream recreation. However, shifts in the natural Ti background due to a storm event and high variability during recreation periods rendered detectability of an anthropogenic effect challenging in the temporal variability study, resulting in only one sampling day in which recreation concentrations were significantly different. The three-river sampling campaign yielded significant differences in oxybenzone during versus outside of recreation use in all streams, and significant changes to Ti mass concentrations in Clear Creek and Salt River, but not Truckee River. Ti NP analysis with single particle ICP-MS (spICP-MS) revealed significant increases in NP concentrations and size distributions for Clear Creek and Salt River, supporting the hypothesis that Ti is elevated during recreation due to bed sediment resuspension.

The second project, Characteristics and Stability of Incidental Iron Oxide Nanoparticles During Remediation of a Mining-impacted Stream (Chapter Three), examined the hypothesis that remediation-induced water chemistry changes would mobilize Fe-oxide incidental nanoparticles (INPs) via increased INP stability in the North Fork of Clear Creek. The research approach to test this hypothesis was to monitor stream water chemistry and Fe- and Cu-containing INPs during the first six months of remediation and examine model Fe INP zeta potentials (ZPs) and aggregation rates when suspended in filtered field waters.

A decrease in INP size and concentrations determined by spICP-MS was observed over the course of remediation and spring snowmelt. The aggregation rate of hematite, a model Fe-oxide INP, decreased over the same time period and correlated inversely with conductivity and positively with pH and DOC, allowing for the creation of a multiple linear regression predictive model. Surface charge likely played a pivotal role influencing INP stability, since aggregation was highest when ZP was near zero and aggregation decreased as ZP became strongly negative, likely due to the pH increase of the water. Physical scouring from increased water velocity during spring snowmelt likely accelerated INP removal, but the experimental evidence supports that chemistry-induced stability changes likely played a role in changes to the INP population in the North Fork of Clear Creek.

The final study, Quantifying Mineral Nanoparticle Hetero- and Homoaggregation Using Single Particle ICP-MS with High Resolution and Time-of-flight Mass Analyzers (Chapter Four), evaluated the hypotheses that 1) spICP-HRMS can detect NP homo- and heteroaggregation based on an increase in measured NP sizes and 2) spICP-TOFMS can detect heteroaggregation between multiple types of NPs by simultaneously detecting multiple elemental pulses caused by the primary element of each NP. These hypotheses were tested by comparing 24-hour old NP suspensions in artificial media that promoted stability versus aggregation in spICP-HRMS and spICP-TOFMS, after confirming aggregation and settling kinetics with Turbiscan analysis.

The spICP-HRMS analysis indicated larger sizes for aggregated samples of CeO_2, goethite, goethite and CeO_2, and goethite and kaolinite than non-aggregated (stable) samples. Changes to size distributions were significant but only small aggregates were measured, up to 200 nm for goethite and 80 nm for CeO_2. Larger aggregates were likely broken up during sample introduction, which would also account for a clumping effect observed in the NP pulses over time in aggregated samples only. Quantifying the clumping in various samples and comparing variances may serve as an additional means to detect aggregates in spICP-MS samples. Finally, examining goethite and CeO_2 samples with spICP-TOFMS yielded co-occurring peaks of Fe and Ce, supporting that this technique is capable of detecting heteroaggregated NPs.

5.2 Future Research

The study on sunscreen and mineralogic Ti NPs in recreational streams over Labor Day weekend demonstrates the importance of establishing background and sampling variability when

attempting to measure ENP inputs to streams. The large number of samples collected and use of different sampling locations allowed for a more robust statistical analysis than previous studies, and future work should consider this approach to improve the certainty of an anthropogenic signal. The wide range of concentrations observed from high frequency sampling during recreation suggests a high degree of variability when measuring poorly-dispersed substances in dynamic systems. This poses a problem, since grab samples are often used in NP studies to represent the system as a whole at a given point of time. Better sampling representativeness could be obtained by using sampling schemes that integrate across multiple widths and depths of the stream cross section

Using spICP-MS to determine concentrations and sizes of INPs formed by mine drainage to the North Fork of Clear Creek alongside water chemistry monitoring and model INP stability experiments allowed for the creation of a predictive model of INP responses to chemistry variables. With this approach, stream INP behavior could be compared to expectations based on surface chemistry theory and established mechanisms of NP stability. This provides compelling evidence for the processes influencing INP behavior during remediation and seasonal changes from snowmelt. While laboratory studies of NP stability in artificial media are essential to determining NP interaction mechanisms, this hybrid approach combining model experiments with field sample analyses should be employed in future studies to further our understanding of NP behavior in real environmental systems.

Future work should continue to examine how homo- and heteroaggregates of NPs are quantified by different spICP-MS instruments and establish their detectability using this technique. While this dissertation research established that aggregates are qualitatively detectable with this method using high resolution and time-of-flight mass analyzers, more work is needed to determine whether and under what conditions the technique can quantify the extent of aggregation in a given sample. This will be essential to using spICP-MS to study the behavior of NPs in an environmental system where aggregation is strongly suspected. The ability to use spICP-MS to measure aggregation and settling kinetics would also be advantageous in mechanistic laboratory studies.

The dissertation research described in this thesis is a valuable contribution to the field of environmental NP analysis. SpICP-MS proved to be a valuable tool in each of these projects and is expected to continue advancing this area of research in future work.

REFERENCES CITED

(1) ASTM International. *Standard Terminology Relating to Nanotechnology*; West Conshohocken, PA, 2012.

(2) Stone, V.; Miller, M. R.; Clift, M. J. D.; Elder, A.; Mills, N. L.; Møller, P.; Schins, R. P. F.; Vogel, U.; Kreyling, W. G.; Jensen, K. A.; Kuhlbusch, T. A. J.; Schwarze, P. E.; Hoet, P.; Pietroiusti, A.; de Vizcaya-Ruiz, A.; Baeza-Squiban, A.; Teixeira, J. P.; Tran, C. L.; Cassee, F. R. Nanomaterials versus Ambient Ultrafine Particles: An Opportunity to Exchange Toxicology Knowledge. *Environ. Health Perspect.* **2017**, *125* (10) DOI: 10.1289/EHP424.

(3) Mueller, N. C.; Nowack, B. Exposure Modeling of Engineered Nanoparticles in the Environmment. *Environ. Sci. Technol.* **2008**, *42* (0), 4447–4453.

(4) Nowack, B.; Bucheli, T. D. Occurrence, Behavior and Effects of Nanoparticles in the Environment. *Environ. Pollut.* **2007**, *150* (1), 5–22 DOI: 10.1016/j.envpol.2007.06.006.

(5) Hochella, M. F.; Mogk, D. W.; Ranville, J.; Allen, I. C.; Luther, G. W.; Marr, L. C.; McGrail, B. P.; Murayama, M.; Qafoku, N. P.; Rosso, K. M.; Sahai, N.; Schroeder, P. A.; Vikesland, P.; Westerhoff, P.; Yang, Y. Natural, Incidental, and Engineered Nanomaterials and Their Impacts on the Earth System. *Science.* **2019**, *363* (6434), 1–10 DOI: 10.1126/science.aau8299.

(6) Guzmán, K. A. D.; Taylor, M. R.; Banfield, J. F. Environmental Risks of Nanotechnology: National Nanotechnology Initiative Funding, 2000-2004. *Environ. Sci. Technol.* **2006**, *40* (5), 1401–1407 DOI: 10.1021/es0515708.

(7) Baalousha, M.; Yang, Y.; Vance, M. E.; Colman, B. P.; McNeal, S.; Xu, J.; Blaszczak, J.; Steele, M.; Bernhardt, E.; Hochella, M. F. Outdoor Urban Nanomaterials: The Emergence of a New, Integrated, and Critical Field of Study. *Sci. Total Environ.* **2016**, *557–558*, 740–753 DOI: 10.1016/j.scitotenv.2016.03.132.

(8) Hassellöv, M.; Readman, J. W.; Ranville, J. F.; Tiede, K. Nanoparticle Analysis and Characterization Methodologies in Environmental Risk Assessment of Engineered Nanoparticles. *Ecotoxicology* **2008**, *17* (5), 344–361 DOI: 10.1007/s10646-008-0225-x.

(9) Hristozov, D.; Malsch, I. Hazards and Risks of Engineered Nanoparticles for the Environment and Human Health. *Sustainability* **2009**, *1* (4), 1161–1194 DOI: 10.3390/su1041161.

(10) Madl, A. K.; Pinkerton, K. E. Health Effects of Inhaled Engineered and Incidental Nanoparticles. *Crit. Rev. Toxicol.* **2009**, *39* (8), 629–658 DOI: 10.1080/10408440903133788.

(11) Som, C.; Berges, M.; Chaudhry, Q.; Dusinska, M.; Fernandes, T. F.; Olsen, S. I.; Nowack, B. The Importance of Life Cycle Concepts for the Development of Safe Nanoproducts. *Toxicology* **2010**, *269* (2–3), 160–169 DOI: 10.1016/j.tox.2009.12.012.

(12) Hochella, M. F.; Lower, S. K.; Maurice, P. A.; Penn, R. L.; Sahai, N.; Sparks, D. L.; Twining, B. S. Nanominerals, Mineral Nanoparticles, and Earth Systems. *Science.* **2008**,

319 (5870), 1631–1635 DOI: 10.1126/science.1141134.

(13) Wigginton, N. S.; Haus, K. L.; Hochella Jr, M. F. Aquatic Environmental Nanoparticles. *J. Environ. Monit.* **2007**, *9* (12), 1306–1316 DOI: 10.1039/b712709j.

(14) Lead, J. R.; Wilkinson, K. J. Aquatic Colloids and Nanoparticles: Current Knowledge and Future Trends. *Environ. Chem.* **2006**, *3* (3), 159–171 DOI: 10.1071/EN06025.

(15) Slomberg, D. L.; Ollivier, B. P.; Radakovitch, C. O.; Borschneck, A. D.; Baran, N.; Sanikast, C. N.; H, D. Characterisation of Suspended Particulate Matter in the Rhone River : Insights into Analogue Selection. **2016**, 804–815.

(16) Theng, B. K. G.; Yuan, G. Nanoparticles in the Soil Environment. *Elements* **2008**, *4* (6), 395–399 DOI: 10.2113/gselements.4.6.395.

(17) Viers, J.; Dupré, B.; Gaillardet, J. Chemical Composition of Suspended Sediments in World Rivers: New Insights from a New Database. *Sci. Total Environ.* **2009**, *407* (2), 853–868 DOI: 10.1016/j.scitotenv.2008.09.053.

(18) Zänker, H.; Schierz, A. Engineered Nanoparticles and Their Identification Among Natural Nanoparticles. *Annu. Rev. Anal. Chem.* **2012**, *5* (1), 107–132 DOI: 10.1146/annurev-anchem-062011-143130.

(19) Banfield, J. F.; Zhang, H. Nanoparticles in the Environment. *Rev. Mineral. Geochemistry* **2001**, *44*, 1–58 DOI: 10.2138/rmg.2001.44.01.

(20) Buffle, J.; Leppard, G. G. Characterization of Aquatic Colloids and Macromolecules. 1. Structure and Behavior of Colloidal Material. *Environ. Sci. Technol.* **1995**, *29* (9), 2169–2175.

(21) Westerhoff, P.; Atkinson, A.; Fortner, J.; Wong, M. S.; Zimmerman, J.; Gardea-Torresdey, J.; Ranville, J.; Herckes, P. Low Risk Posed by Engineered and Incidental Nanoparticles in Drinking Water. *Nat. Nanotechnol.* **2018**, *13* (8), 661–669 DOI: 10.1038/s41565-018-0217-9.

(22) Filella, M. Colloidal Properties of Submicron Particles in Natural Waters. *Environmental Colloids and Particles*. IUPAC Series on Analytical and Physical Chemistry of Environmental Systems; John Wiley & Sons, Ltd.: Triangle Park, N.C. 2003, pp 17–93.

(23) Guo, H.; Barnard, A. S. Naturally Occurring Iron Oxide Nanoparticles: Morphology, Surface Chemistry and Environmental Stability. *J. Mater. Chem. A* **2013**, *1* (1), 27–42 DOI: 10.1039/C2TA00523A.

(24) Moreau, J. W.; Webb, R. I.; Banfield, J. F. Ultrastructure, Aggregation-State, and Crystal Growth of Biogenic Nanocrystalline Sphalerite and Wurtzite. *Am. Mineral.* **2004**, *89*, 950–960.

(25) Rees, T. F.; Ranville, J. F. Collection and Analysis of Colloidal Particles Transported in the Mississippi River, U.S.A. *J. Contam. Hydrol.* **1990**, *6*, 241–250.

(26) Hassellöv, M.; von der Kammer, F. Iron Oxides as Geochemical Nanovectors for Metal Transport in Soil-River Systems. *Elements* **2008**, *4* (6), 401–406 DOI: 10.2113/gselements.4.6.401.

(27) Malengreau, N.; Muller, J. P.; Calas, G. Spectroscopic Approach for Investigating the Status and Mobility of Ti in Kaolinitic Materials. *Clays Clay Miner.* **1995**, *43* (5), 615–621 DOI: 10.1346/CCMN.1995.0430511.

(28) Gilbert, B.; Huang, F.; Zhang, H.; Waychunas, G. A.; Banfield, J. F. Nanoparticles: Strained and Stiff. *Science.* **2004**, *305* (5684), 651–654 DOI: 10.1126/science.1098454.

(29) Myers, D. Colloids and Colloidal Stability. In *Surfaces, Interfaces, and Colloids: Principles and Applications*; John Wiley & Sons: New York, 1999; pp 223–248.

(30) White, W. M. Mineral Surfaces and Their Interaction with Solutions. In *Geochemistry*; Wiley-Blackwell: Oxford, 2013; pp 244–253.

(31) Tipping, E.; Higgins, D. C. The Effect of Adsorbed Humic Substances on the Colloid Stability of Haematite Particles. *Colloids and Surfaces* **1982**, *5*, 85–92 DOI: 10.1016/0166-6622(82)80064-4.

(32) Franchi, A.; O'Melia, C. R. Effects of Natural Organic Matter and Solution Chemistry on the Deposition and Reentrainment of Colloids in Porous Media. *Environ. Sci. Technol.* **2003**, *37* (6), 1122–1129 DOI: 10.1021/es015566h.

(33) Baalousha, M. Aggregation and Disaggregation of Iron Oxide Nanoparticles: Influence of Particle Concentration, PH and Natural Organic Matter. *Sci. Total Environ.* **2009**, *407* (6), 2093–2101 DOI: 10.1016/j.scitotenv.2008.11.022.

(34) Xu, C.; Deng, K.-Y.; Li, J.; Xu, R. Impact of Environmental Conditions on Aggregation Kinetics of Hematite and Goethite Nanoparticles. *J. Nanoparticle Res.* **2015**, *17* (10), 1–13 DOI: 10.1007/s11051-015-3198-8.

(35) Montano, M. D.; Ranville, J.; Lowry, G. V; Blue, J.; Hiremath, N.; Koenig, S.; Tuccillo, M. E.; Gardner, S. P. *Detection and Characterization of Engineered Nanomaterials in the Environment : Current State-of-the-Art and Future Directions*; U.S. Environmental Protection Agency: Washington, DC, 2014.

(36) von der Kammer, F.; Ferguson, P. L.; Holden, P. A.; Masion, A.; Rogers, K. R.; Klaine, S. J.; Koelmans, A. A.; Horne, N.; Unrine, J. M. Analysis of Engineered Nanomaterials in Complex Matrices (Environment and Biota): General Considerations and Conceptual Case Studies. *Environ. Toxicol. Chem.* **2012**, *31* (1), 32–49 DOI: 10.1002/etc.723.

(37) Zbik, M.; St.C. Smart, R. Nanomorphology of Kaolinites: Comparative SEM and AFM Studies. *Clays Clay Miner.* **1998**, *46* (2), 153–160.

(38) Leppard, G. G. Nanoparticles in the Environment as Revealed by Transmission Electron Microscopy: Detection, Characterisation and Activities. *Curr. Nanosci.* **2008**, *4* (3), 278–301 DOI: 10.2174/157341308785161109.

(39) Degueldre, C.; Favarger, P. Y. Colloid Analysis by Single Particle Inductively Coupled Plasma-Mass Spectroscopy: A Feasibility Study. *Colloids Surfaces A Physicochem. Eng. Asp.* **2003**, *217*, 137–142 DOI: 10.1016/S0927-7757(02)00568-X.

(40) Montaño, M. D.; Olesik, J. W.; Barber, A. G.; Challis, K.; Ranville, J. F. Single Particle ICP-MS: Advances toward Routine Analysis of Nanomaterials. *Anal. Bioanal. Chem.* **2016**, *408* (19), 5053–5074 DOI: 10.1007/s00216-016-9676-8.

(41) Pace, H. E.; Rogers, N. J.; Jarolimek, C.; Coleman, V. A.; Higgins, C. P.; Ranville, J. F. Determining Transport Efficiency for the Purpose of Counting and Sizing Nanoparticles via Single Particle Inductively Coupled Plasma Mass Spectrometry. *Anal. Chem.* **2011**, *83*, 9361–9369.

(42) Popov, A. P.; Priezzhev, A. V.; Lademann, J.; Myllylä, R. TiO2 Nanoparticles as an Effective UV-B Radiation Skin-Protective Compound in Sunscreens. *J. Phys. D. Appl. Phys.* **2005**, *38* (15), 2564–2570 DOI: 10.1088/0022-3727/38/15/006.

(43) Serpone, N.; Dondi, D.; Albini, A. Inorganic and Organic UV Filters: Their Role and Efficacy in Sunscreens and Suncare Products. *Inorganica Chim. Acta* **2007**, *360* (3), 794–802 DOI: 10.1016/j.ica.2005.12.057.

(44) Petrazzuoli, M. Advances in Sunscreens. *Curr. Probl. Dermatol.* **2000**, *12* (6), 287–290 DOI: 10.1016/S1040-0486(00)90027-9.

(45) Botta, C.; Labille, J.; Auffan, M.; Borschneck, D.; Miche, H.; Cabié, M.; Masion, A.; Rose, J.; Bottero, J. Y. TiO2-Based Nanoparticles Released in Water from Commercialized Sunscreens in a Life-Cycle Perspective: Structures and Quantities. *Environ. Pollut.* **2011**, *159* (6), 1543–1550 DOI: 10.1016/j.envpol.2011.03.003.

(46) Johnson, A. C.; Bowes, M. J.; Crossley, A.; Jarvie, H. P.; Jurkschat, K.; Jürgens, M. D.; Lawlor, A. J.; Park, B.; Rowland, P.; Spurgeon, D.; Svendsen, C.; Thompson, I. P.; Barnes, R. J.; Williams, R. J.; Xu, N. An Assessment of the Fate, Behaviour and Environmental Risk Associated with Sunscreen TiO2 Nanoparticles in UK Field Scenarios. *Sci. Total Environ.* **2011**, *409* (13), 2503–2510 DOI: 10.1016/j.scitotenv.2011.03.040.

(47) Labille, J.; Feng, J.; Botta, C.; Borschneck, D.; Sammut, M.; Cabie, M.; Auffan, M.; Rose, J.; Bottero, J. Y. Aging of TiO2 Nanocomposites Used in Sunscreen. Dispersion and Fate of the Degradation Products in Aqueous Environment. *Environ. Pollut.* **2010**, *158* (12), 3482–3489 DOI: 10.1016/j.envpol.2010.02.012.

(48) Adams, L. K.; Lyon, D. Y.; Alvarez, P. J. J. Comparative Eco-Toxicity of Nanoscale TiO2, SiO2, and ZnO Water Suspensions. *Water Res.* **2006**, *40* (19), 3527–3532 DOI: 10.1016/j.watres.2006.08.004.

(49) Dransfield, G.; Guest, P. J.; Lyth, P. L.; McGarvey, D. J.; Truscott, T. G. Photoactivity Tests of TiO2-Based Inorganic Sunscreens. Part 1: Non-Aqueous Dispersions. *J. Photochem. Photobiol. B.* **2000**, *59* (1–3), 147–151.

(50) Brezová, V.; Gabčová, S.; Dvoranová, D.; Staško, A. Reactive Oxygen Species Produced upon Photoexcitation of Sunscreens Containing Titanium Dioxide (an EPR Study). *J. Photochem. Photobiol. B Biol.* **2005**, *79* (2), 121–134 DOI: 10.1016/j.jphotobiol.2004.12.006.

(51) Johnston, H. J.; Hutchison, G. R.; Christensen, F. M.; Peters, S.; Hankin, S.; Stone, V. Identification of the Mechanisms That Drive the Toxicity of TiO2 Particulates: The Contribution of Physicochemical Characteristics. *Part. Fibre Toxicol.* **2009**, *6* DOI: 10.1186/1743-8977-6-33.

(52) Auffan, M.; Pedeutour, M.; Rose, J.; Masion, A.; Ziarelli, F.; Borschneck, D.; Chaneac,

C.; Botta, C.; Chaurand, P.; Labille, J.; Bottero, J. Y. Structural Degradation at the Surface of a TiO2-Based Nanomaterial Used in Cosmetics. *Environ. Sci. Technol.* **2010**, *44* (7), 2689–2694 DOI: 10.1021/es903757q.

(53) Holbrook, R. D.; Motabar, D.; Quiñones, O.; Stanford, B.; Vanderford, B.; Moss, D. Titanium Distribution in Swimming Pool Water Is Dominated by Dissolved Species. *Environ. Pollut.* **2013**, *181*, 68–74 DOI: 10.1016/j.envpol.2013.05.044.

(54) Gondikas, A. P.; von der Kammer, F.; Reed, R. B.; Wagner, S.; Ranville, J. F.; Hofmann, T. Release of TiO2 Nanoparticles from Sunscreens into Surface Waters: A One-Year Survey at the Old Danube Recreational Lake. *Environ. Sci. Technol.* **2014**, *48* (10), 5415–5422 DOI: 10.1021/es405596y.

(55) Reed, R. B.; Martin, D. P.; Bednar, A. J.; Montaño, M. D.; Westerhoff, P.; Ranville, J. F. Multi-Day Diurnal Measurements of Ti-Containing Nanoparticle and Organic Sunscreen Chemical Release during Recreational Use of a Natural Surface Water. *Environ. Sci. Nano* **2017**, *4* (1), 69–77 DOI: 10.1039/C6EN00283H.

(56) Venkatesan, A. K.; Reed, R. B.; Lee, S.; Bi, X.; Hanigan, D.; Yang, Y.; Ranville, J. F.; Herckes, P.; Westerhoff, P. Detection and Sizing of Ti-Containing Particles in Recreational Waters Using Single Particle ICP-MS. *Bull. Environ. Contam. Toxicol.* **2018**, *100* (1), 120–126 DOI: 10.1007/s00128-017-2216-1.

(57) Praetorius, A.; Gundlach-Graham, A.; Goldberg, E.; Fabienke, W.; Navratilova, J.; Gondikas, A.; Kaegi, R.; Gunther, D.; Hofmann, T.; von der Kammer, F. Single-Particle Multi-Element Fingerprinting (SpMEF) Using Inductively-Coupled Plasma Time-of-Flight Mass Spectrometry (ICP-TOFMS) to Identify Engineered Nanoparticles against the Elevated Natural Background in Soils. *Environ. Sci. Nano* **2017**, *4*, 307–314 DOI: 10.1039/C6EN00455E.

(58) Reed, R. B.; Higgins, C. P.; Westerhoff, P.; Tadjiki, S.; Ranville, J. F. Overcoming Challenges in Analysis of Polydisperse Metal-Containing Nanoparticles by Single Particle Inductively Coupled Plasma Mass Spectrometry. *J. Anal. At. Spectrom.* **2012**, *27* (7), 1093 DOI: 10.1039/c2ja30061c.

(59) Schwertfeger, D. M.; Velicogna, J. R.; Jesmer, A. H.; Scroggins, R. P.; Princz, J. I. Single Particle-Inductively Coupled Plasma Mass Spectroscopy Analysis of Metallic Nanoparticles in Environmental Samples with Large Dissolved Analyte Fractions. *Anal. Chem.* **2016**, *88* (20), 9908–9914 DOI: 10.1021/acs.analchem.6b02716.

(60) *Test Methods for Evaluating Solid Waste: Physical/Chemical Methods (SW-846)*; U.S. Environmental Protection Agency, 2007.

(61) Peck, A. M. Analytical Methods for the Determination of Persistent Ingredients of Personal Care Products in Environmental Matrices. *Anal. Bioanal. Chem.* **2006**, *386*, 907–939 DOI: 10.1007/s00216-006-0728-3.

(62) Kaegi, R.; Sinnet, B.; Zuleeg, S.; Hagendorfer, H.; Mueller, E.; Vonbank, R.; Boller, M.; Burkhardt, M. Release of Silver Nanoparticles from Outdoor Facades. *Environ. Pollut.* **2010**, *158* (9), 2900–2905 DOI: 10.1016/j.envpol.2010.06.009.

(63) Gomi, T.; Moore, R. D.; Hassan, M. A. Suspended Sediment Dynamics in Small Forest

Streams of the Pacific Northwest. *J. Am. Water Resour. Assoc.* **2005**, *41* (4), 877–898 DOI: 10.1111/j.1752-1688.2005.tb03775.x.

(64) *Acid Mine Drainage Prediction*; US Environmental Protection Agency: Washington, DC, 1994.

(65) Metesh, J. J.; Jarrell, T.; Oravetz, S. *Treating Acid Mine Drainage from Abandoned Mines in Remote Areas*; USDA Forest Service Technology and Development Program: Missoula, MT, 1998.

(66) Drever, J. I. *The Geochemistry of Natural Waters: Surface and Groundwater Environment*; Prentice Hall: Upper Saddle River, NJ, 1997.

(67) Akcil, A.; Koldas, S. Acid Mine Drainage (AMD): Causes, Treatment and Case Studies. *J. Clean. Prod.* **2006**, *14*, 1139–1145 DOI: 10.1016/j.jclepro.2004.09.006.

(68) Johnson, D. B.; Hallberg, K. B. Acid Mine Drainage Remediation Options: A Review. *Sci. Total Environ.* **2005**, *338*, 3–14 DOI: 10.1016/j.scitotenv.2004.09.002.

(69) Chapman, B. M.; Jones, D. R.; Jung, R. F. Processes Controlling Metal Ion Attenuation in Acid Mine Drainage Streams. *Geochim. Cosmochim. Acta* **1983**, *47* (11), 1957–1973 DOI: 10.1016/0016-7037(83)90213-2.

(70) Butler, B. A.; Ranville, J. F.; Ross, P. E. Spatial Variations in the Fate and Transport of Metals in a Mining-Influenced Stream, North Fork Clear Creek, Colorado. *Sci. Total Environ.* **2009**, *407* (24), 6223–6234 DOI: 10.1016/j.scitotenv.2009.08.040.

(71) Butler, B. A.; Ranville, J. F.; Ross, P. E. Direct versus Indirect Determination of Suspended Sediment Associated Metals in a Mining-Influenced Watershed. *Appl. Geochemistry* **2008**, *23*, 1218–1231 DOI: 10.1016/j.apgeochem.2007.11.021.

(72) Murad, E.; Rojik, P. Iron-Rich Precipitates in a Mine Drainage Environment : Influence of PH on Mineralogy. *Am. Mineral.* **2003**, *88*, 1915–1918.

(73) He, Y. T.; Wan, J.; Tokunaga, T. Kinetic Stability of Hematite Nanoparticles: The Effect of Particle Sizes. *J. Nanoparticle Res.* **2008**, *10* (2), 321–332 DOI: 10.1007/s11051-007-9255-1.

(74) Butler, B. A.; Ranville, J. F.; Ross, P. E. Observed and Modeled Seasonal Trends in Dissolved and Particulate Cu, Fe, Mn, and Zn in a Mining-Impacted Stream. *Water Res.* **2008**, *42* (12), 3135–3145 DOI: 10.1016/j.watres.2008.03.004.

(75) Dong, D.; Nelson, Y. M.; Lion, L. W.; Shuler, M. L.; Ghiorse, W. C. Adsorption of Pb and Cd onto Metal Oxides and Organic Material in Natural Surface Coating as Determined by Selective Extractions: New Evidence for the Importance of Mn and Fe Oxides. *Water Res.* **2000**, *34* (2), 427–436.

(76) Rose, S.; Ghazi, A. M. Experimental Study of the Stability of Metals Associated with Iron Oxyhydroxides Precipitated in Acid Mine Drainage. *Environ. Geol.* **1998**, *36* (3–4), 364–370 DOI: 10.1007/s002540050352.

(77) Moreira, R. F. P. M.; Vandresen, S.; Luiz, D. B.; José, H. J.; Puma, G. L. Adsorption of Arsenate, Phosphate and Humic Acids onto Acicular Goethite Nanoparticles Recovered from Acid Mine Drainage. *J. Environ. Chem. Eng.* **2017**, *5*, 652–659 DOI:

10.1016/j.jece.2016.12.018.

(78) Equeenuddin, S. M.; Tripathy, S.; Sahoo, P. K.; Panigrahi, M. K. Metal Behavior in Sediment Associated with Acid Mine Drainage Stream: Role of PH. *J. Geochemical Explor.* **2013**, *124*, 230–237 DOI: 10.1016/j.gexplo.2012.10.010.

(79) Schwertfeger, D. M.; Velicogna, J. R.; Jesmer, A. H.; Scroggins, R. P.; Princz, J. I. Single Particle-Inductively Coupled Plasma Mass Spectroscopya Analysis of Metallic Nanoparticles in Environmental Samples with Large Dissolved Analyte Fractions. *Anal. Chem.* **2016**, *88* (20), 9908–9914 DOI: 10.1021/acs.analchem.6b02716.

(80) McDonald, D. G.; Grandt, A. F. *Limestone - Lime Treatment of Acid Mine Drainage - Full Scale*; Cincinnati, OH, 1981.

(81) Kalin, M.; Fyson, A.; Wheeler, W. N. The Chemistry of Conventional and Alternative Treatment Systems for the Neutralization of Acid Mine Drainage. *Sci. Total Environ.* **2006**, *366*, 395–408 DOI: 10.1016/j.scitotenv.2005.11.015.

(82) Carlson, J. J.; Kawatra, S. K. Factors Affecting Zeta Potential of Iron Oxides. *Miner. Process. Extr. Metall. Rev.* **2013**, *34* (5), 269–303 DOI: 10.1080/08827508.2011.604697.

(83) Burns, J. L.; Yan, Y.; Jameson, G. J.; Biggs, S. A Light Scattering Study of the Fractal Aggregation Behavior of a Model Colloidal System. *Langmuir* **1997**, *13* (24), 6413–6420 DOI: 10.1021/la970303f.

(84) Sinha, P.; Szilagyi, I.; Montes Ruiz-Cabello, F. J.; Maroni, P.; Borkovec, M. Attractive Forces between Charged Colloidal Particles Induced by Multivalent Ions Revealed by Confronting Aggregation and Direct Force Measurements. *J. Phys. Chem. Lett.* **2013**, *4* (4), 648–652 DOI: 10.1021/jz4000609.

(85) French, R. A.; Jacobson, A. R.; Kim, B.; Isley, S. L.; Penn, R. L.; Baveye, P. C. Influence of Ionic Strength, PH, and Cation Valence on Aggregation Kinetics of Titanium Dioxide Nanoparticles. *Environ. Sci. Technol.* **2009**, *43* (5), 1354–1359 DOI: 10.1021/es802628n.

(86) Chen, K. L.; Elimelech, M. Aggregation and Deposition Kinetics of Fullerene (C60) Nanoparticles. *Langmuir* **2006**, *22* (26), 10994–11001 DOI: 10.1021/la062072v.

(87) Lee, B.; Ranville, J. F. The Effect of Hardness on the Stability of Citrate-Stabilized Gold Nanoparticles and Their Uptake by Daphnia Magna. *J. Hazard. Mater.* **2012**, *213–214*, 434–439 DOI: 10.1016/j.jhazmat.2012.02.025.

(88) Trefalt, G.; Szilagyi, I.; Oncsik, T.; Sadeghpour, A.; Borkovec, M. Probing Colloidal Particle Aggregation by Light Scattering. *CHIMIA.* **2013**, *67* (11), 772–776 DOI: 10.2533/chimia.2013.772.

(89) Trefalt, G.; Behrens, S. H.; Borkovec, M. Charge Regulation in the Electrical Double Layer: Ion Adsorption and Surface Interactions. *Langmuir* **2016**, *32* (2), 380–400 DOI: 10.1021/acs.langmuir.5b03611.

(90) Wang, Y.; Li, Y.; Pennel, K. D. Influence of Electrolyte Species and Concentration on the Aggregation and Transport of Fullerene Nanoparticles in Quartz Sands. *Environ. Toxicol.* **2008**, *27* (9), 1860–1867.

(91) Chen, K. L.; Elimelech, M. Relating Colloidal Stability of Fullerene (C60) Nanoparticles

to Nanoparticle Charge and Electrokinetic Properties. *Environ. Sci. Technol.* **2009**, *43* (19), 7270–7276 DOI: 10.1021/es900185p.

(92) Trefalt, G.; Palberg, T.; Borkovec, M. Forces between Colloidal Particles in Aqueous Solutions Containing Monovalent and Multivalent Ions. *Curr. Opin. Colloid Interface Sci.* **2017**, *27*, 9–17.

(93) Park, C. M.; Heo, J.; Her, N.; Chu, K. H.; Jang, M.; Yoon, Y. Modeling the Effects of Surfactant, Hardness, and Natural Organic Matter on Deposition and Mobility of Silver Nanoparticles in Saturated Porous Media. *Water Res.* **2016**, *103*, 38–47 DOI: 10.1016/j.watres.2016.07.022.

(94) Zhou, D.; Abdel-Fattah, A. I.; Keller, A. A. Clay Particles Destabilize Engineered Nanoparticles in Aqueous Environments. *Environ. Sci. Technol.* **2012**, *46* (14), 7520–7526 DOI: 10.1021/es3004427.

(95) Dale, A. L.; Lowry, G. V.; Casman, E. A. Much Ado about α: Reframing the Debate over Appropriate Fate Descriptors in Nanoparticle Environmental Risk Modeling. *Environ. Sci. Nano* **2015**, *2* (1), 27–32 DOI: 10.1039/C4EN00170B.

(96) Buettner, K. M.; Rinciog, C. I.; Mylon, S. E. Aggregation Kinetics of Cerium Oxide Nanoparticles in Monovalent and Divalent Electrolytes. *Colloids Surfaces A Physicochem. Eng. Asp.* **2010**, *366*, 74–79 DOI: 10.1016/j.colsurfa.2010.05.024.

(97) Phenrat, T.; Saleh, N.; Sirk, K.; Tilton, R. D.; Lowry, G. V. Aggregation and Sedimentation of Aqueous Nanoscale Zerovalent Iron Dispersions. *Environ. Sci. Technol.* **2007**, *41* (1), 284–290 DOI: 10.1021/es061349a.

(98) Li, K.; Chen, Y. Effect of Natural Organic Matter on the Aggregation Kinetics of CeO2 Nanoparticles in KCl and CaCl2 Solutions: Measurements and Modeling. *J. Hazard. Mater.* **2012**, *209–210*, 264–270 DOI: 10.1016/j.jhazmat.2012.01.013.

(99) Oncsik, T.; Trefalt, G.; Csendes, Z.; Szilagyi, I.; Borkovec, M. Aggregation of Negatively Charged Colloidal Particles in the Presence of Multivalent Cations. *Langmuir* **2014**, *30* (3), 733–741 DOI: 10.1021/la4046644.

(100) Cao, T.; Szilagyi, I.; Oncsik, T.; Borkovec, M.; Trefalt, G. Aggregation of Colloidal Particles in the Presence of Multivalent Co-Ions: The Inverse Schulze-Hardy Rule. *Langmuir* **2015**, *31* (24), 6610–6614 DOI: 10.1021/acs.langmuir.5b01649.

(101) Szilagyi, I.; Trefalt, G.; Tiraferri, A.; Maroni, P.; Borkovec, M. Polyelectrolyte Adsorption, Interparticle Forces, and Colloidal Aggregation. *Soft Matter* **2014**, *10* (15), 2479–2502 DOI: 10.1039/c3sm52132j.

(102) Laaksonen, T.; Ahonen, P.; Johans, C.; Kontturi, K. Stability and Electrostatics of Mercaptoundecanoic Acid-Capped Gold Nanoparticles with Varying Counterion Size. *ChemPhysChem* **2006**, *7* (10), 2143–2149 DOI: 10.1002/cphc.200600307.

(103) Herbillon, A. J. Introduction to the Surface Charge Properties of Iron Oxides and Oxidic Soils. In *Iron in Soils and Clay Minerals*; Stucki, J. W., Goodman, B. A., Schwertmann, U., Eds.; D. Reidel Publishing Company: Boston, 1988; pp 251–266.

(104) Oriekhova, O.; Stoll, S. Effects of PH and Fulvic Acids Concentration on the Stability of

Fulvic Acids - Cerium (IV) Oxide Nanoparticle Complexes. *Chemosphere* **2016**, *144*, 131–137 DOI: 10.1016/j.chemosphere.2015.08.057.

(105) Juang, R.; Wu, W. Adsorption of Sulfate and Copper(II) on Goethite in Relation to the Changes of Zeta Potentials. *Colloid Interface Sci.* **2002**, *249*, 22–29 DOI: 10.1006/jcis.2002.8240.

(106) Keller, A. A.; Wang, H.; Zhou, D.; Lenihan, H. S.; Cherr, G.; Cardinale, B. J.; Miller, R.; Ji, Z. Stability and Aggregation of Metal Oxide Nanoparticles in Natural Aqueous Matrices. *Environ. Sci. Technol.* **2010**, *44* (6), 1962–1967 DOI: 10.1021/es902987d.

(107) Sims, L.; Guerra, J. *Update Fact Sheet: Central City/Clear Creek Superfund Site*; Denver, CO, 2014.

(108) Laudeman, S.; Boardman, M.; Smith, W.; Sims, L. *Grand Opening Fact Sheet: Central City/Clear Creek Superfund Site*; 2017.

(109) Bigham, J. M.; Schwertmann, U.; Traina, S. J.; Winland, R. L.; Wolf, M. Schwertmannite and the Chemical Modeling of Iron in Acid Sulfate Waters. *Geochim. Cosmochim. Acta* **1996**, *60* (12), 2111–2121 DOI: 10.1016/0016-7037(96)00091-9.

(110) Penners, N. H. G.; Koopal, L. K. Preparation and Optical Properties of Homodisperse Haematite Hydrosols. *Colloids and Surfaces* **1986**, *19* (2), 337–349 DOI: 10.1016/0166-6622(86)80343-2.

(111) Brooks, P. D.; Mcknight, D. M.; Bencala, K. E. The Relationship between Soil Heterotrophic Activity , Soil Dissolved Organic Carbon (DOC) Leachate, and Catchment-Scale DOC Export in Headwater Catchments. *Water Resour. Res.* **1999**, *35* (6), 1895–1902 DOI: 10.1029/1998WR900125.

(112) Surfleet, C. G.; Tullos, D. Variability in Effect of Climate Change on Rain-on-Snow Peak Flow Events in a Temperate Climate. *J. Hydrol.* **2013**, *479*, 24–34 DOI: 10.1016/j.jhydrol.2012.11.021.

(113) Thurman, E. M. *Organic Geochemistry of Natural Waters*; Springer Netherlands: Dordrecht, 1985.

(114) Miller, M. P.; Mcknight, D. M. Comparison of Seasonal Changes in Fluorescent Dissolved Organic Matter among Aquatic Lake and Stream Sites in the Green Lakes Valley. *J. Geophys. Res.* **2010**, *115*, 1–14 DOI: 10.1029/2009JG000985.

(115) Oriekhova, O.; Stoll, S. Stability of Uncoated and Fulvic Acids Coated Manufactured CeO2 Nanoparticles in Various Conditions: From Ultrapure to Natural Lake Geneva Waters. *Sci. Total Environ.* **2016**, *562*, 327–334 DOI: 10.1016/j.scitotenv.2016.03.184.

(116) Hotze, E. M.; Phenrat, T.; Lowry, G. V. Nanoparticle Aggregation: Challenges to Understanding Transport and Reactivity in the Environment. *J. Environ. Qual.* **2010**, *39* (6), 1909–1924 DOI: 10.2134/jeq2009.0462.

(117) Klaine, S. J.; Alvarez, P. J. J.; Batley, G. E.; Fernandes, T. F.; Handy, R. D.; Lyon, D. Y.; Mahendra, S.; McLaughlin, M. J.; Lead, J. R. Nanomaterials in the Environment: Behavior, Fate, Bioavailability, and Effects. *Environ. Toxicol. Chem.* **2008**, *27* (9), 1825–1851.

(118) Velzeboer, I.; Quik, J. T. K.; van de Meent, D.; Koelmans, A. A. Rapid Settling of Nanoparticles Due to Heteroaggregation with Suspended Sediment. *Environ. Toxicol. Chem.* **2014**, *33* (8), 1766–1773 DOI: 10.1002/etc.2611.

(119) Chen, K. L.; Mylon, S. E.; Elimelech, M. Aggregation Kinetics of Alginate-Coated Hematite Nanoparticles in Monovalent and Divalent Electrolytes. *Environ. Sci. Technol.* **2006**, *40* (5), 1516–1523.

(120) *Turbiscan LAB User Guide*, 1st ed.; Formulaction: L'Union, France, 2013.

(121) Luo, M.; Qi, X.; Ren, T.; Huang, Y.; Keller, A. A.; Wang, H.; Wu, B.; Jin, H.; Li, F. Heteroaggregation of CeO2 and TiO2 Engineered Nanoparticles in the Aqueous Phase: Application of Turbiscan Stability Index and Fluorescence Excitation-Emission Matrix (EEM) Spectra. *Colloids Surfaces A Physicochem. Eng. Asp.* **2017**, *533*, 9–19 DOI: 10.1016/j.colsurfa.2017.08.014.

(122) Kim, H.-A.; Lee, B.-T.; Na, S.-Y.; Kim, K.-W.; Ranville, J. F.; Kim, S.-O.; Jo, E.; Eom, I.-C. Characterization of Silver Nanoparticle Aggregates Using Single Particle-Inductively Coupled Plasma-Mass Spectrometry (SpICP-MS). *Chemosphere* **2017**, *171*, 468–475 DOI: 10.1016/j.chemosphere.2016.12.063.

(123) Donovan, A. R.; Adams, C. D.; Ma, Y.; Stephan, C.; Eichholz, T.; Shi, H. Fate of Nanoparticles during Alum and Ferric Coagulation Monitored Using Single Particle ICP-MS. *Chemosphere* **2018**, *195*, 531–541 DOI: 10.1016/j.chemosphere.2017.12.116.

(124) Borovinskaya, O.; Gschwind, S.; Hattendorf, B.; Tanner, M.; Günther, D. Simultaneous Mass Quantification of Nanoparticles of Different Composition in a Mixture by Microdroplet Generator-ICPTOFMS. *Anal. Chem.* **2014**, *86* (16), 8142–8148 DOI: 10.1021/ac501150c.

(125) Naasz, S.; Weigel, S.; Borovinskaya, O.; Serva, A.; Peters, R. J. B. Multi-Element Analysis of Single Nanoparticles by ICP-MS Using Quadrupole and Time-of-Flight Technologies. *J. Anal. At. Spectrom.* **2018** DOI: 10.1039/C7JA00399D.

(126) Hiemstra, T.; De Wit, J. C. M.; Van Riemsdijk, W. H. Multisite Proton Adsorption Modeling at the Solid/Solution Interface of (Hydr)Oxides: A New Approach II. Application to Various Important (Hydr)Oxides. *J. Colloid Interface Sci.* **1989**, *133* (1), 105–117.

(127) Guinoiseau, D.; Gélabert, A.; Moureau, J.; Louvat, P.; Benedetti, M. F. Zn Isotope Fractionation during Sorption onto Kaolinite. *Environ. Sci. Technol.* **2016**, *50* (4), 1844–1852 DOI: 10.1021/acs.est.5b05347.

(128) Waychunas, G. A.; Kim, C. S.; Banfield, J. F. Nanoparticulate Iron Oxide Minerals in Soils and Sediments: Unique Properties and Contaminant Scavenging Mechanisms. *J. Nanoparticle Res.* **2005**, *7* (4–5), 409–433 DOI: 10.1007/s11051-005-6931-x.

APPENDIX A

ADDITIONAL RECREATIONAL RIVER STUDY RESULTS

A.1 Ti and Al Loads in Clear Creek, Colorado 2016

Loads were calculated from Ti and Al concentration data and the USGS recorded discharge at the time of sampling. Loads were then grouped by site, day, and recreation use (Figure A.1, Figure A.2 on page 93) and the same statistical analyses were conducted as described in section 2.3.2 (Table A.1 on page 94).

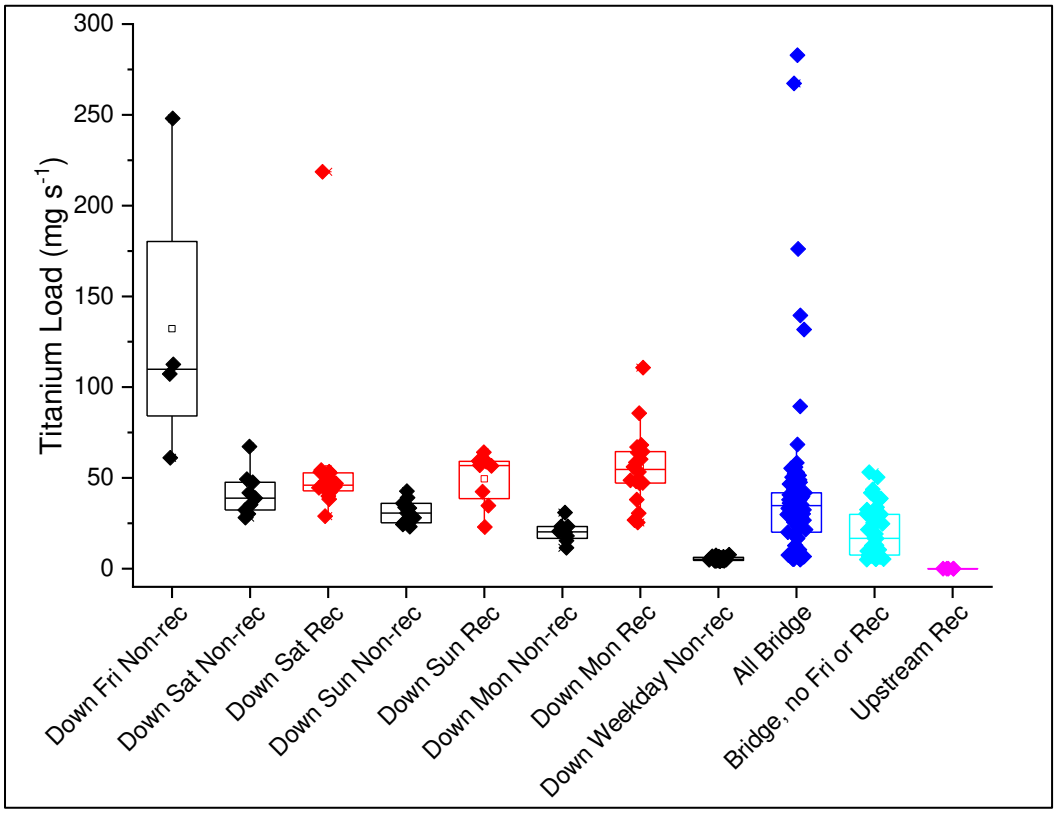

Figure A.1 Ti loads from Labor Day week, 2016. Downstream data are grouped by day and recreation use at the time of sampling (black, non-recreation times; red, recreation times). Bridge data are grouped together (blue) and together minus Friday 9/2 and recreation times (cyan). Upstream data (magenta) include four samples collected Saturday, Sunday, and Monday only.

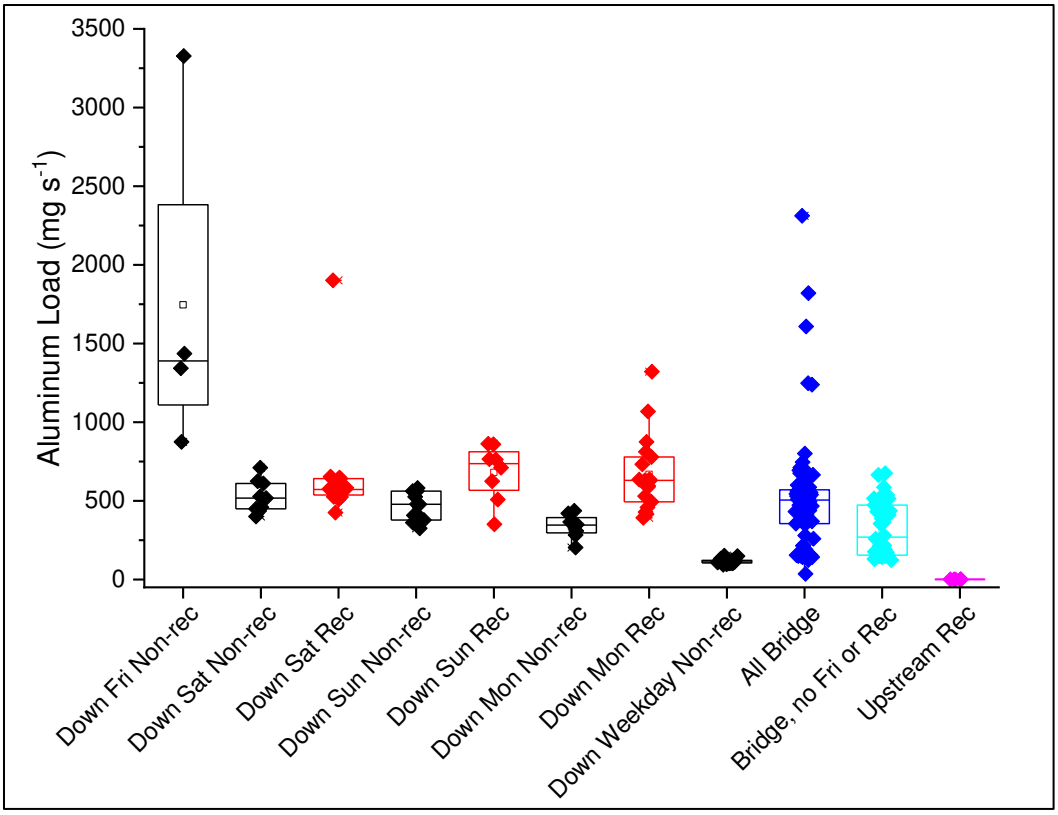

Figure A.2 Al loads from Labor Day week, 2016. Downstream data are grouped by day and recreation use at the time of sampling (black, non-recreation times; red, recreation times). Bridge data are grouped together (blue) and together minus Friday 9/2 and recreation times (cyan). Upstream data (magenta) include four samples collected Saturday, Sunday, and Monday only.

Significant differences between load groups are identical to those between concentration groups (section 2.3.2), except "upstream" differs from five additional groups when comparing loads (Table A.1 on page 94). The differences in loads that were not present when comparing concentrations are "downstream Friday non-recreation", "downstream Saturday non-recreation", "downstream Saturday recreation", "downstream Sunday recreation", "downstream Monday recreation", and "all bridge".

"Upstream" differs significantly from the recreation (but not non-recreation) in the Sunday and Monday downstream loads, which may be considered additional evidence that Sunday and Monday recreation produced significantly different Ti levels in Clear Creek.

The other conclusions drawn from concentration comparisons in section 2.3.2 remain true for loads.

Table A.1 Matrix of Dunn's Test p-values comparing Ti loads grouped by sampling location, day, and recreation (R) versus non-recreation (NR). Significant p-values (α = 0.05) are shaded green while results indicating non-significant p-values are shaded yellow.

			Downstream								Bridge		Upstream
			Fri	Sat		Sun		Mon		Wkdy	All	No Fri	All
			NR	NR	R	NR	R	NR	R	NR	All	NR	R
Downstream	Fri	NR		1	1	0.332	1	0.0264	1	1.09E-06	0.227	0.00279	4.88E-05
	Sat	NR	1		1	1	1	1	1	2.36E-05	1	0.201	0.00316
		R	1	1		0.658	1	0.0230	1	7.01E-13	0.063	3.73E-06	7.74E-06
	Sun	NR	0.332	1	0.658		1	1	0.348	0.00485	1	1	0.0929
		R	1	1	1	1		0.159	1	3.06E-07	1	0.00712	1.86E-04
	Mon	NR	0.0264	1	0.0230	1	0.159		0.01107	1	1	1	1
		R	1	1	1	0.348	1	0.01107		1.68E-13	0.0217	9.96E-07	3.32E-06
	Wkdy	NR	1.09E-06	2.36E-05	7.01E-13	0.00485	3.06E-07	1	1.68E-13		3.08E-10	0.0113	1
Bridge	All	All	0.227	1	0.063	1	1	1	0.0217	3.08E-10		0.00862	0.00324
	No Fri	NR	0.00279	0.201	3.73E-06	1	0.00712	1	9.96E-07	0.0113	0.00862		0.609
Upstream	All	R	4.88E-05	0.00316	7.74E-06	0.0929	1.86E-04	1	3.32E-06	1	0.00324	0.609	

A.2 Filtered Versus Unfiltered Ti Concentrations in Three Rivers, 2017

The unfiltered versus filtered (0.02 µm) triplicate Ti concentrations from upstream and downstream in all three rivers are shown below in Figure A.3. With the exception of two upstream unfiltered sample from Clear Creek, elevated concentrations of Ti occurred only in the downstream unfiltered samples. Filtered Ti concentrations were similar to or below the concentrations upstream unfiltered or non-recreation downstream unfiltered concentrations.

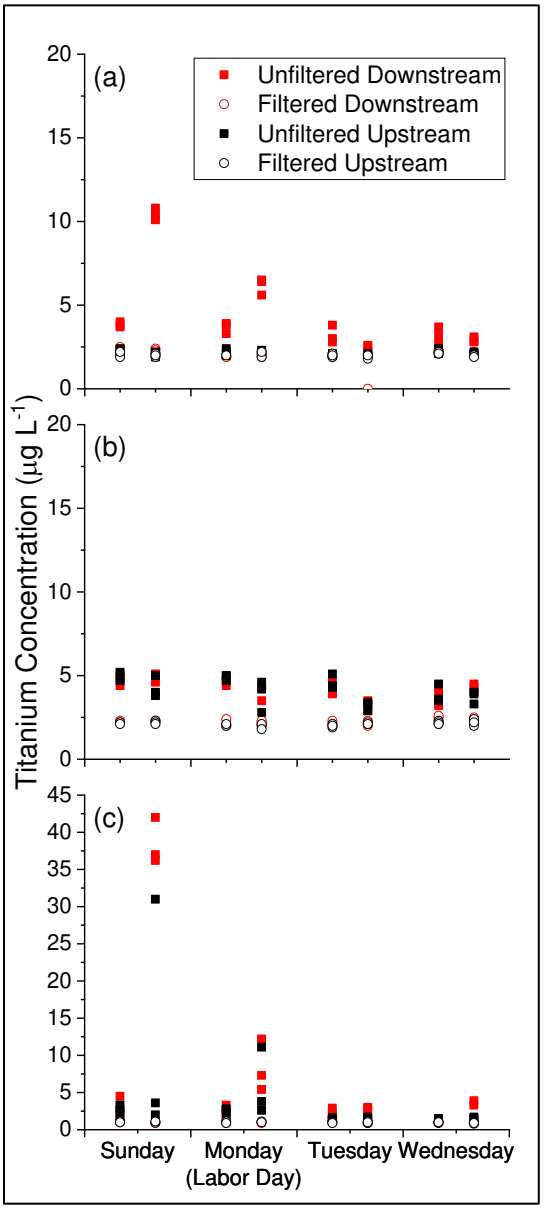

Figure A.3 Mass concentrations of Ti in unfiltered (solid squares) and filtered (open circles) samples from downstream (red) and upstream (black) sampling locations in (a) Salt River, Arizona, (b) Truckee River, Nevada, and (c) Clear Creek, Colorado.

A.3 Ti spICP-MS Size Distributions in Three Rivers, 2017

The Ti NP distributions of all samples analyzed with spICP-MS and compared with Kruskal-Wallis ANOVA and Dunn's test ($\alpha = 0.05$), as discussed in section 2.3.4, are shown below. The Salt River size distributions (Figure A.3) are all statistically different from each other with downstream Sunday afternoon sizes being ~20 nm larger and concentrations double that of the same site on Sunday morning. While this supports the hypothesis that recreation resuspends bed sediments, causing increased particle concentration and number, it also illustrates an issue of variability in the background NP population, as the four non-recreation samples are not equivalent to each other.

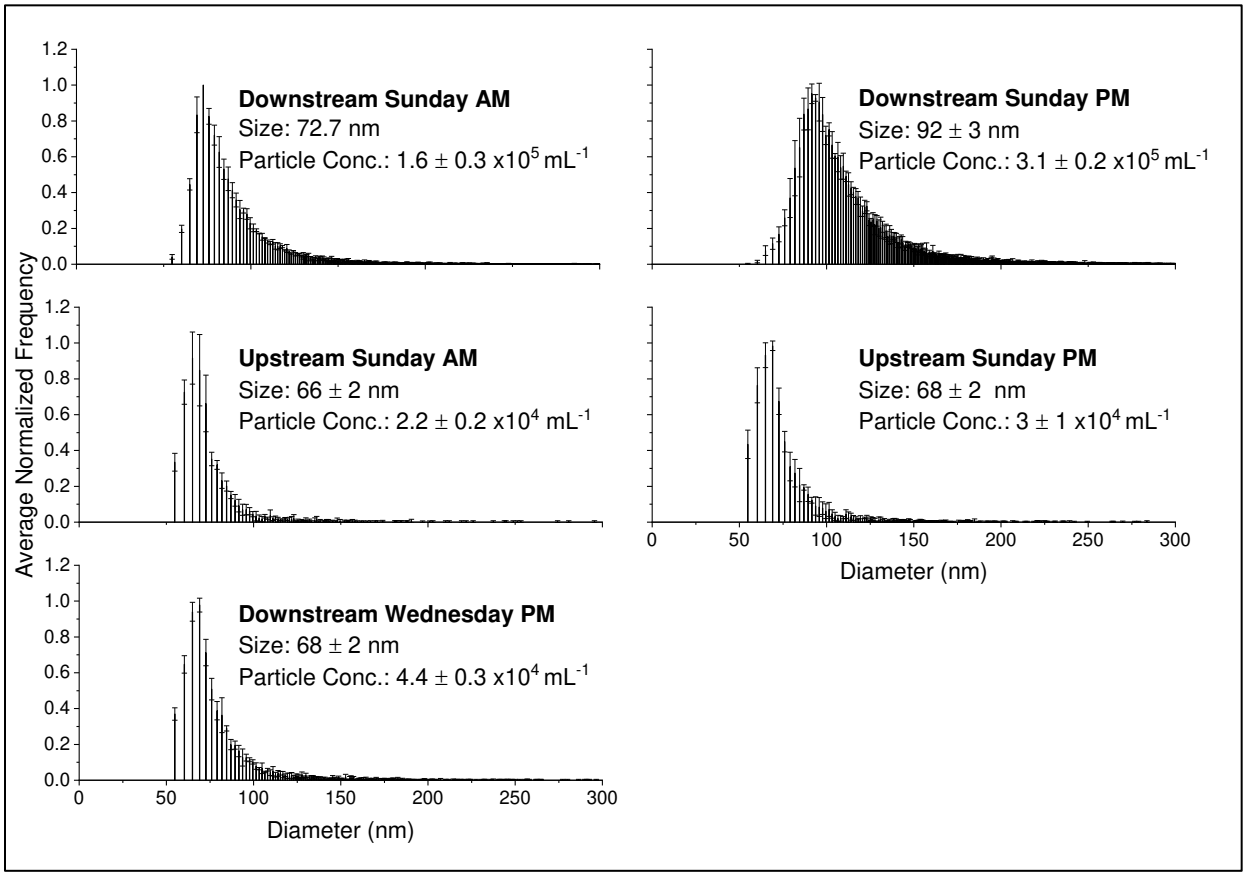

Figure A.4 Size distributions of Ti NPs measured with spICP-MS in the Salt River, Arizona with recreational impacts (top right, Downstream Sunday PM) and without recreational impacts (all other histograms). Sizes and concentrations are given as the mean ± standard deviation of triplicate analyses. The largest sizes and NP concentrations occurred in the Downstream Sunday PM sample, but all background samples are statistically different from each other.

The Truckee River size distributions (Figure A.4) are all statistically identical. This is unsurprising given the similarity of Ti mass concentrations observed over the different recreation use times (Figure 2.7b on page 28) and the lack of bed sediments available for resuspension (see Truckee River site description in section 2.3.1.

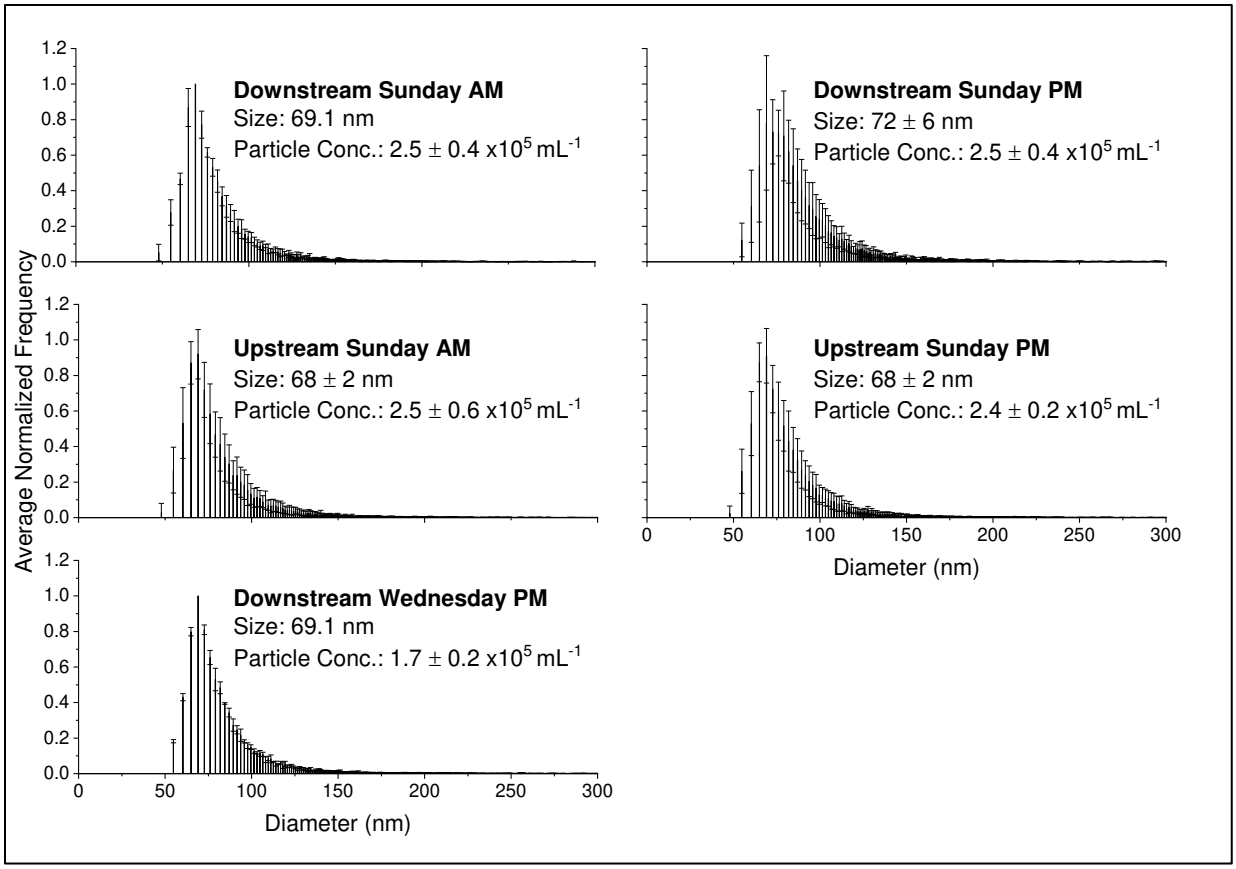

Figure A.5 Size distributions of Ti NPs measured with spICP-MS in the Truckee River, Nevada with recreational impacts (top right, Downstream Sunday PM) and without recreational impacts (all other histograms). Sizes and concentrations are given as the mean ± standard deviation of triplicate analyses. All samples are statistically identical with no significant change occurring in water during recreation.

Clear Creek Ti NP size distributions in the four background-only samples (Figure 4.5 Downstream Sunday AM, Upstream Sunday AM, Upstream Sunday PM, Downstream Wednesday PM) were all statistically equivalent to each other whereas the sample impacted by recreation activity is significantly different. Concentrations in this sample are greater than the others by nearly an order of magnitude and the average NP diameter increased by ~20 nm.

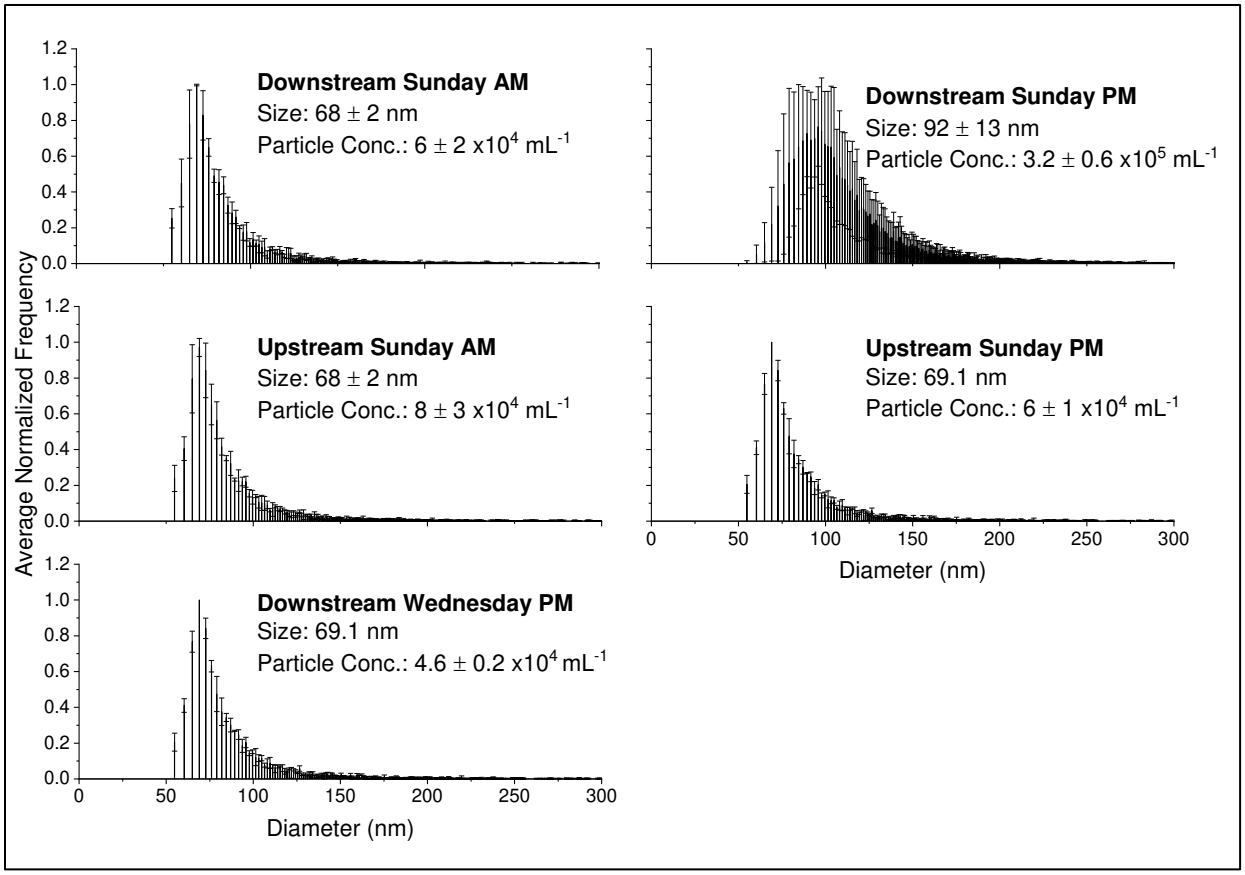

Figure A.6 Size distributions of Ti NPs measured with spICP-MS in Clear Creek, Colorado with recreational impacts (top right, Downstream Sunday PM) and without recreational impacts (all other histograms). Sizes and concentrations are given as the mean ± standard deviation of triplicate analyses. The four non-recreation samples are not statistically different from each other whereas the recreation-impacted sample is significantly different from all of them.

APPENDIX B

TURBISCAN DATA

B.1 CeO_2 Homoaggregation Turbiscan Results

This section contains the Turbiscan graph exports for transmittance (Figures B.1, B.2), delta transmittance (Figures B.3, B.4), Global Turbsiscan Stability Index (Figure B.5), mean delta transmittance (Figure B.6), particle diameter (Figure B.7), and volume fraction (Figure B.8) of CeO_2 homoaggregation experiments in stable and unstable media.

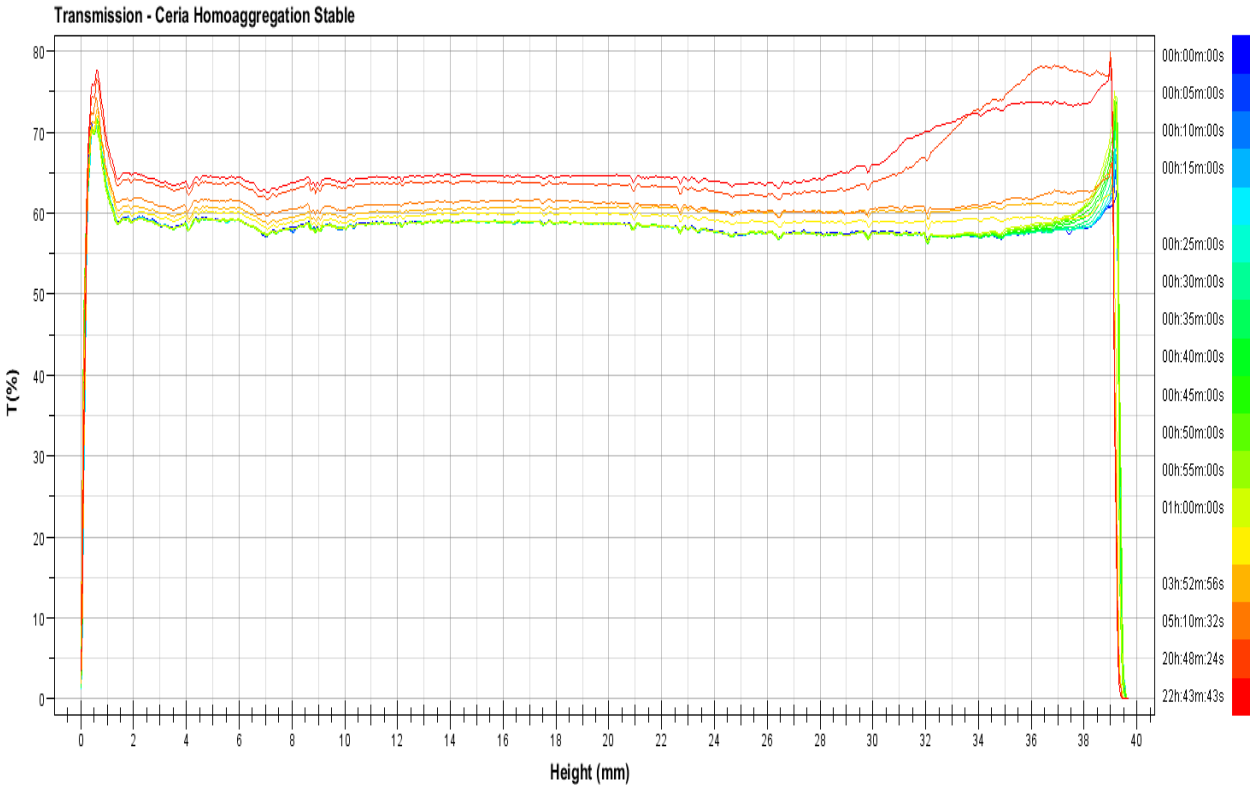

Figure B.1 Original Turbiscan transmittance data (y-axis) across the sample height measured from bottom to top (x-axis) over time (blue to red) for CeO_2 in the stable medium.

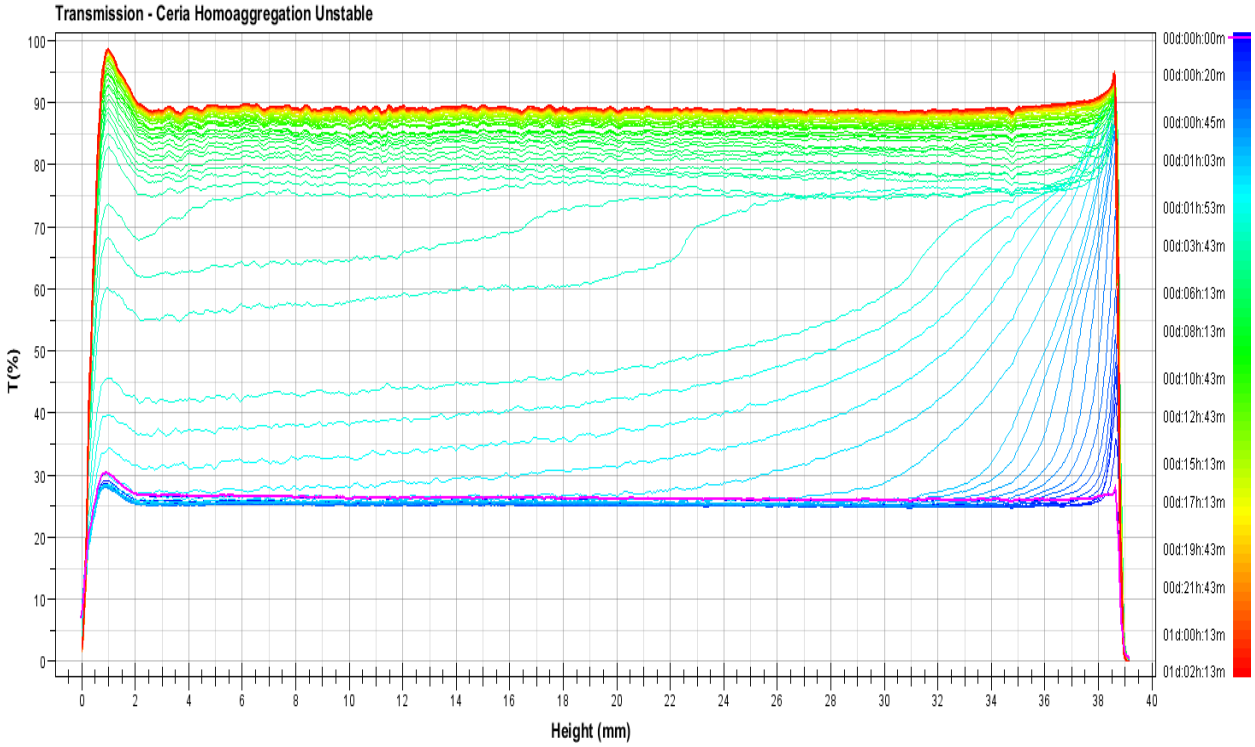

Figure B.2 Original Turbiscan transmittance data (y-axis) across the sample height measured from bottom to top (x-axis) over time (blue to red) for CeO_2 in the unstable medium.

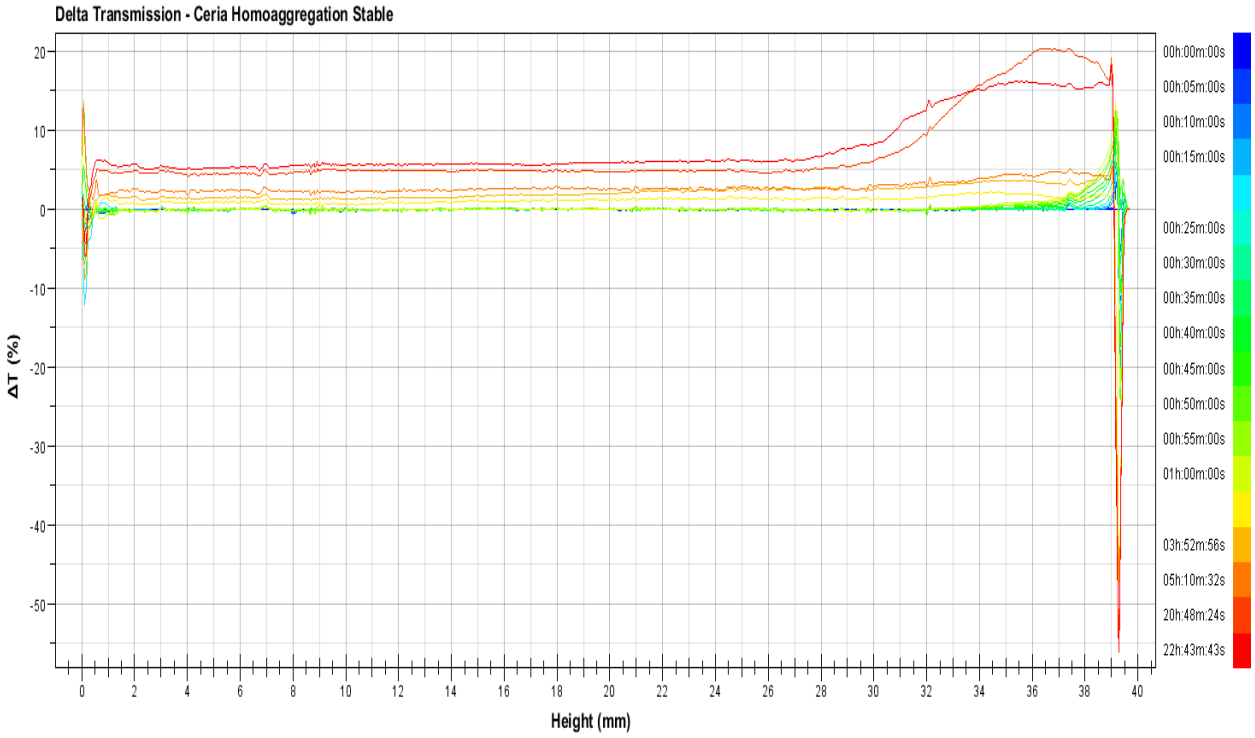

Figure B.3 Delta Turbiscan transmittance data (y-axis) across the sample height measured from bottom to top (x-axis) over time (blue to red) for CeO_2 in the stable medium.

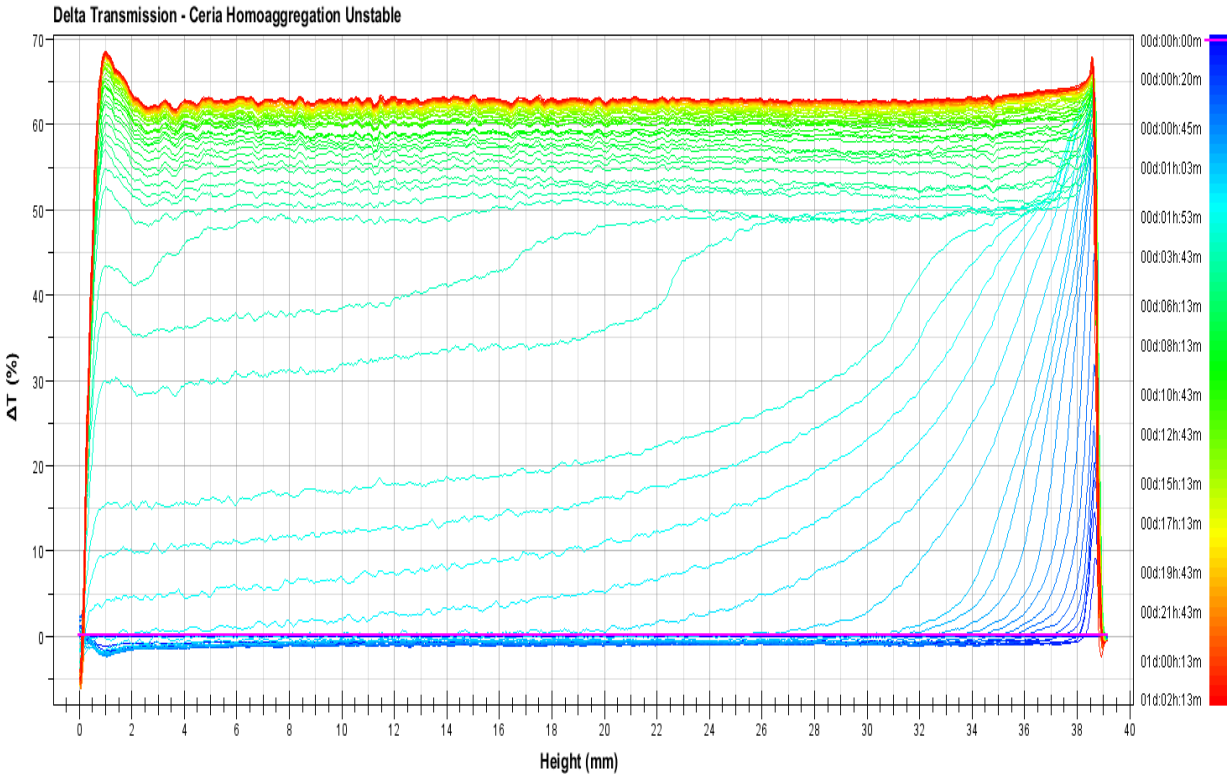

Figure B.4 Delta Turbiscan transmittance data (y-axis) across the sample height measured from bottom to top (x-axis) over time (blue to red) for CeO_2 in the unstable medium.

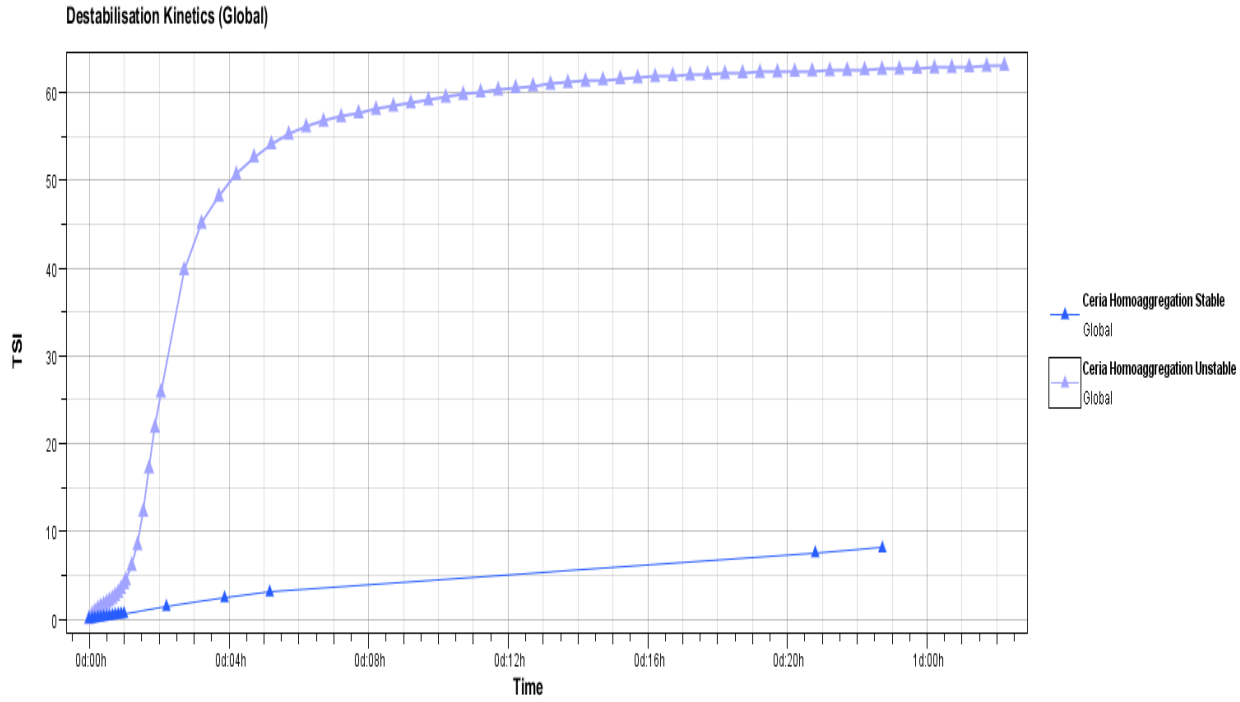

Figure B.5 Global Turbiscan Stability Index of CeO_2 in stable (blue) versus unstable (violet) media over time.

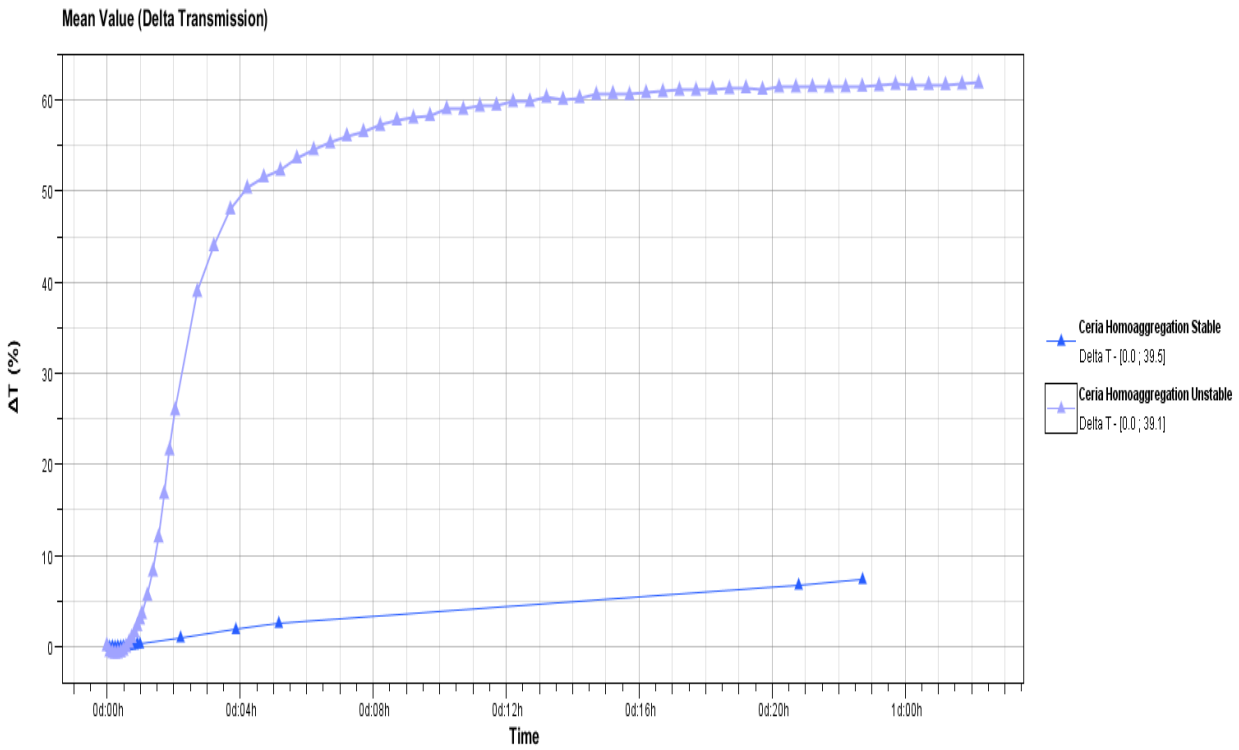

Figure B.6 Mean delta transmittance values (averaged over all sample heights) for CeO_2 in stable (blue) versus unstable (violet) media over time.

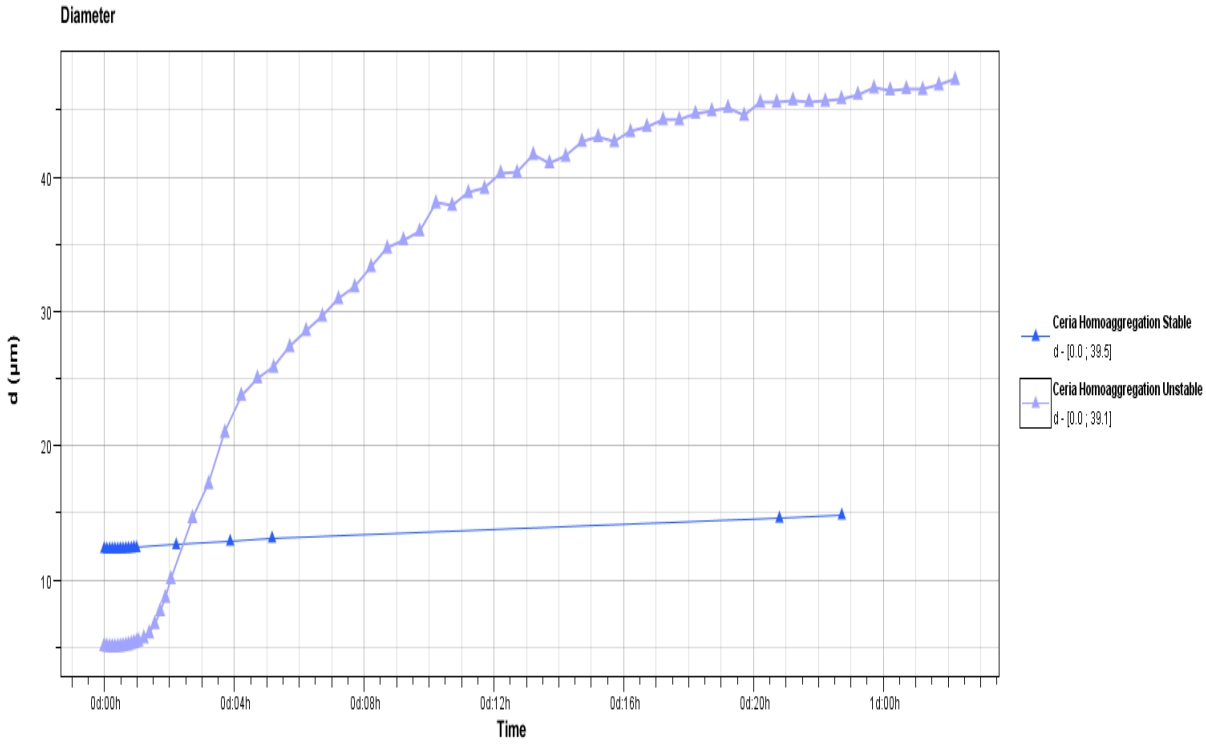

Figure B.7 Particle diameter of CeO_2 in stable (blue) versus unstable (violet) media over time.

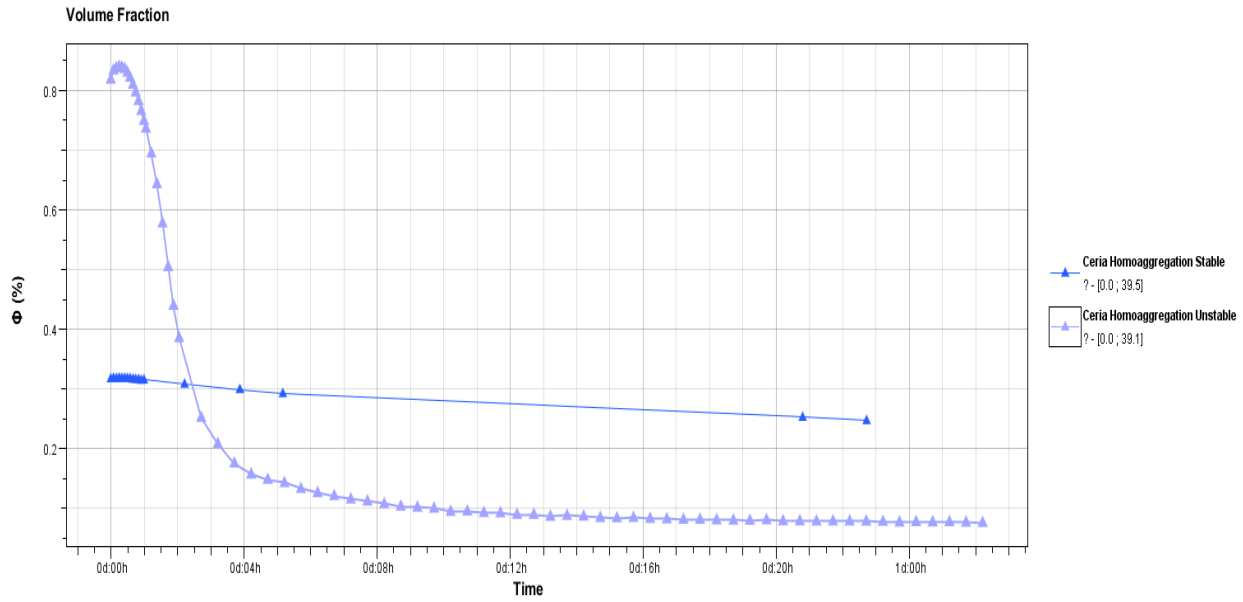

Figure B.8 Volume fraction of CeO_2 in stable (blue) versus unstable (violet) media over time.

B.2 Goethite Homoaggregation Turbiscan Results

This section contains the Turbiscan graph exports for transmittance (Figures B.9, B.10), delta transmittance (Figures B.11, B.12), Global Turbsiscan Stability Index (Figure B.13), mean delta transmittance (Figure B.14), particle diameter (Figure B.15), and volume fraction (Figure B.16) of goethite homoaggregation experiments in stable and unstable media.

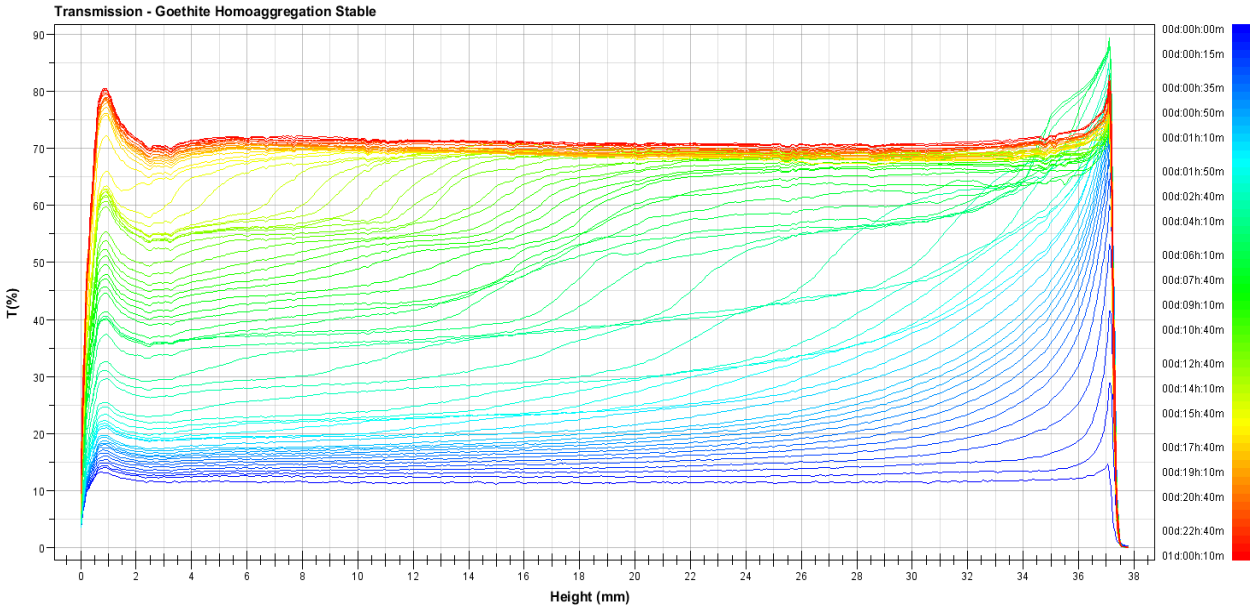

Figure B.9 Original Turbiscan transmittance data (y-axis) across the sample height measured from bottom to top (x-axis) over time (blue to red) for goethite in the stable medium.

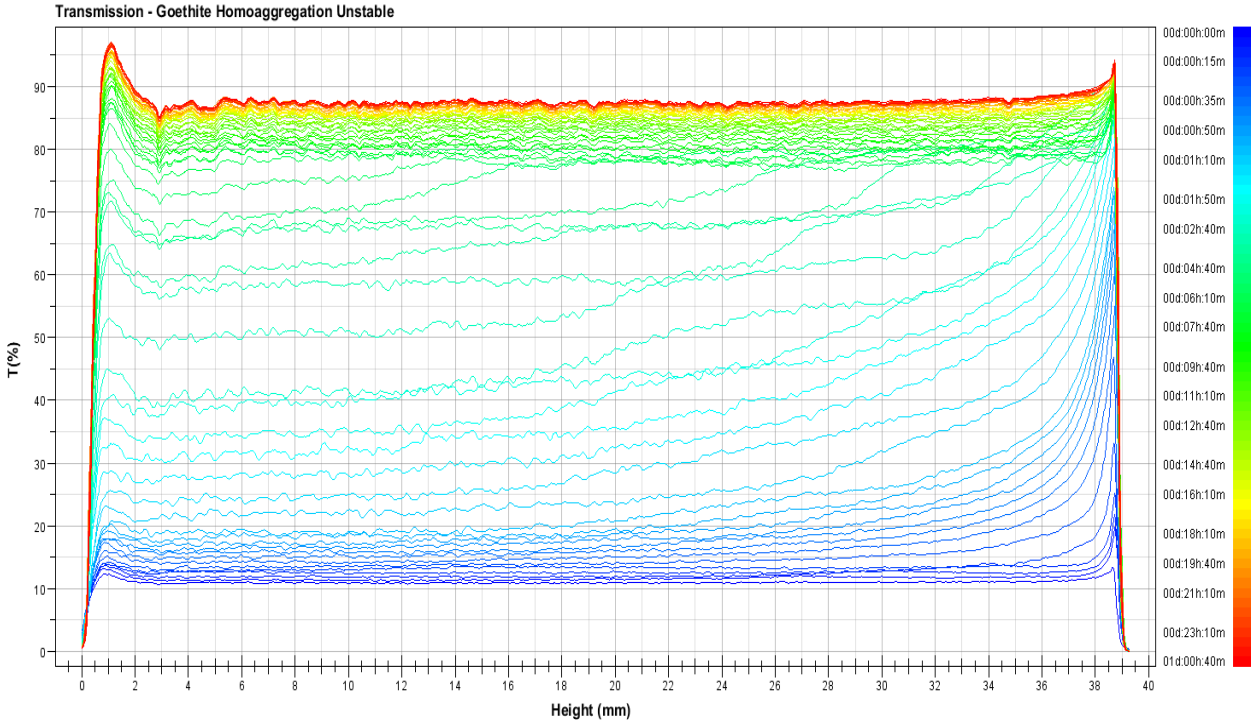

Figure B.10 Original Turbiscan transmittance data (y-axis) across the sample height measured from bottom to top (x-axis) over time (blue to red) for goethite in the unstable medium.

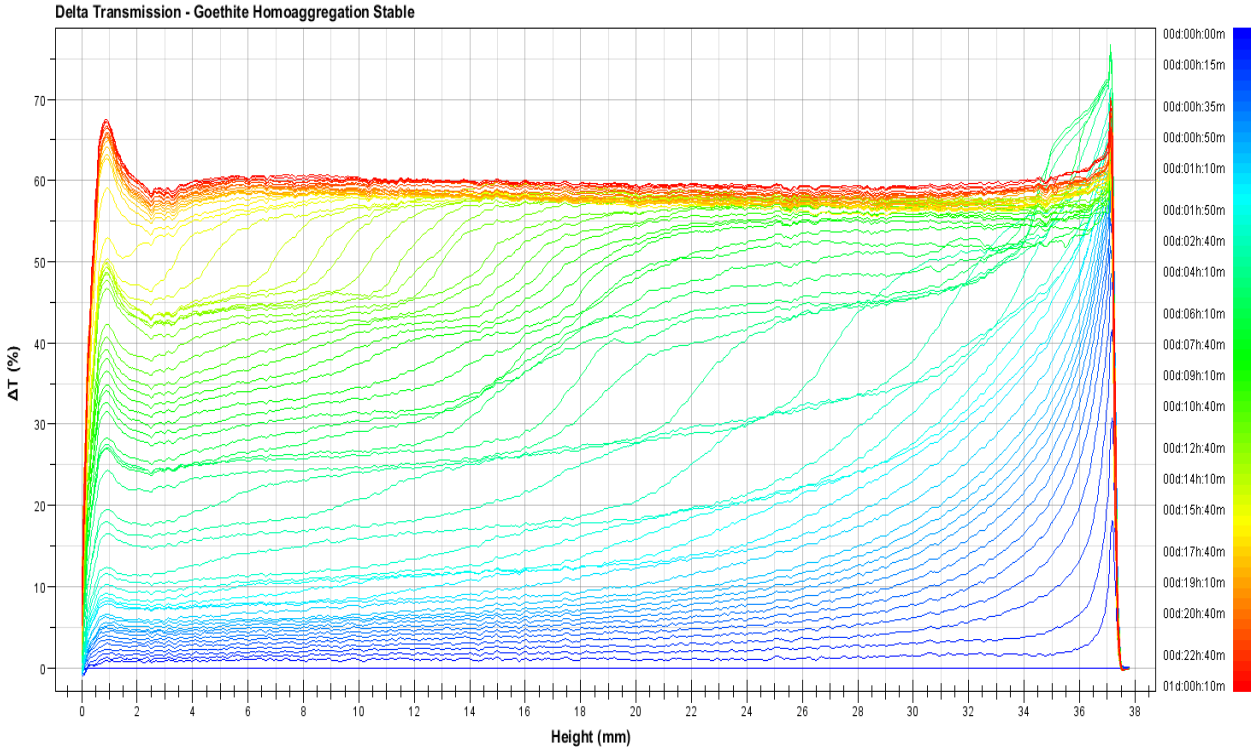

Figure B.11 Delta Turbiscan transmittance data (y-axis) across the sample height measured from bottom to top (x-axis) over time (blue to red) for goethite in the stable medium.

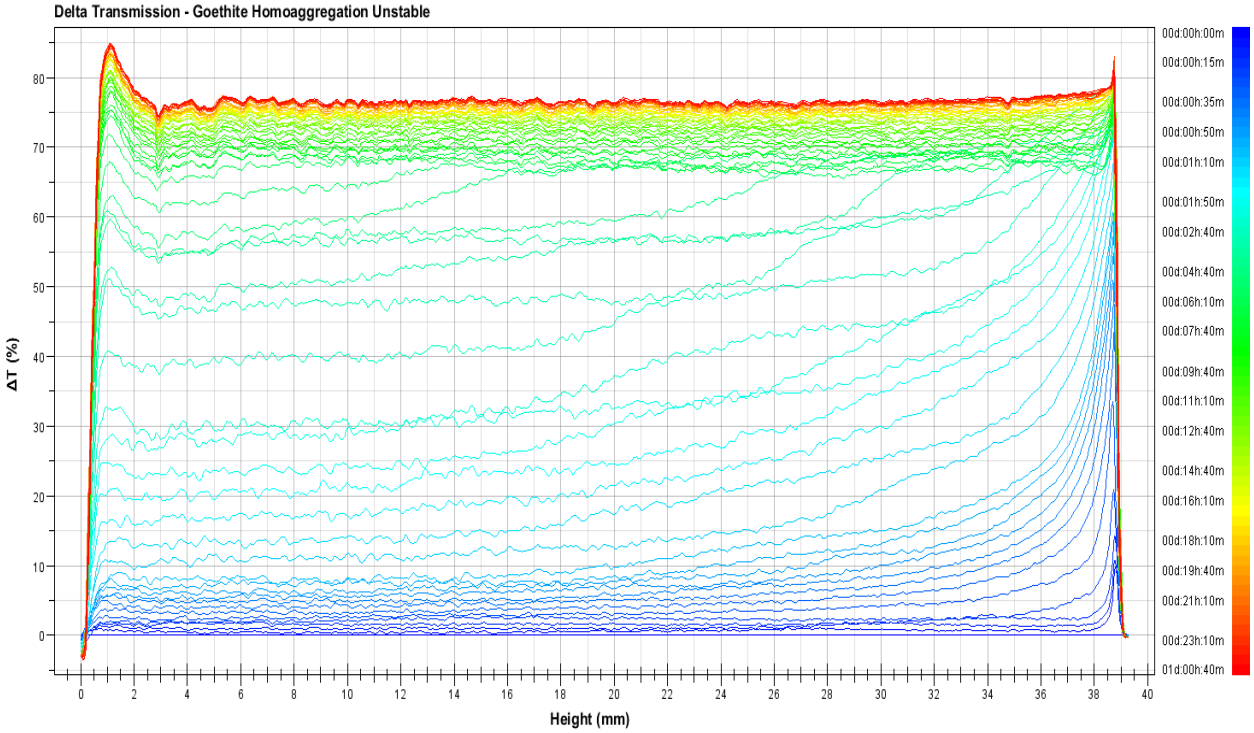

Figure B.12 Delta Turbiscan transmittance data (y-axis) across the sample height measured from bottom to top (x-axis) over time (blue to red) for goethite in the unstable medium.

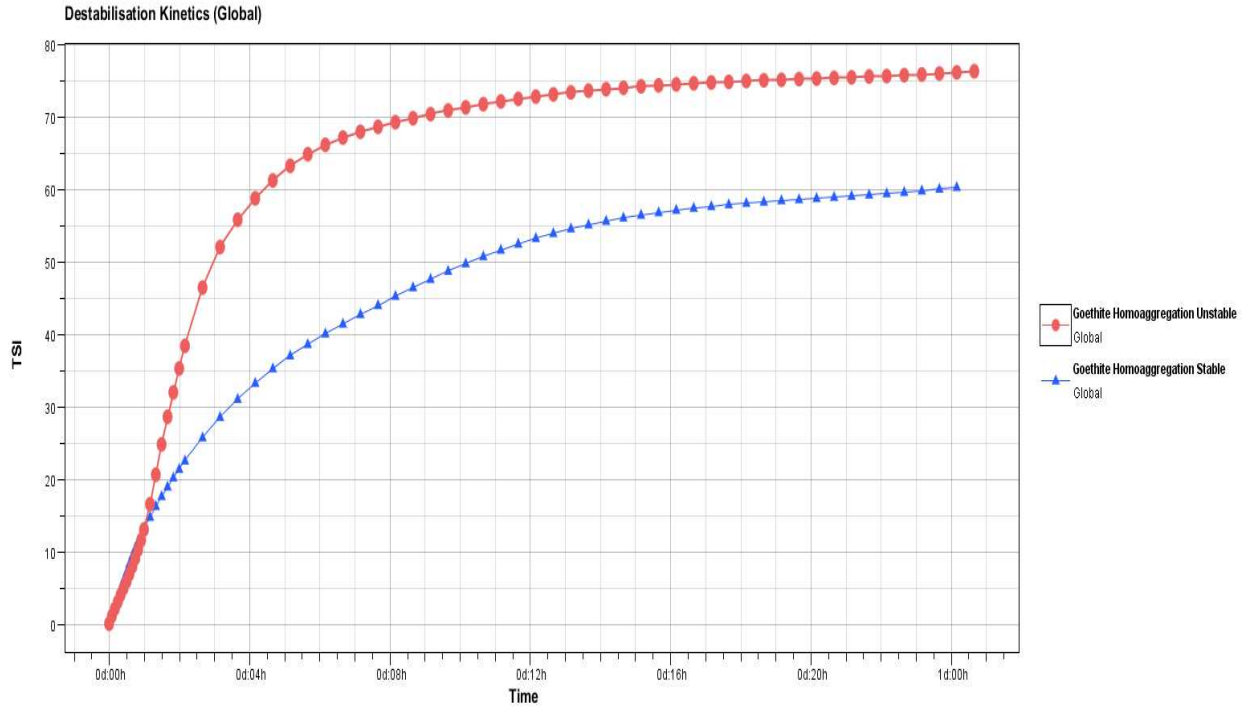

Figure B.13 Global Turbiscan Stability Index of goethite in stable (blue) versus unstable (red) media over time.

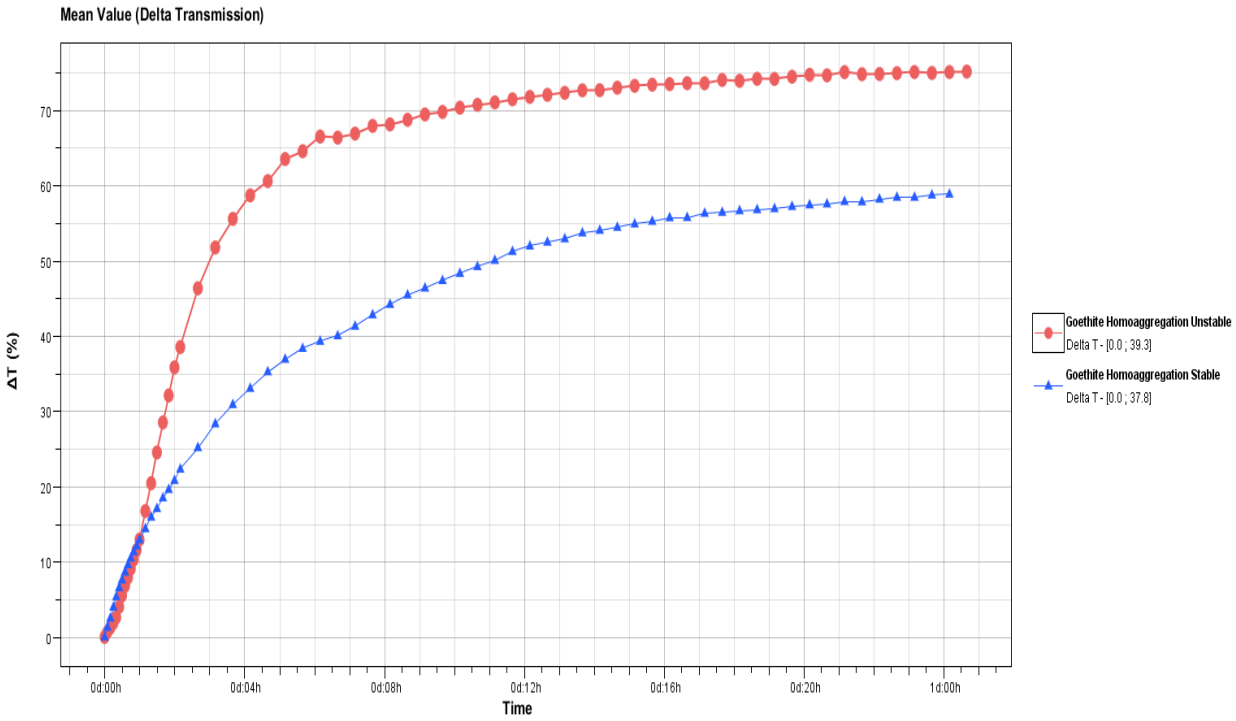

Figure B.14 Mean delta transmittance values (averaged over all sample heights) for goethite in stable (blue) versus unstable (red) media over time.

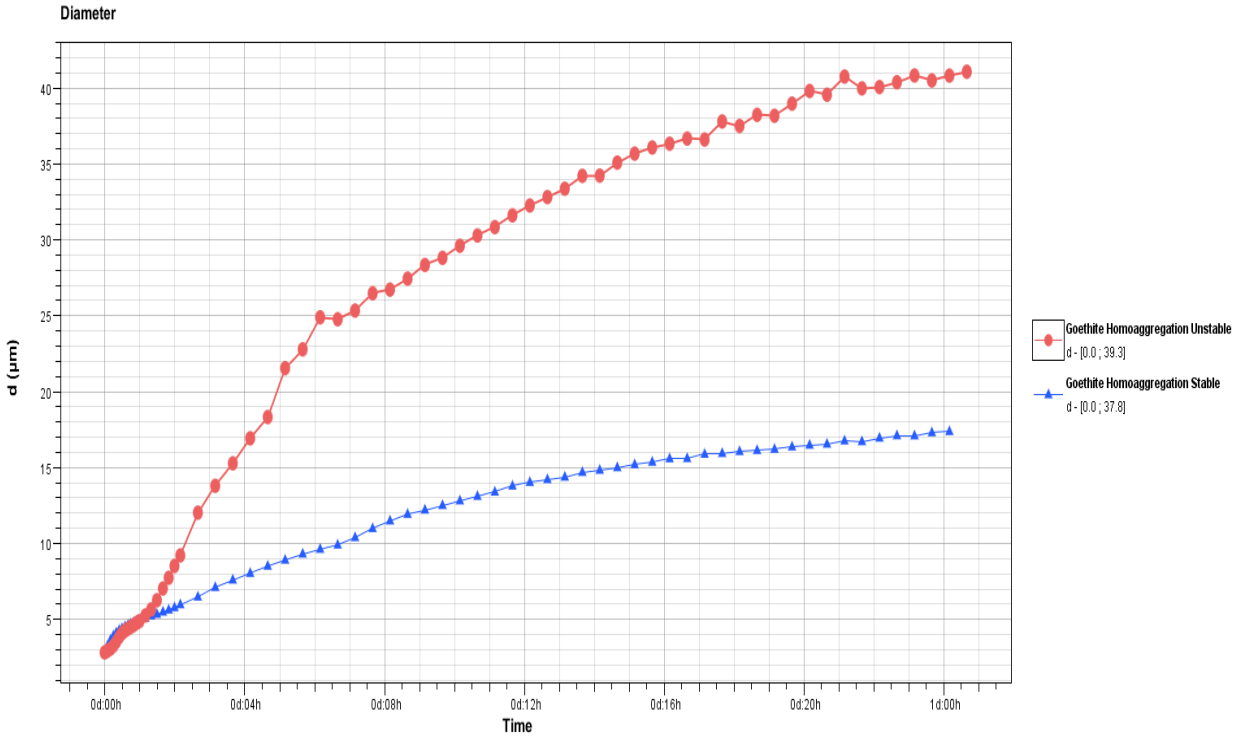

Figure B.15 Particle diameter of goethite in stable (blue) versus unstable (red) media over time.

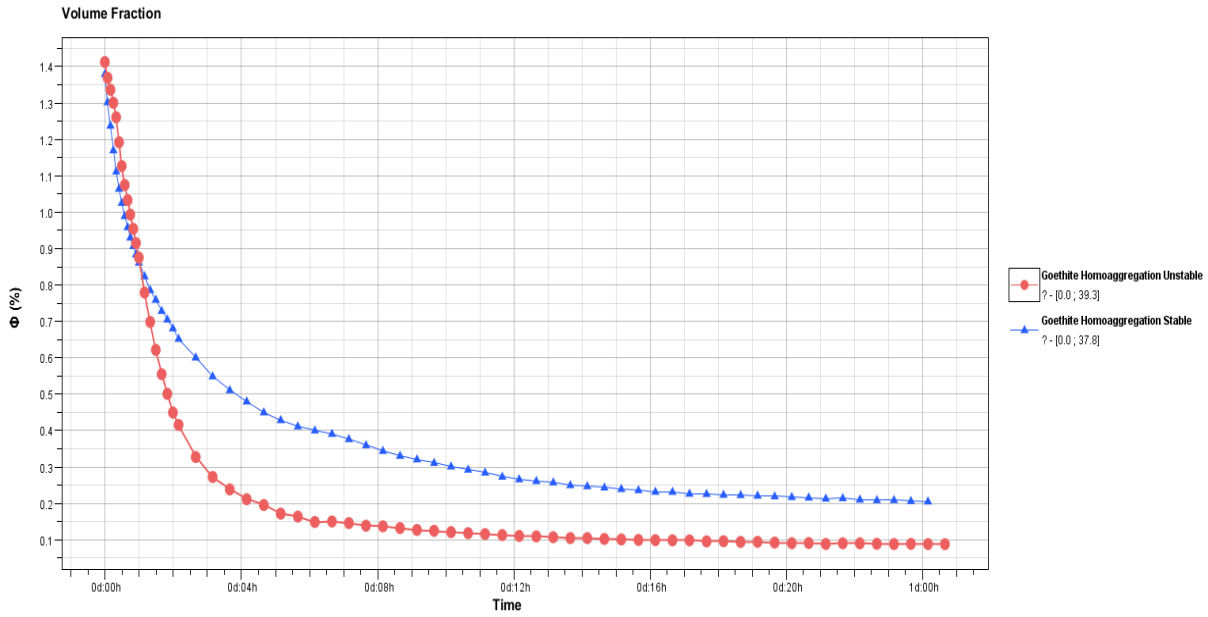

Figure B.16 Volume fraction of goethite in stable (blue) versus unstable (red) media over time.

B.3 Goethite/CeO_2 Heteroaggregation Turbiscan Results

This section contains the Turbiscan graph exports for transmittance (Figures A.17, A.18), delta transmittance (Figures A.19, A.20), Global Turbsiscan Stability Index (Figure A.21), mean delta transmittance (Figure A.22), particle diameter (Figure A.23), and volume fraction (Figure A.24) of goethite/CeO_2 heteroaggregation experiments in stable and unstable media.

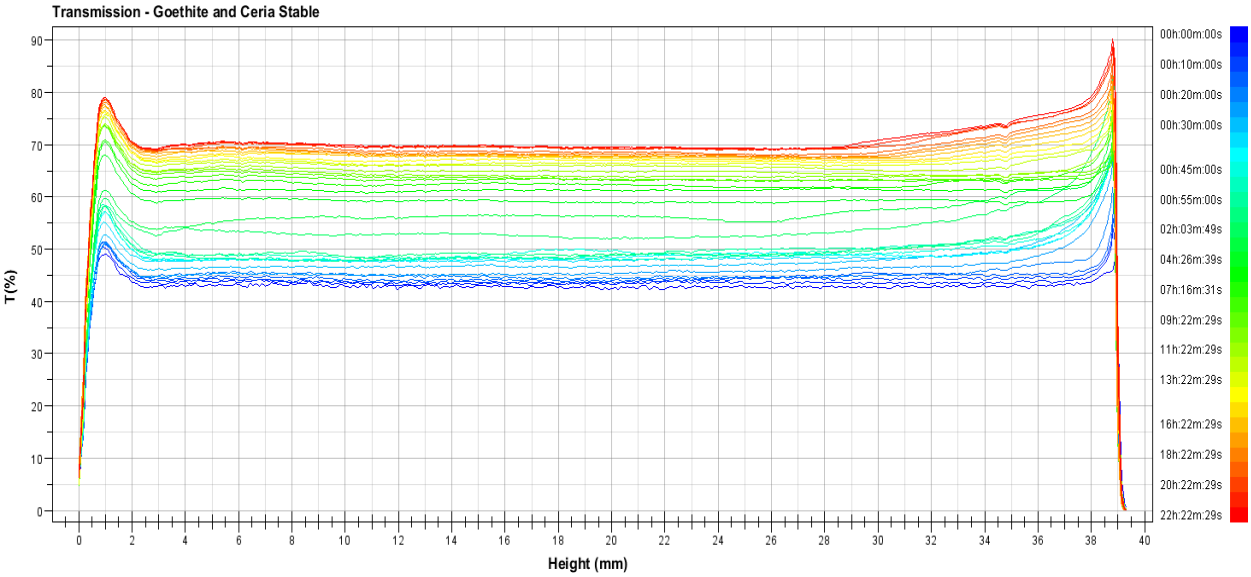

Figure B.17 Original Turbiscan transmittance data (y-axis) across the sample height measured from bottom to top (x-axis) over time (blue to red) for goethite/CeO_2 in the stable medium.

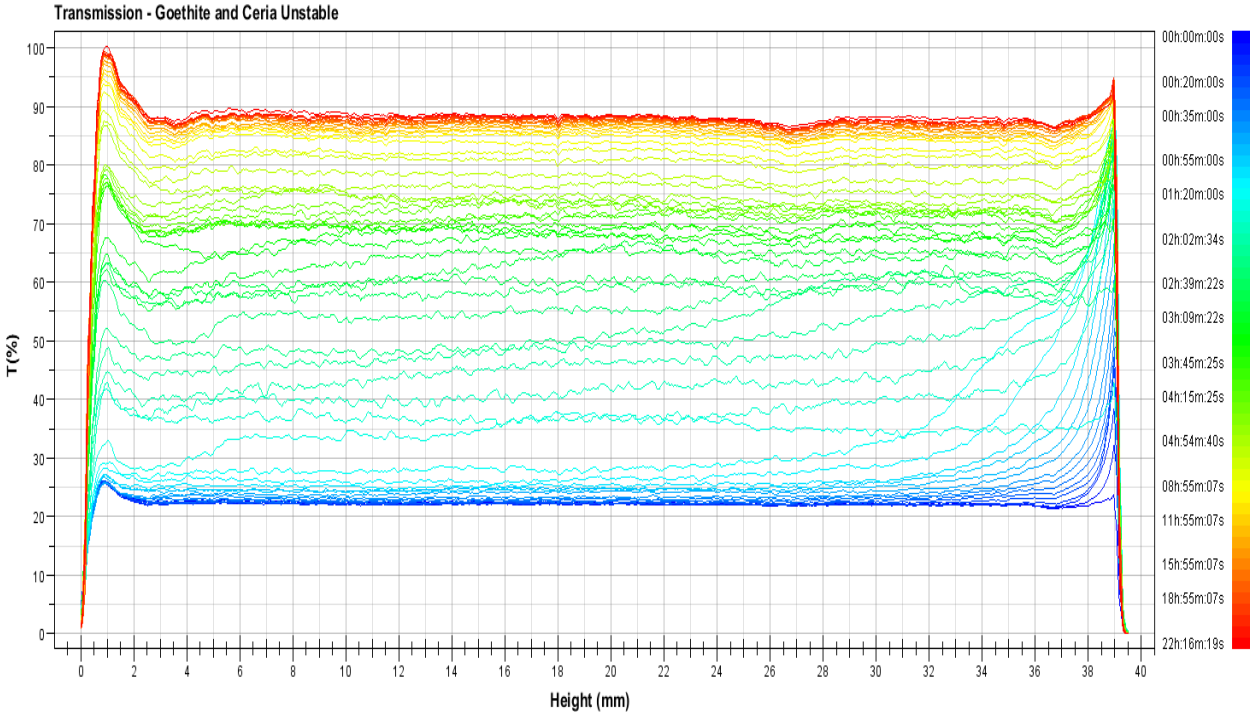

Figure B.18 Original Turbiscan transmittance data (y-axis) across the sample height measured from bottom to top (x-axis) over time (blue to red) for goethite/CeO_2 in the unstable medium.

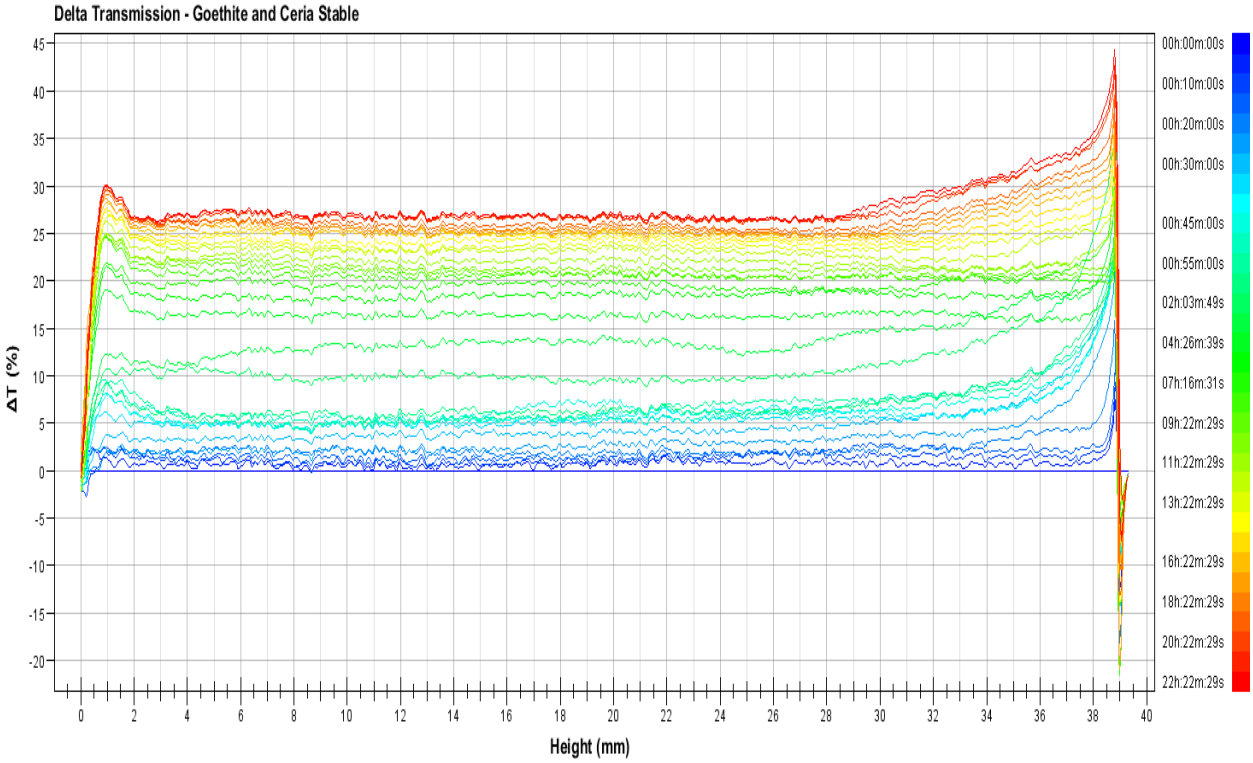

Figure B.19 Delta Turbiscan transmittance data (y-axis) across the sample height measured from bottom to top (x-axis) over time (blue to red) for goethite/CeO_2 in the stable medium.

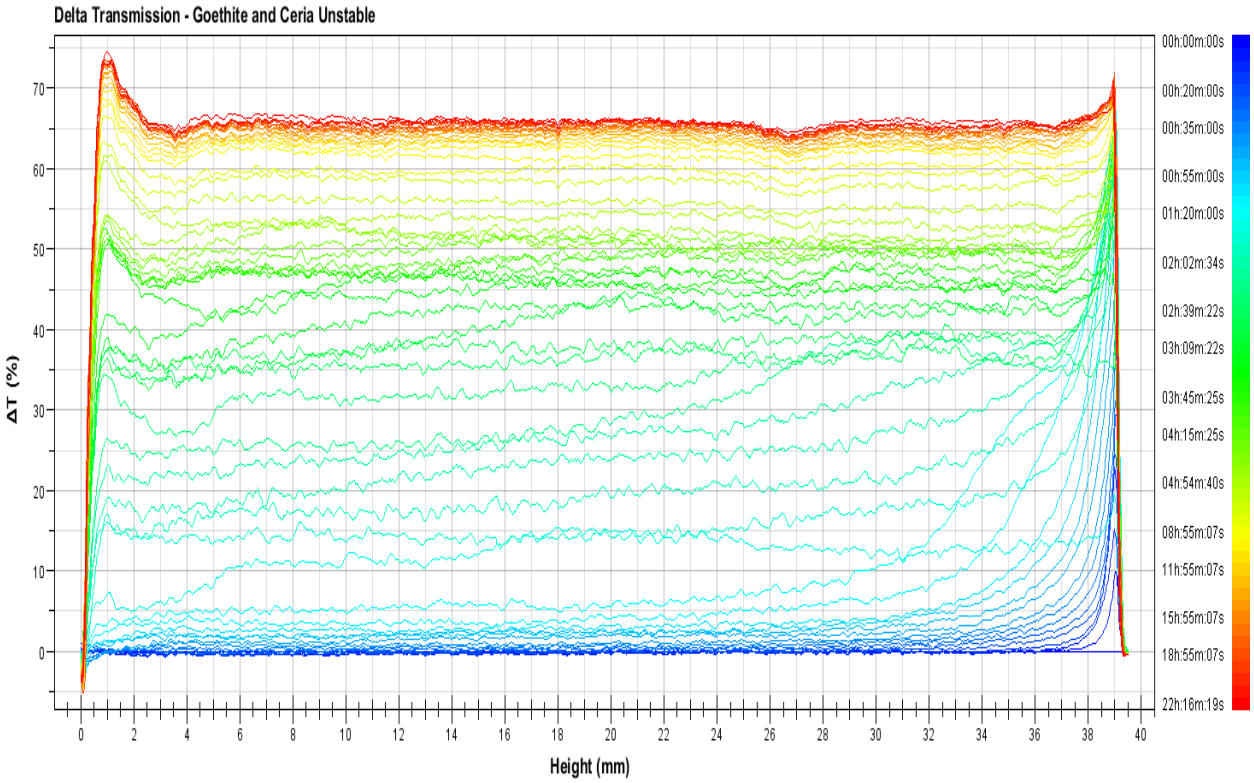

Figure B.20 Delta Turbiscan transmittance data (y-axis) across the sample height measured from bottom to top (x-axis) over time (blue to red) for goethite/CeO_2 in the unstable medium.

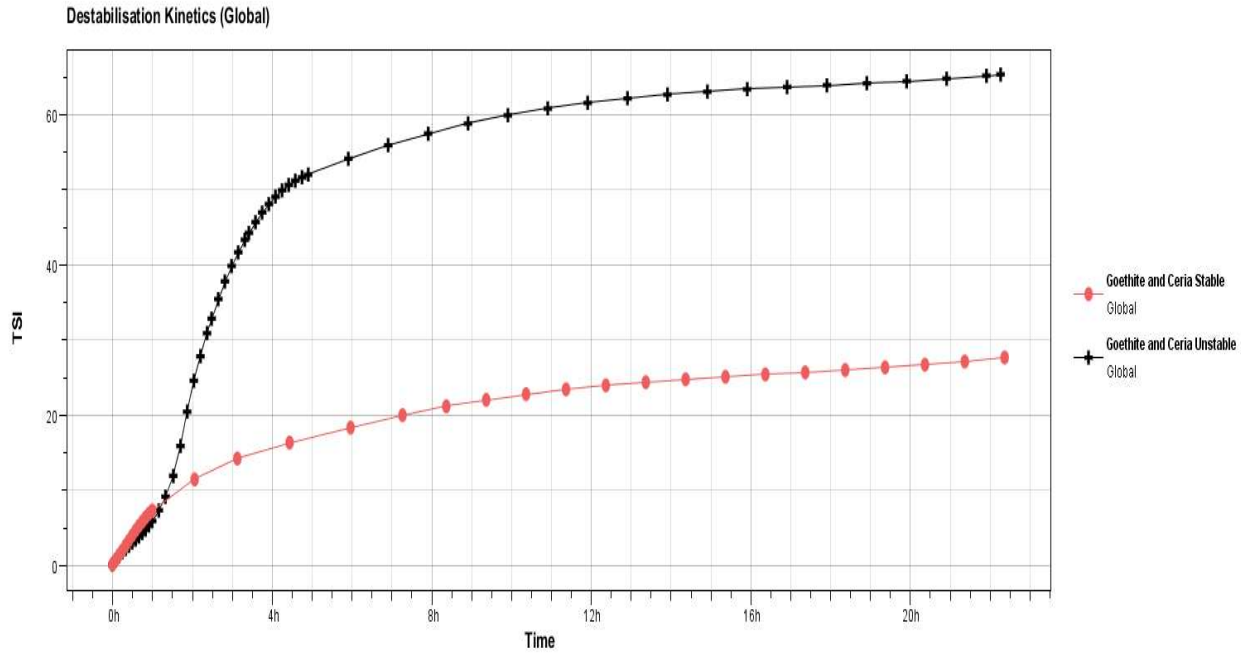

Figure B.21 Global Turbiscan Stability Index of goethite/CeO_2 in stable (red) versus unstable (black) media over time.

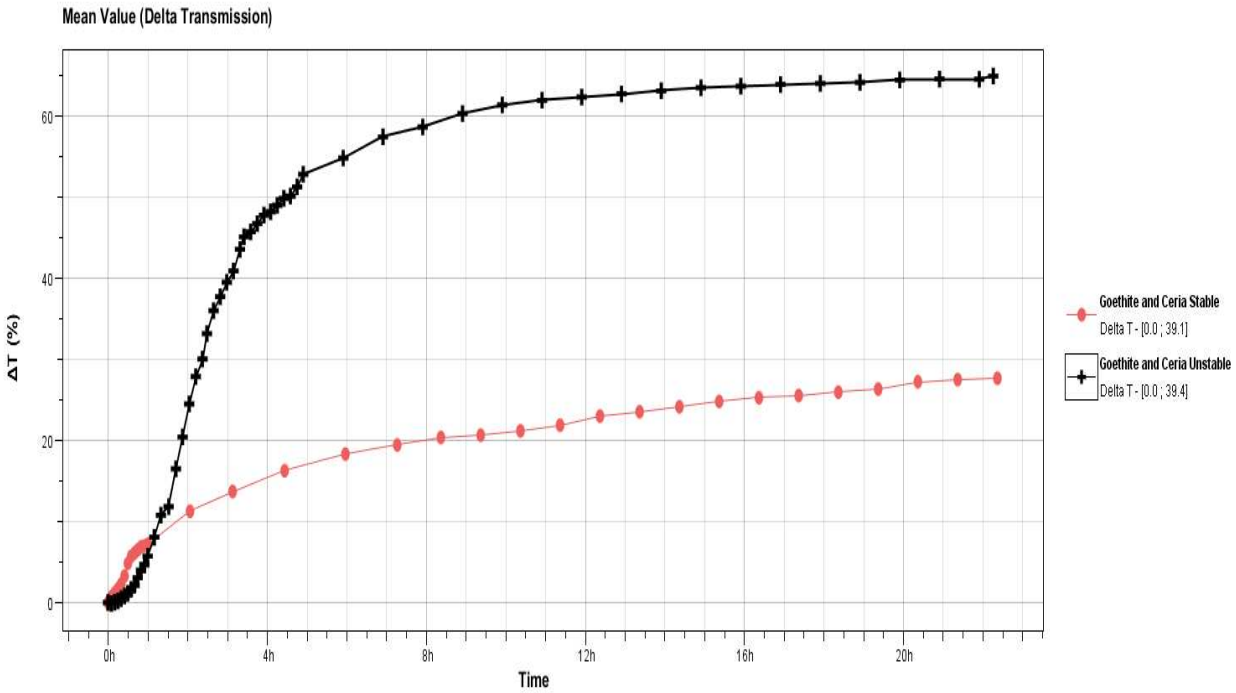

Figure B.22 Mean delta transmittance values (averaged over all sample heights) for goethite/CeO_2 in stable (red) versus unstable (black) media over time.

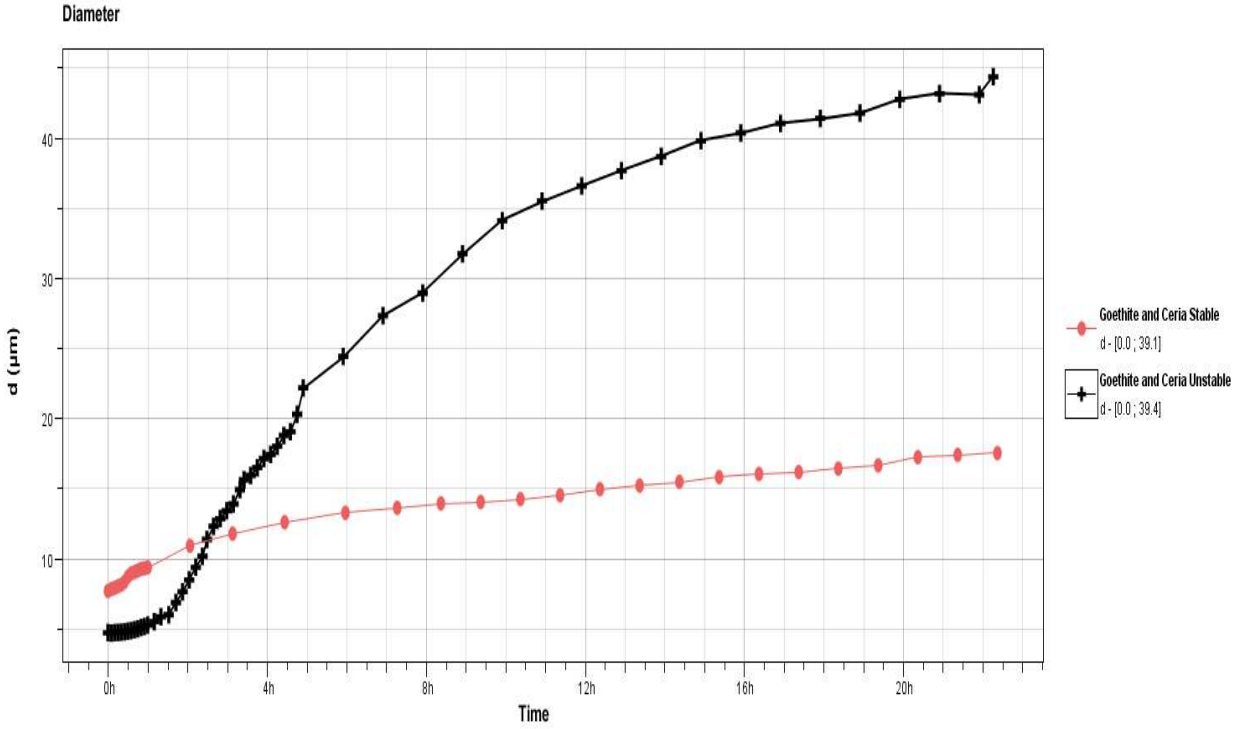

Figure B.23 Particle diameter of goethite/CeO_2 in stable (red) versus unstable (black) media over time.

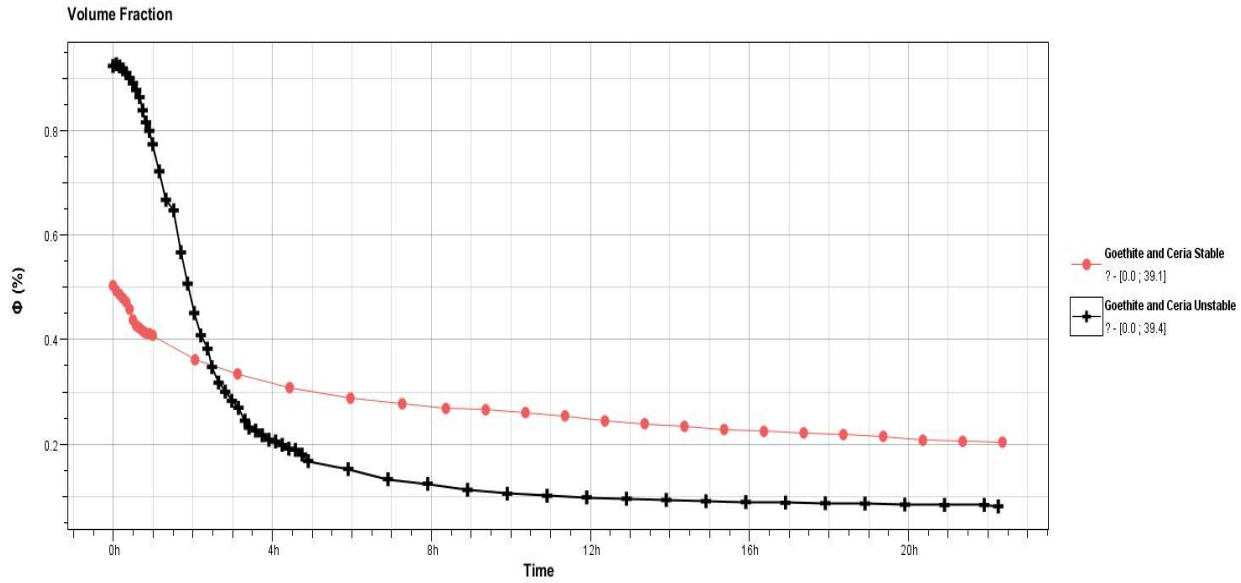

Figure B.24 Volume fraction of goethite/CeO_2 in stable (red) versus unstable (black) media over time.

B.4 Goethite/Kaolinite Heteroaggregation Turbiscan Results

This section contains the Turbiscan graph exports for transmittance (Figures A.25, A.26), delta transmittance (Figures A.27, A.28), Global Turbsiscan Stability Index (Figure A.29), mean delta transmittance (Figure A.30), particle diameter (Figure A.31), and volume fraction (Figure A.32) of goethite/kaolinite heteroaggregation experiments in stable and unstable media.

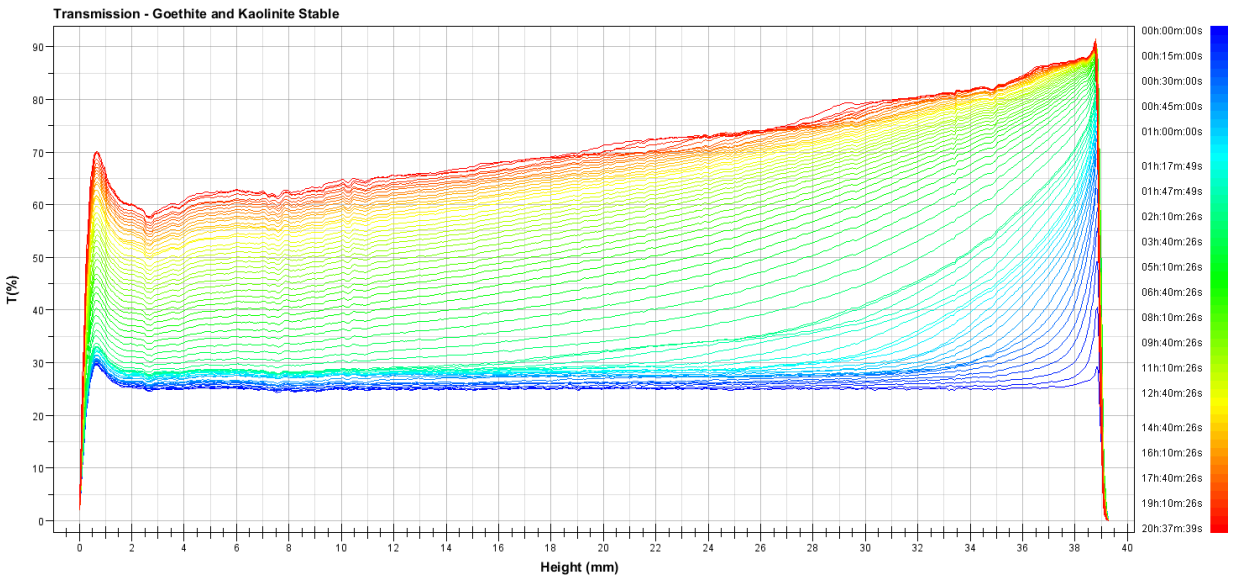

Figure B.25 Original Turbiscan transmittance data (y-axis) across the sample height measured from bottom to top (x-axis) over time (blue to red) for goethite/kaolinite in the stable medium.

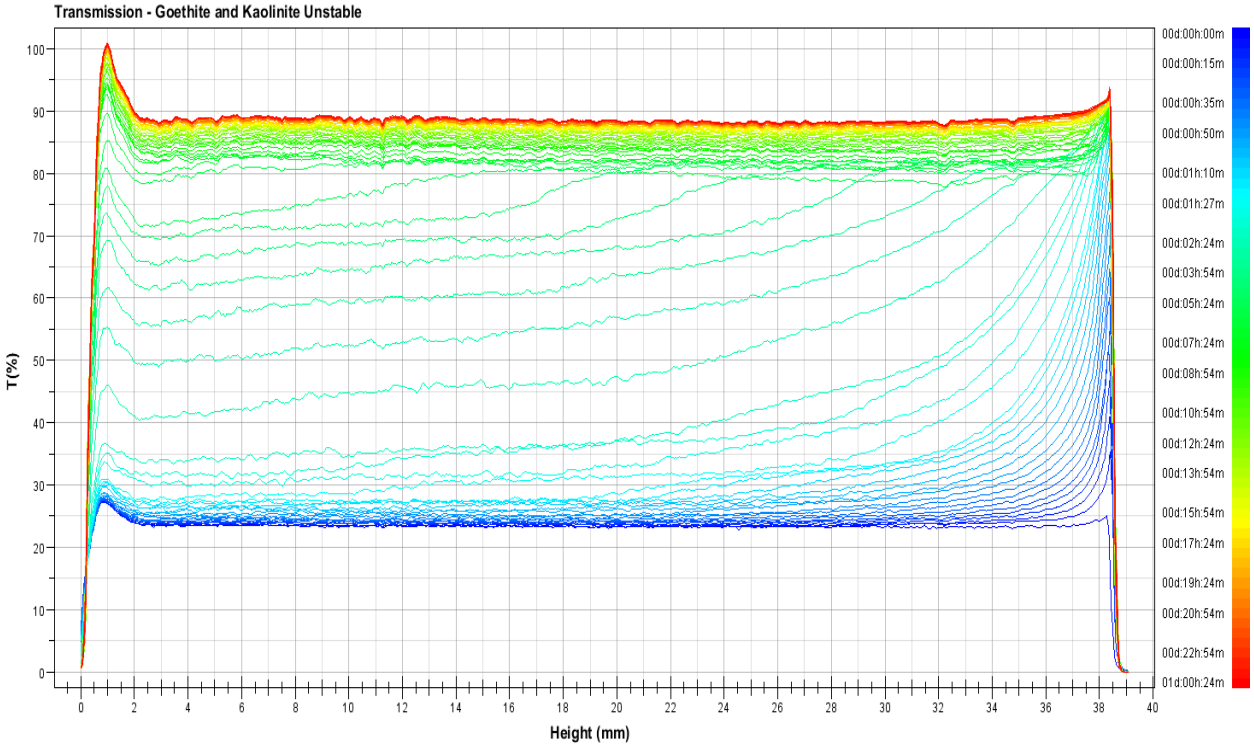

Figure B.26 Original Turbiscan transmittance data (y-axis) across the sample height measured from bottom to top (x-axis) over time (blue to red) for goethite/kaolinite in the unstable medium.

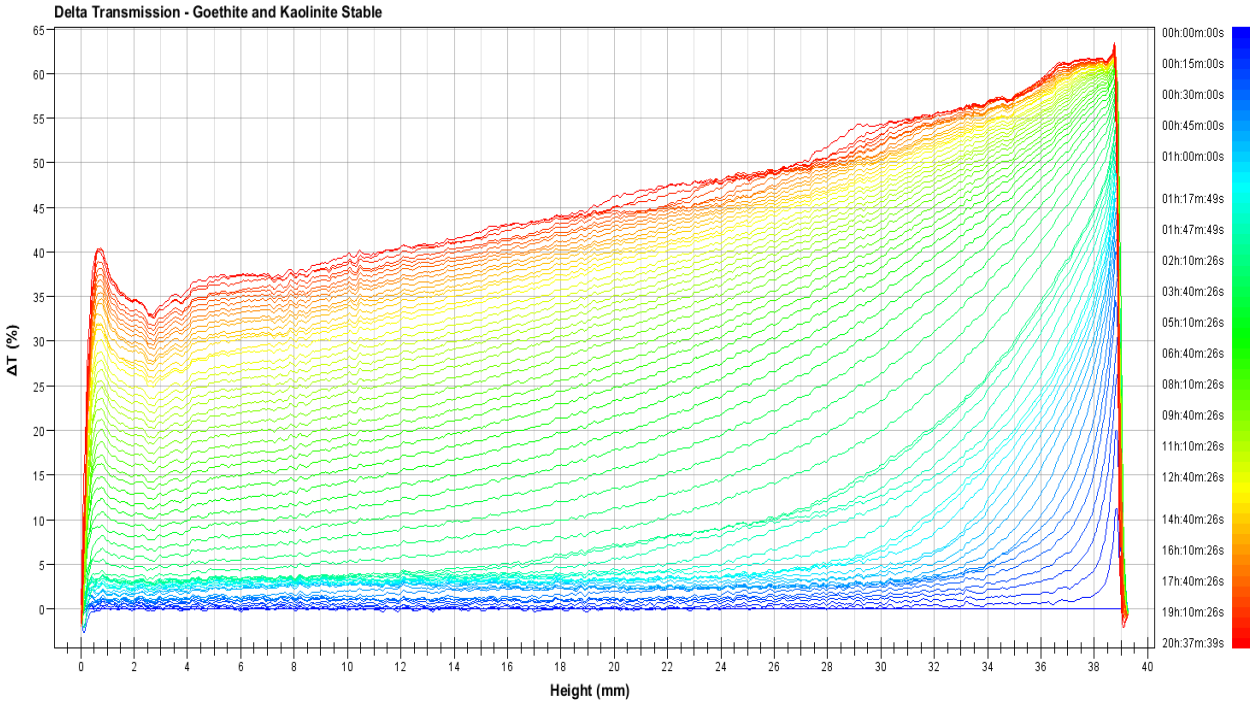

Figure B.27 Delta Turbiscan transmittance data (y-axis) across the sample height measured from bottom to top (x-axis) over time (blue to red) for goethite/kaolinite in the stable medium.

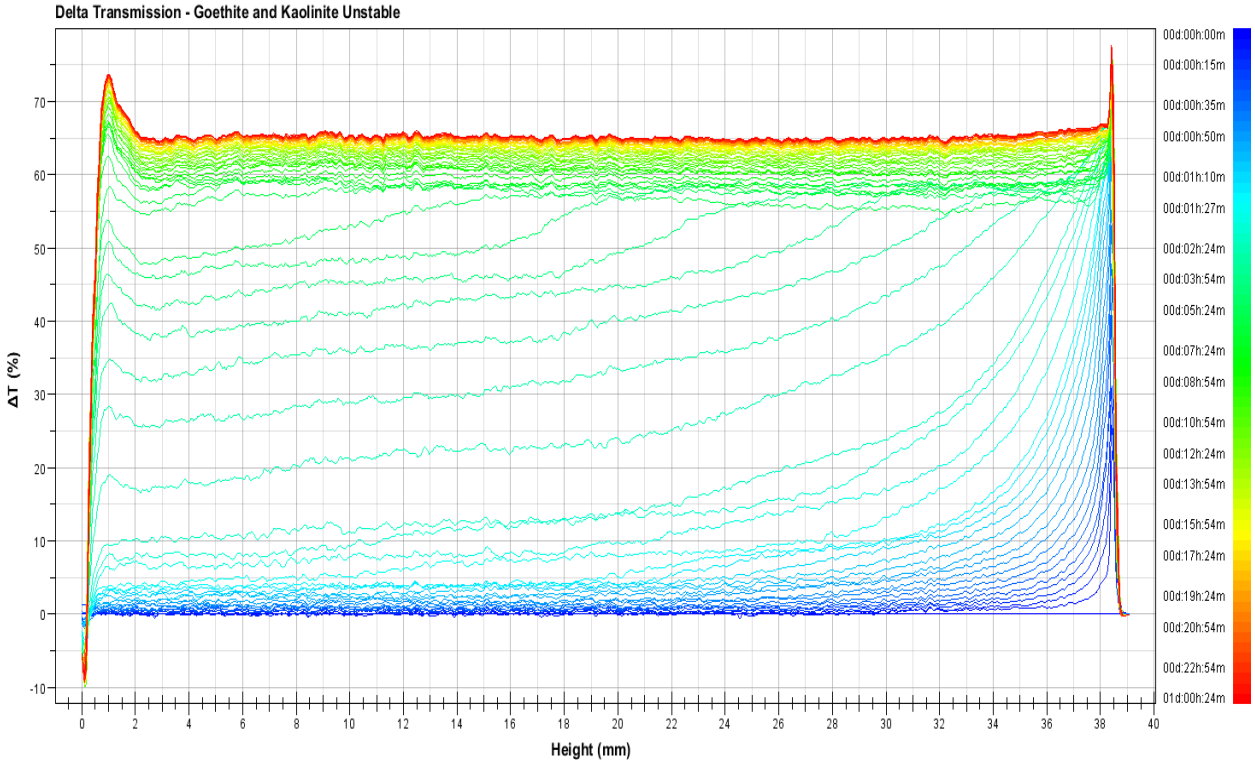

Figure B.28 Delta Turbiscan transmittance data (y-axis) across the sample height measured from bottom to top (x-axis) over time (blue to red) for goethite/kaolinite in the unstable medium.

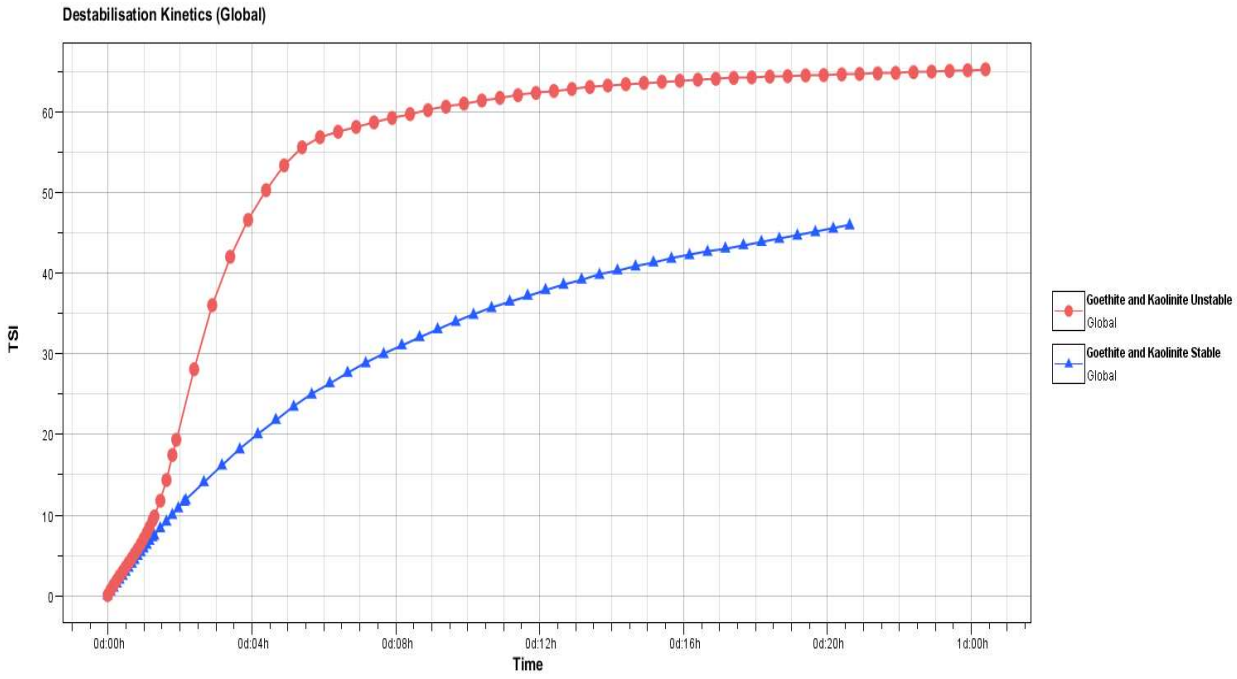

Figure B.29 Global Turbiscan Stability Index of goethite/kaolinite in stable (blue) versus unstable (red) media over time.

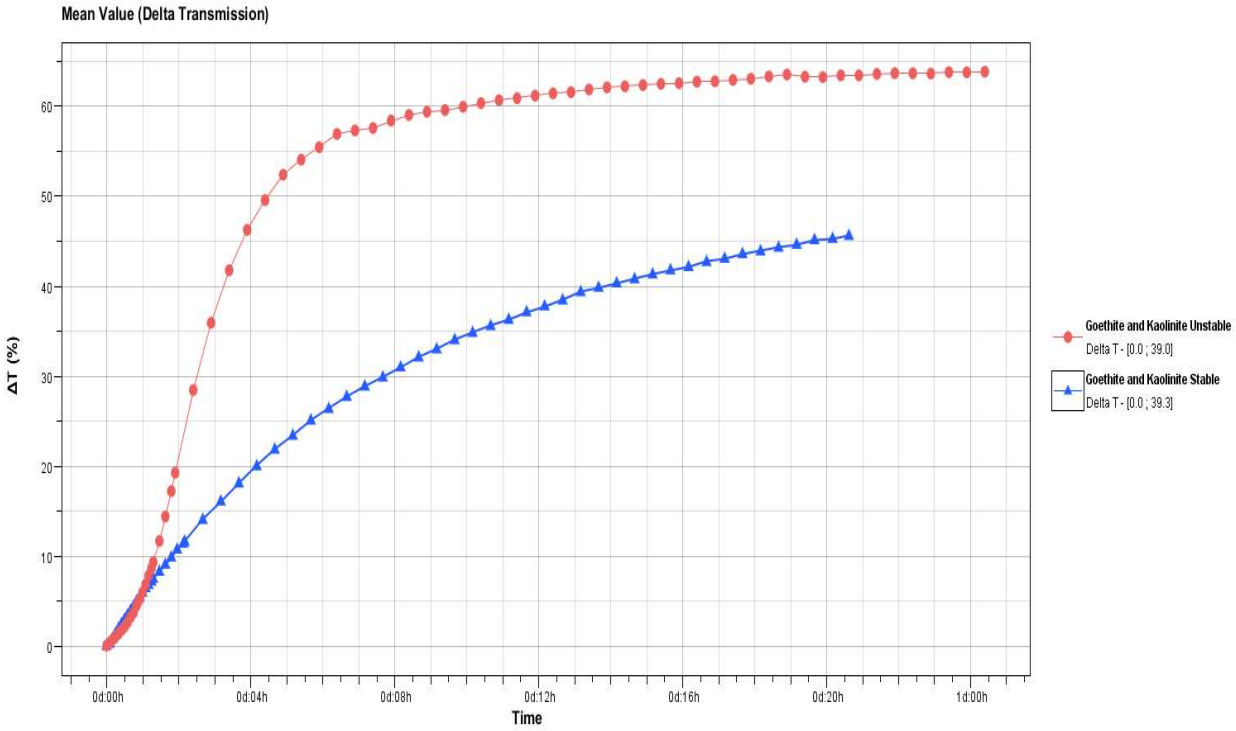

Figure B.30 Mean delta transmittance values (averaged over all sample heights) for goethite/kaolinite in stable (blue) versus unstable (red) media over time.

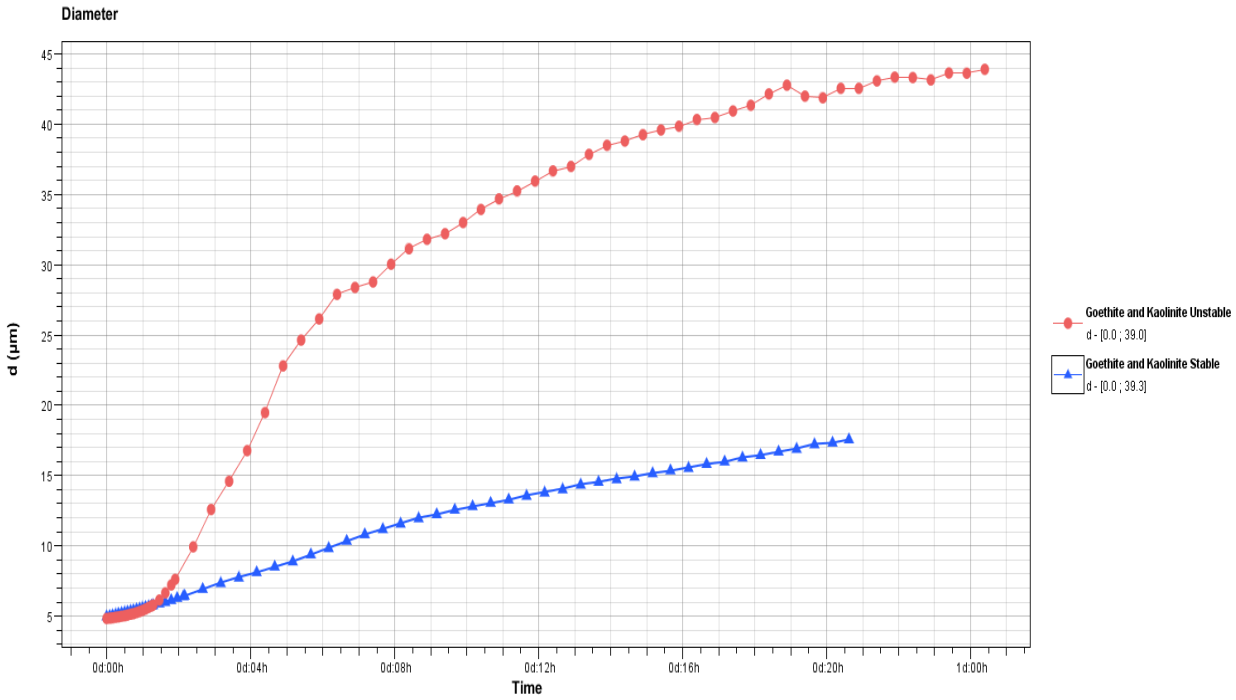

Figure B.31 Particle diameter of goethite/kaolinite in stable (blue) versus unstable (red) media over time.

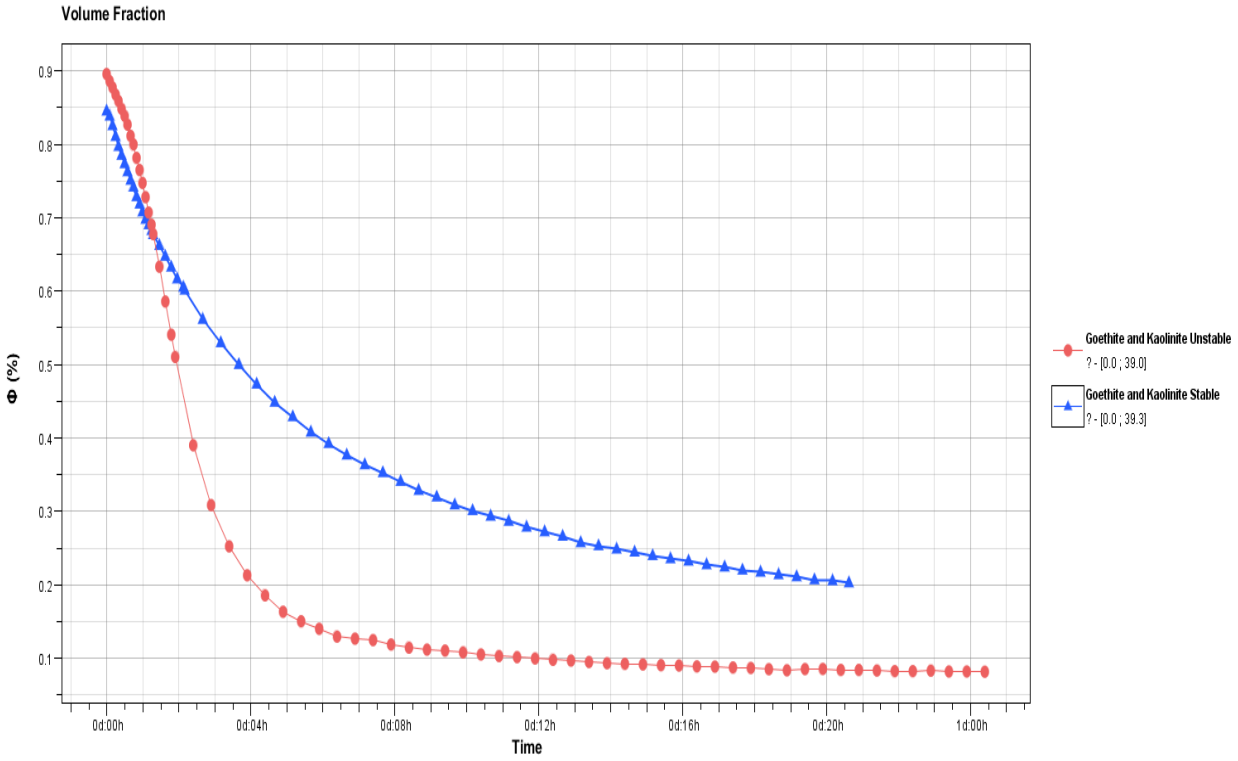

Figure B.32 Volume fraction of goethite/kaolinite in stable (blue) versus unstable (red) media over time.